

University of Windsor

Scholarship at UWindor

Electronic Theses and Dissertations

Theses, Dissertations, and Major Papers

7-11-2015

Experimental Testing of Aluminum Foam Filled Stainless Steel Braided Tubes Subjected to Transverse Impact

Ryan Mark Smith
University of Windsor

Follow this and additional works at: <https://scholar.uwindsor.ca/etd>

Recommended Citation

Smith, Ryan Mark, "Experimental Testing of Aluminum Foam Filled Stainless Steel Braided Tubes Subjected to Transverse Impact" (2015). *Electronic Theses and Dissertations*. 5327.
<https://scholar.uwindsor.ca/etd/5327>

This online database contains the full-text of PhD dissertations and Masters' theses of University of Windsor students from 1954 forward. These documents are made available for personal study and research purposes only, in accordance with the Canadian Copyright Act and the Creative Commons license—CC BY-NC-ND (Attribution, Non-Commercial, No Derivative Works). Under this license, works must always be attributed to the copyright holder (original author), cannot be used for any commercial purposes, and may not be altered. Any other use would require the permission of the copyright holder. Students may inquire about withdrawing their dissertation and/or thesis from this database. For additional inquiries, please contact the repository administrator via email (scholarship@uwindsor.ca) or by telephone at 519-253-3000ext. 3208.

Experimental Testing of Aluminum Foam Filled Stainless Steel Braided Tubes Subjected
to Transverse Impact

By

Ryan Smith

A Thesis
Submitted to the Faculty of Graduate Studies
through the Department of Mechanical, Automotive and Materials Engineering
in Partial Fulfillment of the Requirements for
the Degree of Master of Applied Science
at the University of Windsor

Windsor, Ontario, Canada

2015

© 2015 Ryan Smith

Experimental Testing of Aluminum Foam Filled Stainless Steel Braided Tubes Subjected
to Transverse Impact

by

Ryan Smith

APPROVED BY:

Dr. Hu, Outside Reader
Dept. of Mechanical, Automotive and Materials Engineering

Dr. Green, Internal Reader
Dept. of Mechanical, Automotive and Materials Engineering

Dr. Altenhof, Advisor
Department of Mechanical, Automotive and Materials Engineering

CO-AUTHORSHIP & PREVIOUS PUBLICATION

This thesis contains 3 papers that have been previously published or submitted for publication within peer reviewed journals as follows.

Thesis Chapter	Publication title/full citation	Publication status*
4-9	Audysho R, Smith R, Altenhof W, Patel K. Aluminum foam core density and geometry influences on the deformation mechanisms of foam filled braided tubular structures in tension. <i>Journal of Materials and Design</i> , 2014; 54:394-413.	Published
4-9	Audysho R, Smith R, Altenhof W. Mechanical assessment of deformation mechanisms of aluminum foam filled stainless steel braided tubes subjected to transverse loading. <i>Journal of Thin Walled Structures</i> , 2014; 79:95-107	Published
4-9	Smith. R, Altenhof. W, Lapain. M, Transverse Impact Loading of Aluminum Foam Filled Braided Stainless Steel Tubes. <i>Journal of Impact Engineering</i> . Submitted Mar/5/2015	Submitted

I certify that I have obtained a written permission from the copyright owner(s) to include the above published material(s) in my thesis. I certify that the above material describes work completed during my registration as graduate student at the University of Windsor.

I certify that, to the best of my knowledge, my thesis does not infringe upon anyone's copyright nor violate any proprietary rights and that any ideas, techniques, quotations, or any other material from the work of other people

included in my thesis, published or otherwise, are fully acknowledged in accordance with the standard referencing practices. Furthermore, to the extent that I have included copyrighted material that surpasses the bounds of fair dealing within the meaning of the Canada Copyright Act, I certify that I have obtained a written permission from the copyright owner(s) to include such material(s) in my thesis and have included copies of such copyright clearances to my appendix.

I declare that this is a true copy of my thesis, including any final revisions, as approved by my thesis committee and the Graduate Studies office, and that this thesis has not been submitted for a higher degree to any other University or Institution.

I hereby declare that this thesis incorporates material that is result of joint research, as follows:

This thesis incorporates the outcomes of two joint research projects undertaken in collaboration with Ramsin Audysho under the supervision of Dr. William Altenhof. Elements from these collaborations are covered in Chapters 4-9 of this thesis. The experimental design and data analysis were completed by the author. The contribution of the co-authors was primarily through the provisions of assisting in documenting the experimental findings within the published manuscripts as well as the completion of items such as graphs depicting experimental results.

I am aware of the University of Windsor Senate Policy on Authorship and I certify that I have properly acknowledged the contribution of other researchers to my thesis, and have obtained written permission from each of the co-author(s) to include the above material(s) in my thesis.

I certify that, with the above qualification, this thesis, and the research to which it refers, is the product of my own work.

ABSTRACT

The findings from an experimental study investigating the mechanical response and deformation mechanisms of empty and aluminum foam filled braided stainless steel tubes are presented within this thesis. Tube specimens were impacted using a custom built pneumatic gun and projectile at incident velocities ranging from roughly 21 m/s to 27 m/s. Deformation and failure mechanisms resulting from the impact process were identified through the use of a high speed, high-resolution camera. Aluminum foam cores of density levels ranging from 179.22 kg/m³ to 520.47 kg/m³ were incorporated within the braided tubes having rectangular foam core geometry. Cores possessing density levels greater than 400 kg/m³ were detrimental to structure performance. A comparison of the mechanical responses of empty and foam tube specimens tested under quasi-static and dynamically applied transverse impact loads was also completed. Findings from the comparison indicate braided tube specimens experience an earlier initiation of progressive tube failure when compared to quasi-statically tested specimens.

DEDICATION

To Ian Smith, Antoinette Maitre, and the Pigeon family: For their support and guidance.

ACKNOWLEDGEMENTS

I would like to express my sincere appreciation and gratitude to my advisor Dr. William Altenhof for his support and guidance. Throughout the course of this thesis, his assistance and wisdom have permitted me to not only complete many challenging tasks but do so with a high degree of success. During my time at the university I have tried my best to parallel his level of professionalism and attention to detail which has permitted me to grow not only as an individual but also within my academic and professional career. My time within this program will not be forgotten.

I would like to thank Andy Jenner, Matt St. Louis, and Bruce Durfy for all of their assistance and support throughout the construction of the testing apparatus utilized within this research study. In addition to their assistance, they have taught me many valuable skills that will continue to assist me throughout my career. Additionally, I would like to thank my committee members as well as the faculty and staff of the Department of Mechanical Engineering for their support and assistance.

Finally, I would like to thank Ramsin Audysho for granting me the opportunity to assist in his research. The early exposure I received to a testing lab environment has opened many doors for me and presented many opportunities I would not have had otherwise.

TABLE OF CONTENTS

CO-AUTHORSHIP & PREVIOUS PUBLICATION	iii
DEDICATION	vii
ACKNOWLEDGEMENTS	viii
LIST OF TABLES	xii
LIST OF FIGURES	xiii
LIST OF APPENDICES	xv
LIST OF ABBREVIATIONS	xvi
NOMENCLATURE	xvii
INTRODUCTION	1
2.0 REVIEW OF LITERATURE	8
2.1 Experimental Testing of Braided and Filled Structures	9
2.2 Experimental Testing of Aluminum Foam Filled Braided Stainless Steel Tubes.....	12
2.3 Summary of Literature Review	16
3.0 RESEARCH OBJECTIVES	17
4.0 PNEUMATIC GUN AND PROJECTILE	19
4.1 Introduction.....	19
4.2 Pneumatic Gun and Long Stroke Testing Machine	19
4.3 Structural Analysis of Transverse Fixtures	22
4.4 Finite Element Model Development and Boundary Conditions	22
4.5 Simulation Results	25
5.0 EXPERIMENTAL TESTING METHODS	28
5.1 Compressive Testing of Aluminum Foam Cores.....	29
5.2 Pneumatic Gun Calibration.....	32
5.3 Projectile Load Cell Calibration Process	33
5.4 Transverse Impact Testing of Empty Braided Tubes.....	39
5.5 Transverse Impact of Foam Filled Tubes	47

5.6 Quasi-Static Transverse Testing of Empty and Foam Filled Tube Specimens.....	50
5.7 Quasi-Static Testing of Foam Filled Braided Tubes.....	53
6.0 EXPERIMENTAL OBSERVATIONS AND DISCUSSION	55
6.1 Experimental Observations of Aluminum Foam Core Compressive Tests	55
6.2 Experimental Results From Transverse Impact Tests.....	56
6.2.1 Transverse Impact Response of Empty Braided tubes.....	56
6.2.2 Transverse Impact Response of Low Density Rectangular Foam Filled Tubes	60
6.2.3 Transverse Impact Response of Medium Density Rectangular Foam Filled Tubes.....	67
6.2.4 Transverse Impact Response of High Density Rectangular Foam Filled Tubes.....	74
6.3 FEA Energy Analysis	82
6.3.1 Transverse Assembly F.E.A Model	82
6.3.2 Simulation Results	85
7.0 QUASI-STATIC VERSUS DYNAMIC TEST RESULT COMPARISON.....	87
7.1 Quasi-Static versus Dynamic Transverse Tensile Response of Empty Braided Tubes	87
7.2 Quasi-static versus Dynamic Transverse Tensile Response of Low Density Foam Filled Tubes	91
7.3 Quasi-static versus Dynamic Transverse Tensile Response of Medium Density Foam Filled Tubes	95
7.4 Quasi-static versus Dynamic Transverse Tensile Response of High Density Foam Filled Tubes	97
8.0 VARIABILITY ANALYSIS OF DYNAMIC IMPACT TEST RESULTS.....	101
8.1 Transverse Impact Tests of Rectangular Foam Filled Tube Specimens	101
9.0 Potential Applications of Aluminum Foam Filled Braided Stainless Steel Tubes	105
10.0 CONCLUSIONS.....	106
10.1 Conclusions for Transverse Dynamic Impact Test Trials.....	106
RECOMMENDATIONS FOR FUTURE WORK	111
ACKNOWLEDGEMENTS	112
REFERENCES	113

APPENDIX A: QUASI-STATIC AND DYNAMIC TRANSVERSE TEST DATA COMPARISON	118
APPENDIX B: ENGINEERING STRESS/STRAIN RESPONSES OF ALUMINUM FOAM CORE SAMPLES.....	129
APPENDIX C: ENGINEERING PRINTS FOR PROJECTILE AND IMPACTING CAP.....	132
VITA AUCTORIS	135

LIST OF TABLES

Table 1: Circular Core Foam Compression Test Results.....	31
Table 2: Rectangular Foam Core Compression Test Results	31
Table 3: Computed Projectile Load Cell Sensitivities	37
Table 4: Mechanical properties of AISI 304 Stainless Steel	39
Table 5: Empty Tube Specimen Impact Test Results.....	40
Table 6: Foam filled tube specimen test results.....	47
Table 7: Quasi-static empty tube specimen results.....	53
Table 8: Quasi-static foam filled tube specimen results	54
Table 9: Mechanical properties for ASTM A36 steel.....	84
Table 10: FEA energy balance results	86

LIST OF FIGURES

Figure 1: Constrained nodal rigid bodies (CNRB) and constrained nodes on base of testing machine	24
Figure 2: Discrete spring elements representing stainless steel braided tube specimen	24
Figure 3: Displacement profile in (mm) of transverse fixture assembly under 70 kn applied load.....	25
Figure 4: Von Mises stress distribution in (Pa) within transverse fixture assembly under 70 kN applied load.....	25
Figure 5: Elevated von-mises stress levels within bolted connections of adapter plate (Pa).....	27
Figure 6: Pneumatic gun calibration test footage	32
Figure 7: Muzzle velocity vs. Tank pressure plot.....	33
Figure 8: Projectile load cell calibration process	36
Figure 9: Projectile load cell calibration curves (a) 203b sn 2592 (b) 203b sn 2596 from calibration test 2.....	38
Figure 10: Pneumatic gun and long stroke machine frame.....	41
Figure 11: Projectile and transverse assembly.....	42
Figure 12: Assembly process of high density rectangular core foam filled braided tube.	50
Figure 13: Force/displacement response for empty braided tube.	59
Figure 14: Photographs illustrating the transverse impact deformation process of empty stainless steel braided tube for specimen 1.....	60
Figure 15: Force/displacement response for group a low density foam filled braided tube.	61
Figure 16: Photographs illustrating the transverse impact deformation process of low density group a foam filled braided tube specimen 2.....	62
Figure 17: Force/displacement response for group b low density foam filled braided tubes.....	63
Figure 18: Photographs illustrating the transverse impact deformation process of low density group b foam filled braided tube specimen 2.....	64

Figure 19: Force/displacement response for group a medium density foam filled.	68
Figure 20: Photographs illustrating the transverse impact deformation process of medium density group a foam filled braided tube specimen 3.	69
Figure 21: Force/displacement response for group b medium density foam filled braided tube	70
Figure 22: Photographs illustrating the transverse impact deformation process of medium density group b foam filled braided tube specimen 2.	71
Figure 23: Force/displacement response for group a high density foam filled braided tube.	76
Figure 24: Photographs illustrating the transverse impact deformation process of high density group a foam filled braided tube specimen 1.	77
Figure 25: Force/displacement response for group b high density foam filled braided tube.	78
Figure 26: Photographs illustrating the transverse impact deformation process of high density group b foam filled braided tube specimen 1.	79
Figure 27: Fixture internal energy versus transverse displacement.	83
Figure 28: Quasi-static deformation process of empty braided tube	88
Figure 29: Quasi-static deformation process of low density foam filled braided tubes.	92
Figure 30: Quasi-static deformation process of high density foam filled braided tubes.	98
Figure 31: Minimum, maximum, mean, and median values of metrics computed from foam filled impact test trials (a) FE, (b) TEA, and (c) SEA	104

LIST OF APPENDICES

APPENDIX A:	QUASI-STATIC AND DYNAMIC TRANSVERSE TEST DATA COMPARISON.....	118
APPENDIX B:	ENGINEERING STRESS/STRAIN RESPONSES OF ALUMINUM FOAM CORE SAMPLES.....	129
APPENDIX C:	ENGINEERING PRINTS FOR PROJECTILE AND IMPACTING CAP.....	132

LIST OF ABBREVIATIONS

AISI	American iron and steel institute
ASTM	American Society for Testing and Materials
BIP	black iron pipe
CC	circular core
CFE	crush force efficiency
CNC	computer numeric controlled
CNRB	constrained nodal rigid body
FE	force efficiency
FEA	finite element analysis
FFTI	foam filled transverse impact
IED	improvised explosive devices
IHSA	Infrastructure Health and Safety Association
LVDT	linear voltage differential transducer
NFTI	no foam transverse impact
PPE	personal protective equipment
RC	rectangular core
SEA	specific energy absorption
TEA	total energy absorption
TTL	transistor-transistor logic

NOMENCLATURE

D_t	total displacement (mm)
$E_{(absorbed)}$	sum of energy absorbed by tube specimen and machine frame (kJ)
$E_{(elastic\ frame)}$	energy absorbed by long stroke machine frame (kJ)
$E_{(FE\ sim)}$	estimate of energy absorbed by long stroke machine frame (kJ)
$E_{(projectile)}$	projectile kinetic energy prior to impact (kJ)
F_{ave}	average force (kN)
FE	force efficiency (%)
F_{max}	maximum measured force (kN)
$F_{(measured)}$	reaction force measured by projectile load cells (kN)
m	projectile mass (kg)
SEA	specific energy absorption (kJ/kg)
TEA	energy absorbed by tube specimen (kJ)
TEA^*	energy absorbed by tube specimen computed from FEA (kJ)
v	incident projectile velocity (m/s)

INTRODUCTION

To an unsuspecting individual it may come as a surprise how drastically one's life can be changed as a result of unintentional injury. These injuries deliver not only a personal burden to the victim and their loved ones but also a widespread economic burden resulting from the costs associated with emergency care, chronic care, and rehabilitation. It is estimated by [1] that the cumulative annual cost as a result of injury is roughly 19.8 billion dollars within Canada alone. One particularly devastating form of injuries are those arising from impact. While one may conventionally think of impact injuries within the context of motor vehicle accidents or other extremes, a simple slip and fall can result in significant damage to the human body. Fall accidents are currently accountable for 76% of all head injuries of Canadians 65 years of age and older [2]. Injuries resulting from impact also affect younger demographics with "stuck by" and "struck against" accident types listed as the 2nd and 3rd most cited time loss accidents by young workers in 2008-2012 [3]. When examining strategies to prevent the occurrence of injuries engineering plays an important role, particularly the development of energy absorbing structures within the context of those arising from impact.

Within the workforce employees are instructed to wear personal protective equipment (PPE) to prevent injury. Personal protective equipment exists in many shapes and forms such as hard hats, protective eyewear, and steel toe boots. However even with the wide range of protective equipment currently available to workers, a significant number of accidents occur every year resulting in personal injury. Additionally, statistical data indicates a need for improvement for some particular forms of PPE. Between 2012 and 2013 a 13.2 % increase in the occurrence of fractures was noted within the membership

base of the IHSA [4] with an increase in lower level falls indicated as a primary contributor to the occurrence of fracture injuries. Injuries resulting from overexertion/strenuous movement and falls also accounted for nearly 49% of all injuries reported within [5]

Energy absorbing structures play an important role in the protection of military personnel and structures. From 2001-2014 the use of improvised explosive devices otherwise known as (IEDs) have lead to the deaths of 2349 United States troops [6]. These explosive devices are often triggered remotely or detonated underneath a vehicle as they are passed over. Those fortunate enough to survive a blast are often left with serious injuries to the lower extremities such as the ankles and feet which often lead to long term disability. It was noted within [7] out of a group of 63 U.K military personnel suffering from IED blast injuries to lower extremities occurring between January 2006 to December 2008 only 14% of the service members were fit to return to their pre-injury duties after completion of treatment.

Within the automotive and transportation sectors energy absorbing structures play a crucial role in protecting the lives of both drivers and pedestrians. The world health organization (WHO) estimates approximately 1.24 million people die each year in traffic related accidents with improper use of motorcycle helmets, speed, and improper use of seat belts and child restraints listed as key risk factors [8]. With the ever increasing demand for improved fuel economy to curb CO₂ emissions, the implementation of new materials into vehicle subsystems and safety devices will be important to maintain a suitable vehicle weight while maintaining occupant safety. The use of non ferrous alloys

such as magnesium has been suggested as a promising candidate to replace many conventional steel components [9-10].

Whether it is the crumple zones within an automobile, the road barriers on the side of a highway, or a fall arrest system worn by a construction worker energy absorbing structures play an important role in providing personal protection within our day to day lives. In the scope of many engineering applications, energy absorbing structures may include, but are not limited to, cellular materials, thin walled extrusions, and honeycomb members. Although these familiar structures have proven to be effective in providing the benefits of energy absorption many are only effective under a compressive mode of deformation or a particular mechanism of deformation such as progressive folding. The development of more versatile energy absorbing structures capable of withstanding non conventional modes of loading and deformation such as axial tensile or transverse deformation as well as torsion is necessary to provide the benefits of energy absorption to a more extensive demographic.

In the work of Wagner et al. [11] AM30 magnesium extruded beams were tested under both quasi-static and dynamic axial crushing as well as four point bending loading conditions. The experimental load/displacement results were then compared to those predicted by an FEA model constructed for simulation within LS-DYNA for each respective test. The beams utilized the double top hat geometrical configuration. For both the quasi-static and dynamic axial tests a large section of the flange was removed from each tube and a "bump" was created on the top and bottom tube surface to act as a crush trigger to produce a sequential collapse. Material cracking and separation were observed under all 3 distinct loading conditions. FEA results were observed to have a

tendency to over predict the energy absorbing capabilities of the specimens however experimental load/displacement data demonstrated a high degree of repeatability for all tests. In addition to crushing, axial cutting has been investigated as a means of energy absorption under both quasi-static and dynamic loads. In the work of Majumder et. al [12] AA6061-T4 and -T6 aluminum extrusions were subjected to quasi-static axial cutting using a custom 4 blade cutting tool. Tests were completed using a Tinius Olsen compression testing machine and test specimens machined to a wall thickness of 1.587 mm or 3.175 mm were investigated. It was observed that the cutting deformation mode was stable and repeatable for all specimens considered and a crush force efficiency (CFE) as high as 0.92 was achieved. Jin et. al [13] expanded upon the work of [12] through the completion of a parametric study on AA6061-T6 aluminum extrusions subjected to both quasi-static and dynamic axial cutting. Parameters examined during the study included extrusion diameter, wall thickness, number of cutting blades, and loading condition. Levels of absorbed energy for quasi-static and dynamic axial cutting modes ranged from 1.01 kJ to 3.44 kJ and 1.50 kJ to 2.18 kJ respectively. Additionally, the axial cutting force was noted to increase with the increase in cutting blade quantity and increased wall thickness. The deformation of empty and foam filled aluminum, brass, and titanium tubes subjected to lateral compressive loads was previously investigated by Hall et. al [14]. The addition of foam was noted to produce an increase in specific energy absorption (SEA) performance of the tube specimens and was most prominent within aluminum tube specimens.

One particular structure that shows potential to replace many conventional comparable metallic structures is aluminum foam filled braided stainless steel tubes. The

implementation of braids offers many advantages over traditional solid components such as their increased damage tolerance, containment properties, and reduction in crack propagation [15]. Braided components can often be manufactured using a high level of automation which presents several cost advantages to manufacturers and offer a high degree of design predictability. An additional advantage of the implementation of braids over traditional solid components is that the use of braids presents the ability to tailor the mechanical response of the component through the creation of composite structures. The mechanical response of structures incorporating braids can be changed drastically through the introduction of interior cores constructed from various materials such as metallic or polyurethane foams as well as epoxy impregnation of the surrounding braid material. The creation of composite structures through the implementation of braids allows for improved energy absorption by taking advantage of the unique deformation kinematics and damage mechanisms of braided structures under deformation such as matrix cracking, delamination, and core pulverization.

The primary objectives of this thesis are to examine the mechanical behavior, deformation mechanisms, and to assess the influence of loading rate on aluminum foam filled braided stainless steel tubes subjected to dynamically applied transverse impact loads. This study is an expansion of a number of experimental research studies completed by Powel et al. [16], Cheng et al. [17], and Audysho et al. [18-19]. Within these prior experimental studies, the mechanical response of aluminum foam filled braided stainless steel tubes has been investigated under both axial tensile and transverse quasi-statically applied loads. Currently no study exists which examines the energy absorbing capabilities of this promising structure under dynamic loading conditions.

During the course of this study, transverse impact tests were completed on empty and aluminum foam filled tube specimens using the frame of a custom fabricated long stroke tensile testing machine coupled to a newly fabricated pneumatic gun and projectile. Review of past literature and research has not yielded any indication of a standardized testing protocol for the particular material combination investigated within this study. As such, a methodology consistent with that followed within [18-19] was followed where the tube is loaded continuously from an undisturbed state to a maximum transverse displacement with the only exception being that tube specimens were loaded just prior to the point of complete material failure within this research study. Tube specimens were not loaded beyond the point of complete failure to ensure that the projectile would not completely exit the gun barrel during testing trials. The projectile utilized to load the specimens has a significant mass of 9.73 kg and achieves a muzzle velocity approaching approximately 30 m/s prior to impact with the test specimen. Although there are countermeasures present to decelerate the projectile in the event of an unexpected tube failure, it was decided not to load the tubes beyond the point of material failure in the interest of safety. The experimental findings collected from test trials were compared to the quasi-static experimental data collected by Audyso et al. [18-19] to assess the presence of any loading rate dependent phenomena occurring during the tube deformation process.

Transverse impact loading test trials of empty and aluminum foam filled braided stainless steel tubes have been completed using the frame of a custom fabricated long stroke testing machine coupled to a newly fabricated pneumatically operated gun and projectile. The findings from this thesis are novel as currently no quantitative assessment of the

mechanical performance of aluminum foam filled braided stainless steel tubes under dynamic loading conditions exists. The experimental findings from this thesis will allow for a more complete understanding of the performance of circular braided tubes coupled with an interior foam core as an energy absorbing composite structure.

2.0 REVIEW OF LITERATURE

For the purpose of this thesis, this literature review examines the experimental testing, parametric/theoretical analysis, and finite element simulations of composite structures incorporating braided materials as well as various interior cores. Composite structures of interest have been subjected to a variety of loading conditions including both quasi-static and dynamically applied loads in an effort to study the mechanical response, damage mechanisms and the influence of parameters such as braid architecture and core density on the energy absorbing capacity of the structure. Section 2.1 discusses a variety of experimental studies examining composite structures under dynamic loading conditions as well as FEA simulations of composite structure loading. Section 2.2 discusses past experimental efforts in specific regard to aluminum foam filled braided stainless steel tubes.

2.1 Experimental Testing of Braided and Filled Structures

There are a limited number of publications examining the experimental testing of aluminum foam filled braided stainless steel tubes. However, there have been numerous publications investigating the incorporation of braided materials within energy absorbing structures. Previously, Jenq and Mo [20] performed an experimental study examining the ballistic limit of two-step braided three-dimensional textile composites. The specimens examined within the study were constructed from unidirectional E-Glass fiber roving and infiltrated with an epoxy resin. Prior to the completion of the dynamic impact tests, quasi-static punch tests were performed using a universal testing machine to characterize the damage mechanisms of the structure during the deformation process. Impact tests involved firing a hemispherical tipped projectile towards the specimen utilizing a pneumatic gun. The ballistic limit of the textile composites was determined to be 74 m/s where it was noted that the prominent damage modes of the specimen were indentation, matrix failure, and fiber breakage. Similar damage development was noted in an experimental study completed by Gong et. al [21] examining the mechanical response of braided panels subjected to impact loading by means of a pendulum as well as a gas operated gun. Gning et. al [22] performed drop weight impact tests on $\pm 55^\circ$ filament wound glass/epoxy tubes. The specimens examined within the experimental study were constructed from 2400 Tex E-glass fibres wound around a 55 mm diameter steel mandrel and cured using an epoxy resin. Similar to the methodology followed by [20] quasi-static indentation tests were completed using a universal testing machine equipped with a 50 mm hemispheric indenter in an effort to reproduce any interaction effect between the projectile and tube specimen without an incident velocity. Impact energies ranged from 2

to 45 J. It was observed that low energy impacts resulted in delamination and debonding of braid layer surface interfaces while high energy impacts caused delaminations to propagate and resulted in intralaminar cracking. The influence of prior damage due to lateral impact on the progressive crush behavior of composite tubes was investigated by Karbhari et. al [23]. Crush tests were completed on a total of 14 different braid architectures, it was noted that the presence of damage had a pronounced effect on damage mechanisms within the crush zone under progressive deformation. Zhang et. al [24] completed quasi-static as well as transverse impact tests on four step 3-D rectangular braided composites using a drop-weight impact tester as well as a split Hopkinson pressure bar (SHPB) apparatus. The specimens investigated within the study were comprised of carbon fiber braid tows woven with a four-step 1 x 1 braid architecture and solidified using an epoxy resin by means of resin transfer molding (RTM). During drop-weight test trials, specimens were impacted at an incident velocity of 6 m/s while split Hopkinson pressure bar impact tests were completed at velocities of 13.6 m/s, 17.8 m/s and 22.8 m/s. Drop-weight impact test results demonstrated a sharp rise in the measured force upon impact up to a peak value of 2.5 kN followed by a gradual fluctuating decrease in the measured load with increasing displacement as a result of fiber breakage and matrix cracking. Load/displacement results collected from split Hopkinson pressure bar tests demonstrated greater peak force values at a smaller displacement than that observed during quasi-static tests.

The implementation of various interior core materials has been investigated within a number of studies. Borvik et al. 2003 [25] conducted an experimental study where it was noted that addition of a foam core drastically increased the energy absorbing capabilities

of metallic extrusions under bending loads compared to empty tubes. Bambach et. al [26] completed an experimental and analytical investigation on hollow and concrete filled steel (C350) square section beams subjected to low velocity high mass transverse impact. The test specimens were subjected to impact at the beam mid-span using a drop rig at an incident velocity of 6.2 m/s. Upon examination of the mechanical responses of both the hollow and concrete filled specimens, it was observed that the concrete filling led to a reduction in the transverse failure deflection due to the formation of tensile tears at the beam mid-span. Additionally, an elastic-plastic predictive model was developed and compared to the collected experimental data. Kavi et. al [27] completed an experimental study examining the mechanical response of thin walled circular aluminum tubes filled with either polystyrene or closed cell aluminum foam cores under axial compression. Experimental results demonstrated that regardless of foam type or density, foam filling shifted the deformation mode of tube specimens from diamond to concertina. The action of foam filling was noted to increase the energy absorbing capacity of the tube specimens when compared to empty samples. However, the implementation of foam did not produce a significant increase in specific energy absorption when compared to simply increasing tube wall thickness. The mechanical response of square composite crash boxes subjected to compressive axial impact loads was investigated by Zarei et. al [28]. The outer tube structure of the crash box was comprised of woven glass-fiber solidified within a polyamide matrix. Square tubes were filled with Alporas aluminum foam with a relative density of 0.0085. Experimental findings were similar to those observed by Kavi et al. [27] where the insertion of foam increased the energy absorbing capacity of the structure however, a reduction in specific energy absorption was noted.

Several finite element based research studies have been completed examining composite structures. Previously, Gu and Li [29] developed a simplified structural model to analyze the penetration of three dimensional braided composites by a conical projectile. The model was generated for simulation within LS-DYNA and based upon the fibre inclination model which modeled the braid architecture as a combination of cuboids. Predicted levels of absorbed kinetic energy were found to be in good agreement with previously gathered experimental data however, the model failed to accurately duplicate the damage morphology of the composite structure. Lipa and Kotelko [30] developed an FEA model examining the behavior of singular and multi-member tubular structures subjected to lateral impact. Results predicted by the finite element model were found to be in good agreement with previously collected experimental data however, it was suggested additional simulation trials examining larger impact velocities be completed. A parametric study was completed by Zeng et. al [31] which examined the influence of factors such as tube radius, tube thickness, and braid angle on the levels of energy absorbed by a composite tube struck axially by a rigid plate. The model utilized within the study was constructed for simulation within LS-DYNA and demonstrated good correlation between the alteration of geometric parameters and corresponding changes in the computed results.

2.2 Experimental Testing of Aluminum Foam Filled Braided Stainless Steel Tubes

Within the scope of this literature review, no previous publications examining the mechanical response and assessment of damage mechanisms of aluminum foam filled braided stainless steel tubes under dynamic loading conditions have been found. However, there have been a number of studies completed examining the mechanical

response of aluminum foam filled braided stainless steel tubes under quasi-statically applied axial and transverse loads. Altenhof et. al [16] conducted an experimental study examining the force/displacement and energy/displacement characteristics of aluminum foam filled braided stainless steel tubes subjected to quasi-statically applied axial tensile loads. Visual examination of test data revealed the primary mechanisms of energy absorption to be a combination of foam crushing resulting from the diametrical reduction of the exterior braided tube under elongation followed by the elastoplastic deformation of the braided tube. Due to limitations associated with the stroke length of the test apparatus it was required that test trials be completed in 3 individual stages which involved unloading and disturbing the specimen between stages. Due to the need to complete the tests in stages the force/displacement and energy/displacement results were juxtaposed in order to achieve a continuous data curve. Energy absorption levels ranged from approximately 5.2 to 7.9 kJ. Cheng et al. [17] expanded upon the work of Altenhof et al. [16] through the development of a theoretical model based upon the kinematic relationship between tube elongation and tube diameter. The theoretical model was based upon the concept of the unit cell which relates the instantaneous radius and length of the braided tube to the angle between crossing braid tows. Within the model, energy dissipation was assumed to be a superposition of crushing of the interior foam core prior to tow lockup followed by the elastoplastic deformation of the exterior braided tube after tow lockup. The unit cell model developed by Cheng et al. [17] is a semi-empirical model as experimental data collected from empty tube specimens is required for energy predictions within the second phase of energy absorption associated with the tensile loading and deformation of the exterior braided stainless steel tube. A comparison of

predicted levels of absorbed energy to measured experimental values demonstrated a strong degree of correlation with a maximum percentage error of 25%. No validation of the model prior to tow lockup was completed within the study. Audysho et. al [18-19] expanded upon the work of both Altenhof et al. [16] and Cheng et al. [17] through the completion of a series of experimental studies examining the mechanical response of aluminum foam filled braided stainless steel tubes under quasi-statically applied axial and transverse loads. A new custom fabricated long stroke testing machine was utilized in both the axial and transverse studies. Implementation of the long stroke testing machine allowed for tube specimens to be loaded from rest to the point of failure in a continuous fashion eliminating the need to complete test trials in stages. Both circular and rectangular foam core geometries of varying density were examined within each respective study. Results from axial tensile test trials indicated that braided tube specimens incorporating both high and low density circular cores demonstrate a significant degree of necking as a result of the decoupling of the individual pucks comprising the interior foam core during axial elongation. The formation and propagation of a neck was identified as the primary mechanism of failure for tube specimens incorporating circular foam cores with levels of absorbed energy ranging from 6.46 kJ to 8.34 kJ. Specimens incorporating low density rectangular foam cores demonstrated uniform crushing deformation along the length of the braided tube throughout the deformation process while tube specimens incorporating high density rectangular cores experienced localized necking. Absorbed energy ranged from 8.08 kJ to 10.81 kJ. In addition to the measured experimental data collected within the axial tensile test trials, visual data was collected using a high speed, high resolution camera for

the purpose of validating the unit cell model developed by Cheng et al. [17]. The validation process involved first measuring the instantaneous diameter of the braided tube prior to tow lockup using ProAnalyst [32] digital image tracking software. The measured tube diameter was then compared to that predicted by the theoretical unit cell model. Experimentally collected diameter measurements were found to be in good agreement with predictions of the unit cell model, tube specimens incorporating circular foam cores demonstrated an error of approximately 1.69% while specimens incorporating rectangular cores demonstrated an error of 3.03%.

Results from quasi-static transverse tensile test trials demonstrated that tube specimens incorporating low density circular foam cores experience uniform foam crushing throughout the length of the braided tube during the deformation process with failure initiating at either the right or left side clamp. Tube specimens incorporating high density circular foam cores experienced only a limited degree of foam crushing along the tube length with the exception of highly localized fracture and crushing at the tube mid-span which resulted in tube fracture. Levels of absorbed energy for low and high density circular cores ranged from 5.79 kJ to 7.03 kJ, respectively. Tube specimens incorporating both low and high density rectangular foam cores were observed to fail at the tube mid-span as a result of a combination of highly localized tow elongation and bending. Levels of absorbed energy for specimens containing low and high density rectangular foam cores ranged from 7.44 kJ to 9.13kJ, respectively.

2.3 Summary of Literature Review

The manuscripts presented within this literature review indicate a need for further examination of structures incorporating both foams and braids as energy absorbers. The large majority of studies examining braided structures pertain primarily to structures which utilize a braid in combination with resin impregnation to provide the structure with rigidity. Although the implementation of braids has assisted in improving the energy absorbing performance and damage tolerance of these structures, composite energy absorbers that utilize both braids and foams present a wide array of opportunities to specifically tailor the mechanical response of the structure for a desired application. At the moment the research pertaining to aluminum foam filled braided stainless steel tubes is novel and the structure has only been tested under a limited number of configurations namely, quasi-statically applied axial and transverse loads. As such, there is a need for additional studies on aluminum foam filled braided stainless steel tubes to provide a more extensive comparison to other energy absorbing structures.

3.0 RESEARCH OBJECTIVES

Before aluminum foam filled braided stainless steel tubes can be truly considered for implementation as a versatile composite energy absorbing structure it is important to first develop a comprehensive understanding of the mechanical response of the structure under a diverse variety of loading conditions. Currently, literature associated with the experimental testing of aluminum foam filled braided tubes is very limited and focuses primarily on testing tube specimens under quasi-statically applied loads. Although these preliminary findings are of great significance, many scenarios in which energy absorbing structures are implemented involve rapid loading rates such as a vehicle collision. Additional experimental testing of aluminum foam filled braided stainless steel tubes under dynamic loading conditions is required to both assess and understand the influence of loading rate and other inertial effects on this novel composite structure. To meet this requirement, a pneumatically operated gun and projectile have been integrated within the test apparatus utilized by Audysho et. al [18-19] to provide the capability of performing transverse dynamic impact tests. The experimental testing detailed within this thesis aims to achieve the following goals.

1. Test braided tube specimens coupled with aluminum foam cores of varying density under the previously unexplored transverse impact loading condition.
2. Collect a combination of visual and measured force data to achieve continuous force/displacement and energy/displacement data curves under the transverse impact loading condition.

3. Identify and assess the presence of any loading rate dependent phenomena within the mechanical response of the structure using both measured and visual high speed data.
4. Assess the influence of foam core density on the mechanical response of the structure.
5. Compare the experimental data collected within this study to quasi-static transverse test results collected by Audyshe [18-19] to assess any other factors influenced by the increased loading rate.

4.0 PNEUMATIC GUN AND PROJECTILE

This chapter provides an overview of the design considerations of the pneumatic gun and projectile as well as the finite element simulation completed on the long stroke testing machine frame.

4.1 Introduction

Preliminary research revealed the hydraulic ram of the long stroke testing machine utilized by Audysho et al. [18-19] could not be modified to deliver dynamic transverse tensile loads to braided tube specimens. It was determined that a new structure would need to be added to the machine to perform transverse dynamic impact tests. The capacity to perform dynamic impact tests was achieved through the design and implementation of the pneumatically operated gun and projectile. The implementation of the pneumatic gun and projectile permitted aluminum foam filled braided stainless steel tube specimens to be loaded from a resting state to the point of failure within a matter of milliseconds. The projectile utilized to impact tube specimens is equipped with two ICP load cells, a 500G (4905 m/s^2) accelerometer and a modular data acquisition system. In addition to the measurement instrumentation within the projectile, test trials were filmed using a high speed, high resolution camera which permitted the examination of the interaction between the interior foam core and external braid tow wires as well as the identification of failure and deformation mechanisms arising during the impact event.

4.2 Pneumatic Gun and Long Stroke Testing Machine

The pneumatic gun and projectile were designed as an extension of the existing long stroke testing machine constructed by Audysho et al. [18-19]. The pneumatic gun assembly consists of 3 primary components, which include the pneumatic gun, pneumatic

gun frame, and recoil mounts. The pneumatic gun was pressurized by a 10 gallon TSI Cheetah (CH10AL) air tank coupled to a 50.8 mm diameter, manually operated ball valve by a section of black iron pipe (BIP). The gun barrel is 2.44 m in length and constructed from 114.3 mm x 114.3 mm ASTM A500 square tubular steel with a wall thickness of 4.76 mm. The barrel and air storage tank of the pneumatic gun were supported by the pneumatic gun frame which is constructed from 114.3 mm x 114.3 mm ASTM A500 square structural steel tubing with a wall thickness of 4.76 mm. The length, width, and height of the pneumatic gun frame was 1.43 m x 0.91 m x 1.35 m, respectively, and was used to elevate and position the pneumatic gun such that the central longitudinal axis of the barrel was positioned perpendicular to the braided tube specimen when fully secured within the transverse fixtures of the long stroke testing machine. The base of the pneumatic gun frame was fitted with leveling mounts, which facilitated fine vertical height adjustments of the barrel mouth to ensure proper alignment of the projectile with the braided tube specimen. To prevent the pneumatic gun and frame from being displaced backwards as a result of reaction forces arising from accelerating the projectile, a set of recoil mounts were utilized to secure the gun frame to that of the long stroke testing machine which was bolted securely to the floor. The recoil mounts were constructed from a combination of AISI 304 angle iron and flat bar each possessing a thickness of 6.35 mm. The mounts were slotted to allow for fastening to the long stroke testing machine frame as well as to permit horizontal adjustment of the distance between the edge of the barrel mouth and exterior surface of the braided tube specimen. The recoil mounts possessed a length, width, and height of 311.15 mm x 97.6 mm x 304.8 mm, respectively, and were fastened to the legs of the pneumatic gun frame. A

protective curtain with a width and height of 304.8 mm x 304.8 mm was constructed from 8 layers of ballistic nylon and chained to the long stroke testing machine frame behind the test specimen to safely decelerate the projectile in the event that a tube specimen were to experience an unexpected catastrophic failure. Finally, a wooden support frame was implemented for the purpose of mounting a high-speed camera to record the test trials. The frame positioned the camera directly above the test specimen and was constructed such that it did not physically contact the long stroke testing machine frame in an effort to minimize the transmission of vibrations arising from the impact event to the camera.

4.3 Structural Analysis of Transverse Fixtures

Prior to the completion of experimental impact test trials a three dimensional FE simulation was completed within LS-DYNA™ version 971s R4.2 software. The objective of the simulation was to ensure that the fixture assembly of the long stroke testing machine utilized secure braided tube specimens could withstand the anticipated transverse loads arising during impact test trials.

4.4 Finite Element Model Development and Boundary Conditions

The transverse testing machine frame model geometry utilized in this analysis was previously developed by Audysho et al. [18-19]. The model was originally generated using Catia v5 R20 drafting software which was utilized to generate IGES files for the purpose of meshing. Discretization of the structure was completed within Hypermesh V11 software. An element size of 10 mm x 10 mm was selected for regions where no discontinuities in the structure were present and an element size of 9 mm x 5 mm was selected where circular hole discontinuities existed. The meshed model consisted of 248,405 nodes, 173,260 shell elements, and 52,960 solid elements. All shell elements utilized a fully integrated element formulation (ELFORM 16 within LS-DYNA™) in an effort to minimize computing time. All solid elements utilized the default constant stress element formulation (ELFORM 1 within LS_DYNA™) which uses a Hughes-Liu formulation with cross section integration. Bolted connections present within the model were represented as constrained nodal rigid bodies (CNRB). The CNRB connects the mesh areas of adjacent components and acts as a rigid bolted connection as a result of the translational and rotational constrained imposed on the selected nodes. Bolted connections between the long stroke testing machine frame and floor were represented

through the implementation of boundary constraints on the nodes of the base of the machine which inhibited all translational and rotational motion. All components of the transverse testing machine frame were modeled using an elastic material model (*MAT_ELASTIC within LS-DYNA™) which assumes isotropic material behavior. Representation of the braided tube specimen was accomplished through the insertion of 2 discrete elements with a material model specific for discrete spring elements (*MAT_SPRING_ELASTIC within LS-DYNA™) positioned between the annular clamps of the transverse mounting assembly. The ends of the discrete elements were secured to the annular clamps which were secured to the transverse fixture assemblies using CNRBs. Deformation of the braided tube specimen was accomplished through a prescribed nodal displacement (*BOUNDARY_PRESCRIBED_MOTION) of the centre node joining the 2 discrete elements 280 mm in the positive x-direction. Displacement of the centre node generated a transverse force of 70 kN which was distributed between the transverse assembly arms. The applied transverse load was selected from quasi-static test data on high density foam filled aluminum tube specimens completed by Audysho [18-19]. The 70 kN load was the highest failure load observed within test trials. A contact algorithm (*CONTACT_AUTOMATIC_SURFACE_TO_SURFACE) was implemented to account for the contact interaction between the machine frame columns and transverse fixture arms in addition to the transverse fixture arms and annular clamps. A static and dynamic friction coefficient of 0.25 was implemented. The imposed constraints as well as the spring elements simulating the braided tube specimen are depicted within Figures 1 and 2. An explicit time integration scheme was implemented to simulate the dynamic

impact of tube specimens with the impact event occurring over a time period of 20 ms.

No mass or time scaling was implemented.

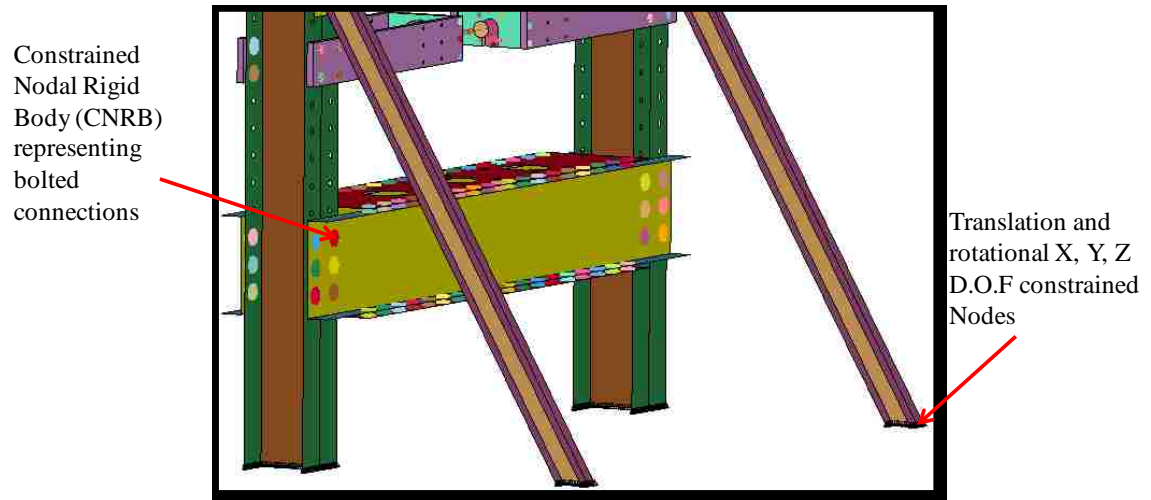


Figure 1: Constrained Nodal Rigid Bodies (CNRB) and constrained nodes on base of testing machine

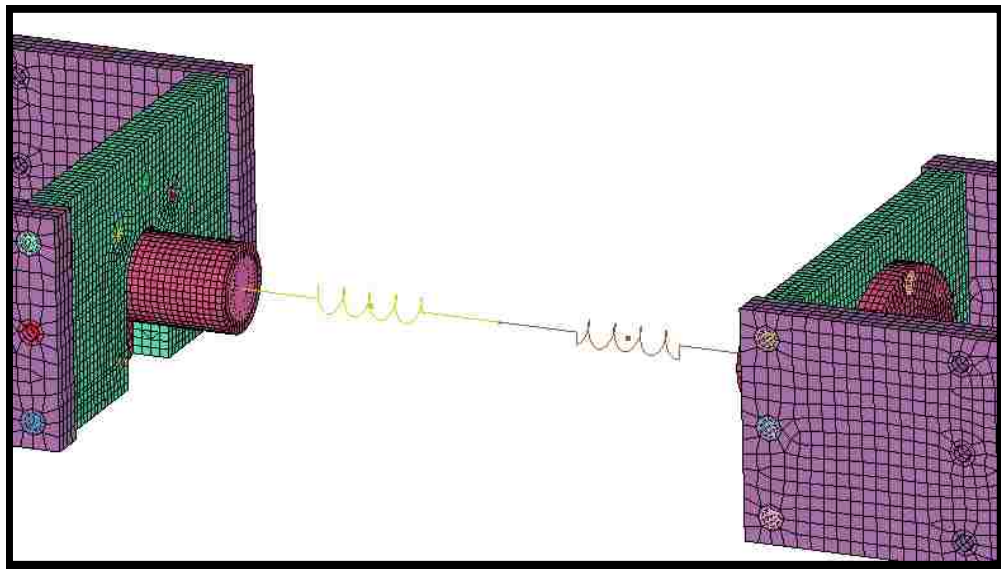


Figure 2: Discrete spring elements representing stainless steel braided tube specimen

4.5 Simulation Results

The resultant displacement profile as well as the von Mises stress distribution within the transverse fixture assembly when subjected to the applied 70 kN transverse load are depicted in Figures 3 and 4.

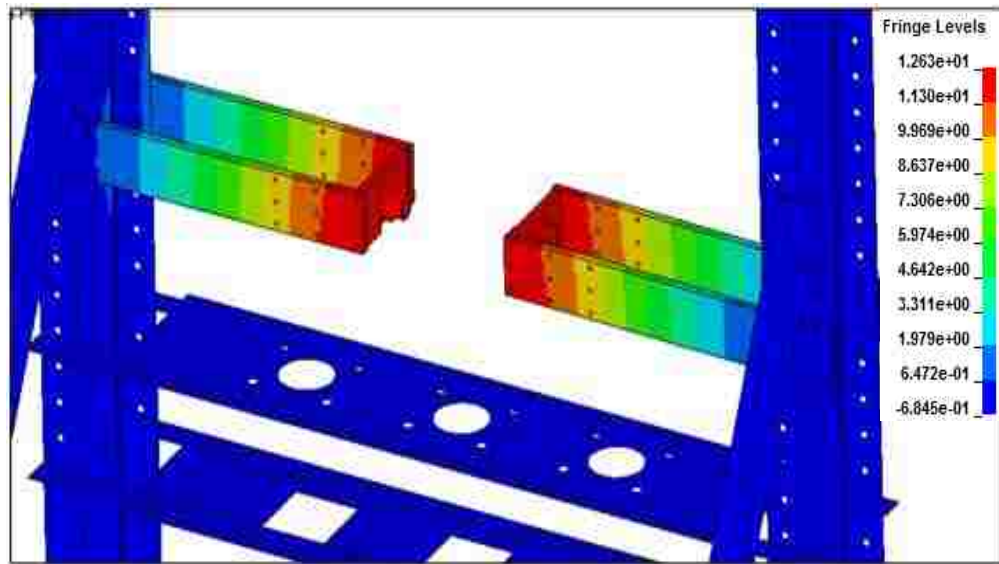


Figure 3: Displacement profile in (mm) of transverse fixture assembly under 70 kN applied load

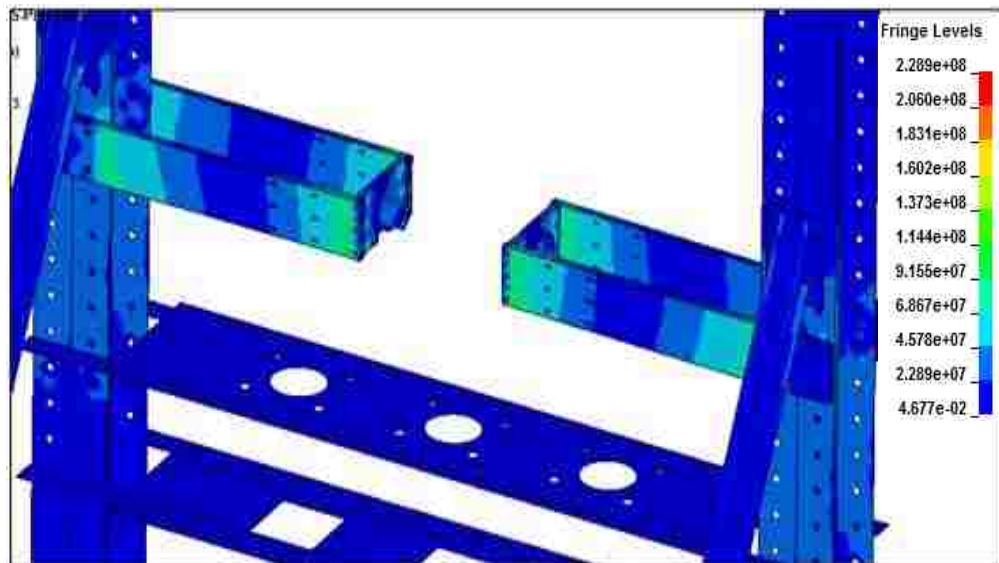


Figure 4: von Mises stress distribution in (Pa) within transverse fixture assembly under 70 kN applied load

From Figure 3 it can be observed that the transverse fixture assembly of the long stroke testing machine experienced a maximum deflection of roughly 12.6 mm measured from the end of the annular clamp as a result of the transverse impact load. Examination of the stress distribution within the transverse mounting assembly revealed a concentrated stress of roughly 228 MPa arising within the bolted connections between the side plates and adapter plate of the transverse fixture assembly as depicted in Figure 4. The elevated stress levels observed within the bolted connection are a result of the reaction bending moment generated through the elongation of the discrete elements between the annular clamps. Additionally, the presence of stress concentrations within the bolted connections is believed to be attributed to the rigid nature of the CNRB connection. In real applications, a minor reduction in stress levels is anticipated due to the small amount of translation permitted by a bolted connection. Examination of the stress levels distributed throughout the long stroke testing machine frame revealed slightly elevated stress levels of approximately 117 MPa in the vicinity of the side plates and adapter plate of the transverse fixture assembly and 141.2 MPa in the vicinity of the side plates and transverse testing machine vertical columns. Although the levels of elevated stress were noted to approach the 248 MPa yield stress of A36 structural steel within the bolted connection between the side plate and adapter plate they did not exceed the yield stress of the material. Due to the fact that the applied 70 kN transverse load was selected from quasi-static test trials completed on high density aluminum foam filled braided stainless steel tubes in which the largest failure loads were observed, it was deemed that the transverse fixture assembly would be suitable for application within transverse impact test trials on empty and foam filled braided tube specimens. However, the displacement

of the transverse assembly resulting from the impact loads arising during test trials would need to be accounted for when measuring the transverse displacement of braided tube specimens.

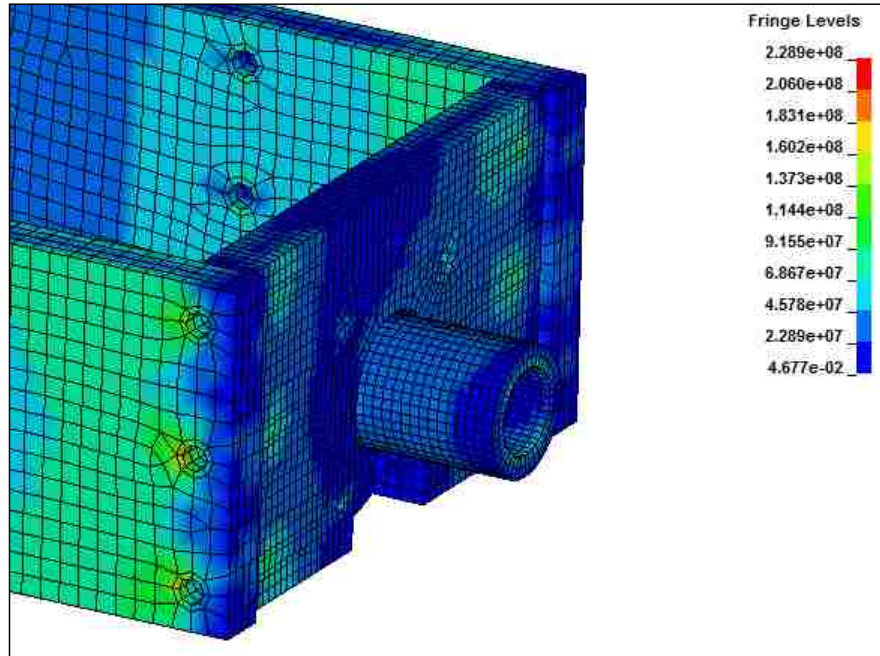


Figure 5: Elevated von-Mises stress levels within bolted connections of adapter plate (Pa)

5.0 EXPERIMENTAL TESTING METHODS

The experimental testing methods implemented during dynamic impact and quasi-static test trials are discussed within this chapter. The collection of transverse dynamic impact test data from empty and aluminum foam filled braided tube specimens required a number of steps. These steps include, mechanical characterization of the interior foam cores, calibration of the projectile load cells, and completion of the dynamic impact testing process. Details associated with the compressive testing of aluminum foam core samples completed within [18] are discussed in Section 5.1. Section 5.2 discusses the details associated with the calibration of the pneumatic gun. Section 5.3 discusses the calibration procedure of the projectile. The transverse impact testing procedure of empty and foam filled tubes is discussed within Sections 5.4 and 5.5. Finally, details of the quasi-static transverse tensile testing of tube specimens are discussed within Sections 5.6 and 5.7.

5.1 Compressive Testing of Aluminum Foam Cores

The aluminum foam cores utilized within this experimental study were constructed from stabilized aluminum foam sheets manufactured by the Cymat Aluminum Corporation (Canada) [33]. The closed cell aluminum foam boards were manufactured using a unique process known as melt gas injection. References [34] and [35] provide a comprehensive overview of the details associated with the melt gas injection process. Cymat [33] indicates that the aluminum foam exhibits typical density, average cell size and cell wall thickness ranging from 0.069 g/cm^3 to 0.54 g/cm^3 , 3 mm to 25 mm, and $50 \text{ }\mu\text{m}$ to $85 \text{ }\mu\text{m}$, respectively.

Compressive testing was completed on rectangular and circular aluminum foam core specimens using a Tinius Olsen compression testing machine. Three individual foam specimens of each respective density were tested to assess the engineering stress/strain response of the interior foam cores. The testing machine was equipped with a linear voltage differential transformer (LVDT) with a functional operating range of 150 mm, which was utilized to monitor the deformation of the foam specimens during compressive loading. Forces arising during the testing process were measured through the implementation of a PCB strain gauge based load cell within the testing machine with an appropriate measurement range for each respective specimen (PCB model numbers 1204-03A (220 kN), 1204-02A (90 kN), or 1203-03A (9 kN) as required). Signals from the load cell and LVDT were measured using National Instruments 9237 and 9215 modules mounted within an NI CompactDAQ chassis. Force and displacement measurements were acquired at a rate of 2 kHz. During each test, foam specimens were oriented such that the translational direction of the testing machine crosshead was parallel to the height

of the test specimen. Each test was completed at a crosshead speed of 1.04 mm/s at room temperature. Five measurements (length, width and height) for rectangular and (height and diameter) for circular specimens were taken prior to each test. An average value was computed for each critical dimension and later utilized to compute the density of each respective specimen. The identification system utilized for rectangular specimens follows the convention $\gamma\rho$ -RC, where γ is either 'H' or 'L' indicating a high or low foam density (ρ), and RC indicates a rectangular core test specimen. The identification system utilized for circular cores follows the convention $\alpha\phi$ - $\beta\rho$ -CC, where α is either 'H' or 'L' indicating whether the specimen is high or low diameter (ϕ), β is either 'H' or 'L' indicating whether the specimen is high or low density (ρ) and CC identifies the specimen as circular core.

Table 1: Circular Core Foam Compression Test Results

Specimen ID	Test #	Density (kg/m ³)	Specimen Geometry(mm)		Load Cell Range (kN)	Elastic Modulus (MPa)	Plateau Stress (MPa)	Densification Strain (%)
			Diameter	Height				
H ϕ -H ρ -CC	1	488.80	84.18	26.18	90	151.29	3.98	33.3
	2	489.98	84.07	26.12	90	139.77	4.01	37.2
	3	474.29	84.29	26.21	90	120.53	3.99	34.1
H ϕ -L ρ -CC	1	315.09	83.24	25.11	90	43.83	0.73	38.6
	2	317.71	83.44	25.11	90	27.50	0.47	40.1
	3	293.86	83.39	25.45	90	39.61	0.50	39.2
L ϕ -H ρ -CC	1	439.47	79.69	26.58	220	158.61	3.15	38.9
	2	451.60	79.49	26.04	90	92.79	2.96	40.4
	3	439.18	79.41	25.91	90	97.60	2.80	39.2
L ϕ -L ρ -CC	1	331.51	79.09	25.05	90	29.48	0.58	35.1
	2	330.46	78.51	25.36	90	14.75	0.41	44.4
	3	348.31	78.46	25.19	90	8.60	0.32	25.2

Table 2: Rectangular Foam Core Compression Test Results

Specimen ID	Test #	Density (kg/m ³)	Specimen Geometry(mm)		Load Cell Range (kN)	Elastic Modulus (MPa)	Plateau Stress (MPa)	Densification Strain (%)
			Width	Height				
H ρ -RC	1	489.68	37.936	24.53	90	201.54	3.80	28.1
	2	477.55	37.256	24.52	90	182.32	3.30	29.7
	3	453.25	36.814	24.71	90	139.81	3.10	30.1
L ρ -RC	1	162.38	64.004	24.21	90	11.18	0.36	43.3
	2	169.42	62.736	24.24	90	16.55	0.40	42.9
	3	163.17	63.738	24.58	90	7.44	0.36	41.2

5.2 Pneumatic Gun Calibration

Prior to the completion of impact test trials, a brief calibration study was completed on the pneumatic gun to correlate the firing pressure with the muzzle velocity. The study involved firing the pneumatic gun over a range of known air pressures and recording the projectile exiting the muzzle using a Photron SA4 high speed camera. All photographic image data recorded during the calibration study was recorded at a rate of 3600 fps at a resolution of 1024 x 1024 pixels².

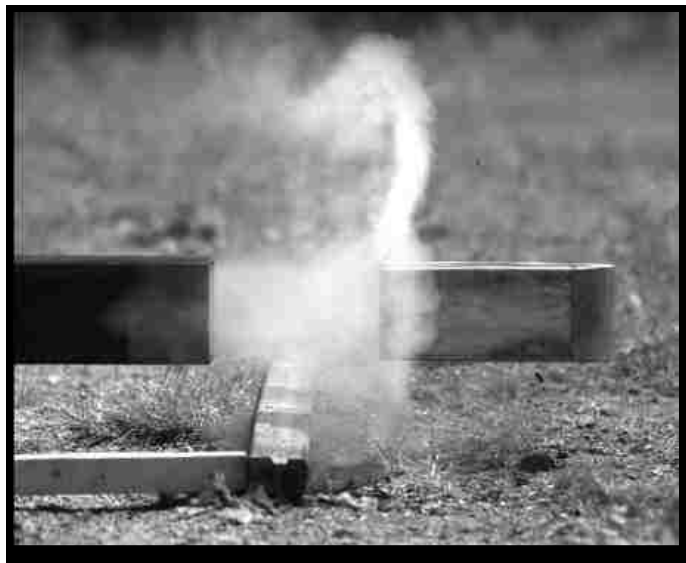


Figure 6: Pneumatic Gun Calibration Test Footage

After collecting the visual data, the test footage was uploaded within ProAnalyst [32] image tracking software and the muzzle velocity was determined for each corresponding air pressure. The computed muzzle velocities and corresponding air pressures were then plotted within Mathcad [36] engineering software and a linear regression curve fit was implemented. It can be observed within Figure 7 that the pneumatic gun was able to produce muzzle velocities with a good degree of repeatability. It should be noted that factors such as frictional forces within the barrel and pressure losses were not accounted

for within the calibration study. The resulting data curve was utilized in test trial preparation to determine the tank pressure required for the desired impact energy.

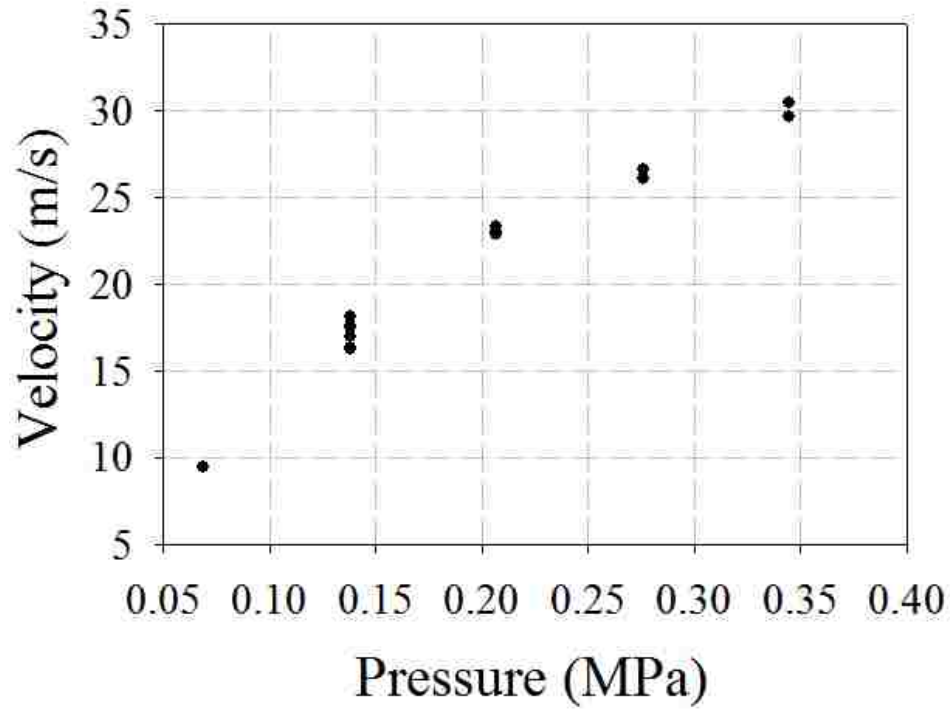


Figure 7: Muzzle velocity vs. tank pressure plot

5.3 Projectile Load Cell Calibration Process

The PCB 203B load cells utilized in this experimental study were originally intended to be mounted in a specific configuration, which utilized a beryllium copper stud supplied by the manufacturer. Use of different mounting hardware was noted to provide errors in sensitivity of up to 50% if the cell was not recalibrated prior to the implementation of alternative fasteners [37]. For the purpose of this study, the load cells were mounted in a non-typical configuration positioned between the flat surfaces of the main body and impacting cap and fastened using 12.7 mm socket head cap screws. To remedy this issue, both PCB 203B load cells incorporated within the projectile were recalibrated in house prior to the completion of impact test trials.

Several steps were taken when performing the in house calibration process to ensure that a linear calibration curve was produced, comparable to that provided by the manufacturer. First, a set of high precision 304 stainless steel washers possessing an outer diameter of 52 mm, inner diameter of 13.1 mm and thickness of 3.175 mm were machined using a manual lathe operated by a skilled technician. The high-precision washers were positioned between the main body of the projectile and the bottom surface of each 203B load cell to ensure that the load cells were resting on flat surface. A secondary set of washers that were provided and recommended by the manufacturer designated as anti-friction washers [37] were placed between the lower face of the impacting cap and upper face of the load cell. After positioning the washers, the load cells were wired with their respective 10-32 coaxial cables. Due to the very rapid signal decay time of the PCB 203B load cells, a PCB 484B signal conditioner was implemented to provide a longer system discharge time and a slower signal decay of the voltage measured throughout the calibration process. Analog voltage output from the load cells was measured using a NI 9237 module and recorded using a laptop computer installed with custom programmed LabVIEW software. A small amount of thread locking compound with the trade name Loctite (blue) was applied on all 10-32 threads as well as all bolted connections to ensure that all fasteners remained secure after repeated test trials. The impacting cap was placed on top of the load cells and loosely fastened using 12.7 mm socket head cap screws. The screws utilized to secure the impacting cap were tightened using a beam style torque wrench in increments of 13.55 N·m until the manufacturer-designated preload of 17.79 kN was achieved. The preload placed upon each load cell was verified by ensuring both cells were supplying a measured potential of

1 V after fastening the screws of the impacting cap. The assembled projectile was then positioned within a Tinius Olsen compression testing machine such that the longitudinal centre axis of the projectile was oriented parallel to the translating direction of the machine crosshead and positioned centered within the machine platen. Compressive forces delivered by the compression testing machine were measured using a PCB 1204-02A 90 kN strain gauge based load cell positioned beneath the projectile. A steel plate was inserted between the load cell and base of the projectile body to ensure it was resting on a flat, level surface. Analog voltage from the 90 kN load cell was measured using a NI 9237 module at a sampling rate of 2 kHz. An additional rectangular aluminum plate possessing a 52.39 mm radius, semi circular cut-out was positioned between the machine crosshead and impacting cap to ensure forces would be distributed evenly across each load cell during the compressive loading process. The configuration of the projectile within the Tinius Olsen machine is depicted in Figure 8.



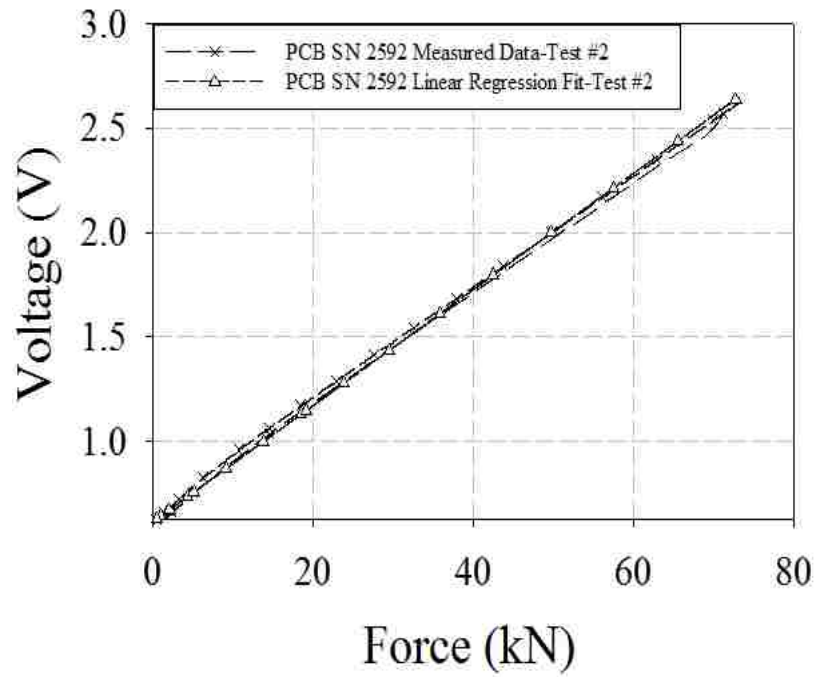
Figure 8: Projectile Load Cell Calibration Process

Calibration test trials involved axially loading the projectile until a compressive force of approximately 80 kN was achieved to ensure each cell was loaded through a sufficient extent of the functional measurement range. After achieving the desired 80 kN compressive load, the projectile was then gradually unloaded until it returned to a resting state. A crosshead speed of approximately 1.3 mm/s was utilized during both the loading and unloading phases. In an effort to ensure consistency within the successive computed load cell sensitivity values, 5 test trials were completed for each load cell. Data from compressive test trials was later imported into Mathcad engineering software [36]. Voltage measurement data collected from the 203B load cells was plotted against force measurement data from the PCB 1204-02A, the slope of the resulting curve was then computed using a linear regression curve fit. The Pearson's correlation coefficient was

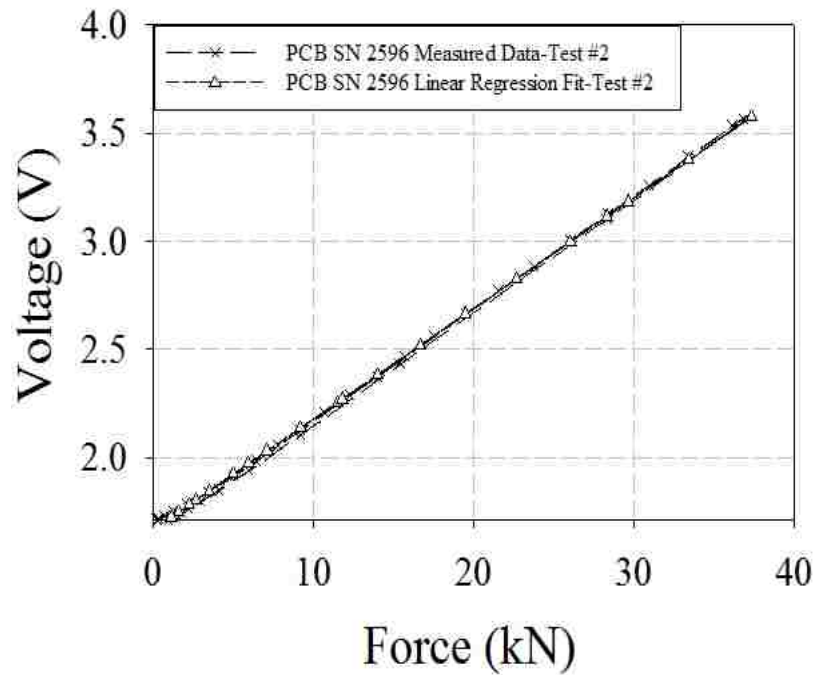
computed to ensure a strong degree of correlation between the approximated curve and raw experimental data existed. Finally, the average sensitivity values were computed and input into the SLICEWare software. The results collected from the calibration test trials as well as a sample calibration, from calibration test 2, representative of all findings from the process described above are presented in Table 3 and Figure 9(a) and (b).

Table 3: Computed Projectile Load Cell Sensitivities

Test #	Load Cell SN	Sensitivity (mV/kN)	Pearson's Coefficient (r²)
1	2592	55.824	0.998
2	2592	55.634	0.999
3	2592	55.444	0.999
4	2592	55.742	0.999
5	2592	55.928	0.999
1	2596	50.896	0.999
2	2596	51.036	0.999
3	2596	50.919	0.999
4	2596	50.922	0.999
5	2596	50.974	0.999



(a)



(b)

Figure 9: Projectile load cell calibration curves (a) 203B SN 2592 (b) 203B SN 2596 from calibration test 2.

5.4 Transverse Impact Testing of Empty Braided Tubes

Braided tube specimens utilized within this experimental study were constructed from American Iron and Steel Institute (AISI) 304 stainless steel wires with a standard "2 over 2 under" braid weave configuration. Cylindrical braids were created by weaving 48 braid tows around the circumference of the tube. Braid tows consisted of 8 individual wire strands each possessing a nominal diameter of 0.51 mm. The nominal external diameters of the braided tubes were 64.5 mm. Prior to testing, the tube diameter was physically measured to ensure that it met with manufacturer specifications. The mechanical properties of AISI 304 stainless steel are listed in Table 4.

Table 4: Mechanical properties of AISI 304 Stainless Steel

Young's Modulus (GPa)	Yield Strength (MPa)	Tensile Strength (MPa)	Elongation (%)	Density (kg/m ³)
193	241	586	55	8027

Transverse impact tests were completed using the frame of a custom long stroke testing machine equipped with transverse mounting fixtures as well as a custom fabricated pneumatically operated gun and projectile. Each side of the long stroke testing machine utilized an identical transverse fixture assembly to secure the braided tube specimens that consisted of two side plates and one adapter plate. The side plates are 1.143 m in length, 165.1 mm in height and 25.4 mm thick, and were fastened to the vertical pillars of the long stroke testing machine. The adapter plate fastened to each side plate and has a width, height, and thickness of 269.7 mm x 165.1 mm x 25.4 mm respectively. Additionally, a semi-circular cutout with a radius of 33.02 mm exists in the adapter plate

to permit coupling and fastening of an annular clamp utilized to secure the braided tube specimens within the transverse fixtures.

The pneumatic gun assembly consists of 3 primary components, which include the pneumatic gun, pneumatic gun frame, and recoil mounts. The pneumatic gun was pressurized by a 10 gallon TSI Cheetah (CH10AL) air tank coupled to a 50.8 mm diameter, manually operated ball valve by a section of black iron pipe (BIP). The gun barrel is 2.44 m in length and constructed from 114.3 mm x 114.3 mm ASTM A500 square tubular steel with a wall thickness of 4.763 mm. The barrel and air storage tank of the pneumatic gun were supported by the pneumatic gun frame which is constructed from 114.3 mm x 114.3 mm ASTM A500 square structural steel tubing with a wall thickness of 4.76 mm. The length, width, and height of the pneumatic gun frame was 1.43 m x 0.91 m x 1.35 m, respectively, and was used to elevate and position the pneumatic gun such that the centre longitudinal axis of the barrel was positioned perpendicular to the braided tube specimen when fully secured within the transverse fixtures of the long stroke testing machine. The base of the pneumatic gun frame was fitted with leveling mounts, which facilitated fine vertical height adjustments of the barrel mouth to ensure proper alignment of the projectile with the braided tube specimen. To prevent the pneumatic gun and frame from being displaced backwards as a result of reaction forces arising from accelerating the projectile, a set of recoil mounts were utilized to secure the gun frame to that of the long stroke testing machine which was bolted securely to the floor. The recoil mounts were constructed from a combination of AISI 304 angle iron and flat bar each possessing a thickness of 6.35 mm. The mounts were slotted to allow for fastening to the long stroke testing machine frame as well as to permit horizontal

adjustment of the distance between the edge of the barrel mouth and exterior surface of the braided tube specimen. The recoil mounts possessed a length, width, and height of 311.15 mm x 97.6 mm x 304.8 mm respectively, and were fastened to the legs of the pneumatic gun frame. A protective curtain with a width and height of 304.8 mm x 304.8 mm was constructed from 8 layers of ballistic nylon and chained to the long stroke testing machine frame behind the test specimen to safely decelerate the projectile in the event that a tube specimen were to experience an unexpected catastrophic failure. Finally, a wooden support frame was implemented for the purpose of mounting a high speed camera to record the test trials. The frame positioned the camera directly above the test specimen and was constructed such that it did not physically contact the long stroke testing machine frame in an effort to minimize the transmission of vibrations arising from the impact event to the camera.

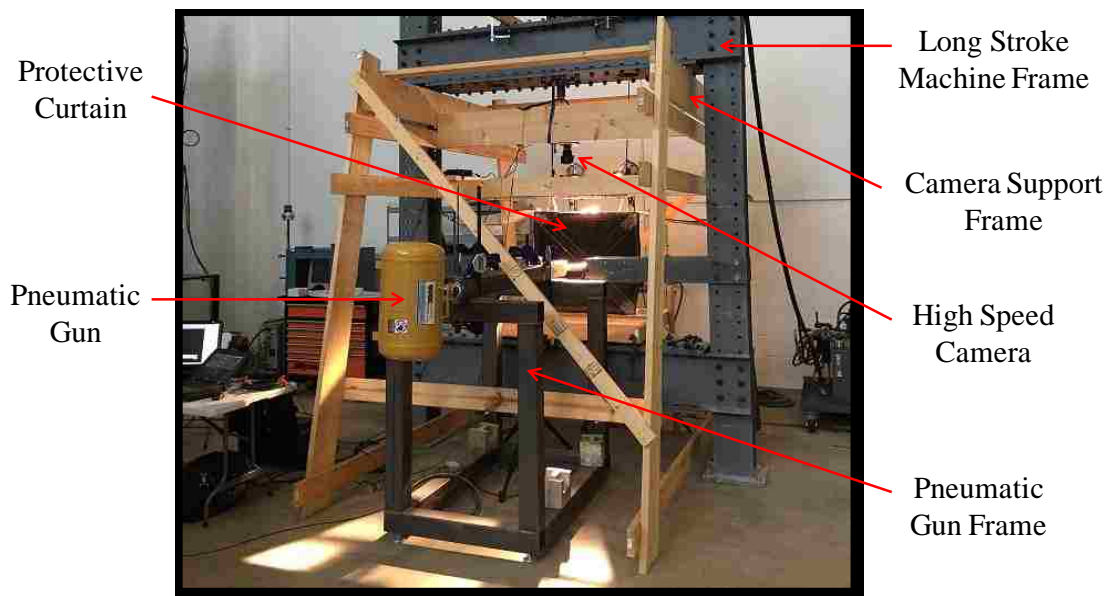


Figure 10: Pneumatic Gun and Long Stroke Machine Frame

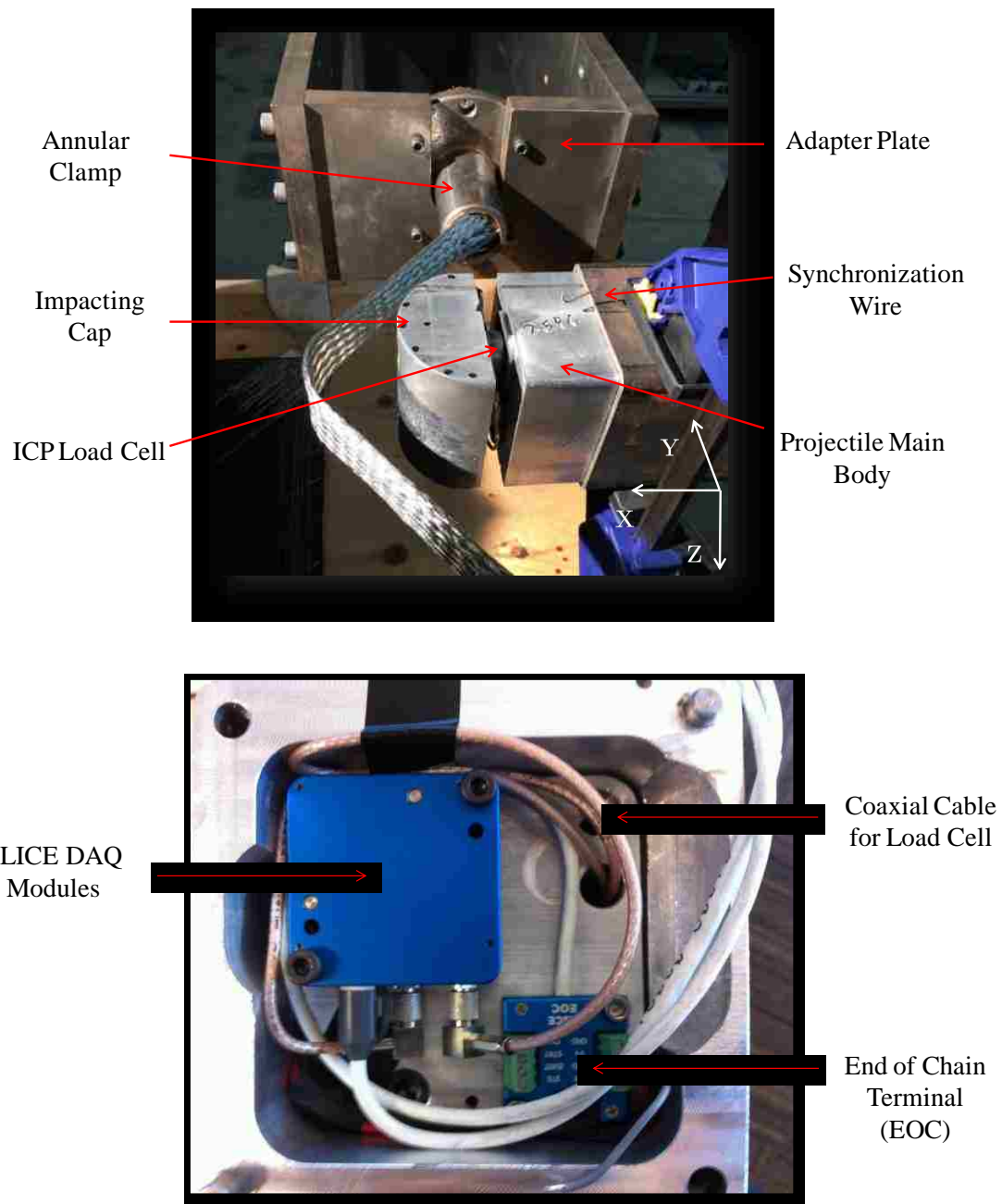


Figure 11: Projectile and Transverse Assembly

The projectile used to impact the test specimens was machined from square and round sections of 6061-T6 aluminum bar stock. The projectile was constructed as two individual components designated as the main body and impacting cap as illustrated in Figure 11. The main body possesses a length, width, and height of 304.8 mm x

104.78 mm x 104.78 mm and the impacting cap has a length, width, and radius of 104.78 mm x 104.78 mm x 52.39 mm respectively. When fully assembled and instrumented, the projectile possesses a total mass of 9.73 kg. Transverse loads arising during the impact event were measured using 2 PCB 203B ICP load cells integrated within the projectile positioned between the impacting cap and main body. A compartment was machined in the rear end of the main body by a computer numeric controlled (CNC) milling machine to mount a PCB 352C03 IEPE accelerometer as well as DTS SLICE Base and IEPE modular DAQ modules as depicted in Figure 11. Force and acceleration data were acquired at a sampling rate of 20 kHz for each test. The main body and impacting cap were machined such that a very tight fit existed between the exterior surface of the projectile and the interior barrel wall of the pneumatic gun. The close fitment of the projectile within the barrel allowed for the gun to be fired without the use of a sabot to prevent a significant loss of air pressure.

Preparation of the pneumatic gun and test specimen for a given test trial involved a number of steps. First, preparation of the tube specimen required measuring approximately 300 mm of manually compressed stainless steel braided tubing and cutting the tube using conventional aviation shears. The mass of braided tube utilized for each test was approximately 500 grams. The SLICE DAQ unit within the projectile was then armed and subsequently triggered using a laptop computer installed with SLICEWare data acquisition software to commence the collection of force and acceleration data. Following the output of the trigger signal, the laptop computer was disconnected from the projectile and the rear cap of the main body was closed and secured. The projectile was then manually loaded into the barrel of the pneumatic gun and the tube specimen was

mounted within the transverse fixtures of the long stroke machine frame. Mounting of the braided tube specimen consisted of first inserting one end of the braided tube through one of the annular clamps and securing it using a taper lock conical wedge with an applied clamping preload of roughly 10 kN. The remaining free end of the braided tube specimen was then fed through the opposing side annular clamp and secured by an identical taper lock conical wedge using the same preload. After securing the braided tube specimen, a small rounded piece of stainless steel wire was positioned and clamped to the barrel in front of the barrel mouth as depicted in Figure 11. The purpose of the wire was to create a small "blip" in the measured force/time history as it was bent by the passing of the projectile upon firing of the pneumatic gun. The small momentary rise in the measured force/time response prior to impact was utilized during the post-processing of test data to ensure the time histories of the collected force and visual data sets were properly synchronized. Finally, the laser beam of an Acuity AR700-12 laser displacement sensor with an operating range of 300 mm was positioned to shine through a small hole in the bottom of the pneumatic gun barrel. Analog voltage output from the laser displacement sensor was measured using a NI 9215 4 channel 16-bit analog input DAQ module mounted within an NI 9274 chassis and connected to a secondary laptop computer installed with custom LabVIEW software. The interference in the beam created by the passing of the projectile resulted in a drop in the measured voltage output of the laser displacement sensor which was registered by the LabVIEW software. The drop in voltage initiated the output of a secondary trigger signal which was delivered to the Photron SA4 high speed camera positioned above the tube specimen and initiated the collection of visual image data. The camera trigger signal was delivered using a NI 9401

TTL module. In addition to identifying the deformation and failure mechanisms of the braided tube specimen, the visual data collected during test trials was utilized within the post-processing of data to determine the displacement/time history of the projectile as well as the flexion of the transverse fixtures for each respective test through the process of digital image tracking. The displacement/time histories of both the projectile and transverse mounting fixtures were utilized to compute the displacement of the braided tube specimen relative to the transverse mounting arms thus accommodating for any deformation of the transverse assembly resulting from the impact event. Image tracking was completed using ProAnalyst motion analysis software [32]. All photographic data collected within this study was acquired at a rate of between 5000 to 10000 images per second, a shutter speed of 33 μ s to 67 μ s at a resolution of no less than 640 x 640 pixels². Lighting was provided by two ARRI 750 W halogen lights. Table 5 provides the lengths as well as the metrics computed from impact test trials on empty tube specimens. The specimen identification in Table 5 utilizes the convention NFTI-# which indicates (No Foam Transverse Impact) followed by the test number. The average force as defined by Eq. (1) is the area bound by the force/displacement response and the abscissa, normalized with respect to the total measured displacement of each respective test. The TEA as defined in Eq. (2) is the area bound by the experimentally recorded force versus transverse displacement curve. The SEA as defined in Eq. (3) is the total energy absorbed normalized with respect to the mass of the test specimen. The FE as defined by Eq. (4) is defined as the average measured force normalized with respect to the largest measured force .

$$F_{ave} = \frac{1}{D_t} \int F_{(measured)} dx \quad (1)$$

$$TEA = \int F_{(measured)} dx \quad (2)$$

$$SEA = \frac{TEA}{m} \quad (3)$$

$$FE = \frac{F_{ave}}{F_{max}} \quad (4)$$

Table 6: Empty Tube Specimen Impact Test Results

Specimen ID	Test #	Tube Length (mm)	Average Force (kN)	FE (%)	TEA (kJ)	SEA (kJ/kg)
NFTI	1	330	11.72	26.8	1.78	3.17
	2	330	11.83	26.7	1.70	3.04
	3	330	13.07	31.2	1.99	3.55

Table 7: Foam filled tube specimen test results.

Specimen ID	Test #	Tube Length (mm)	Core Geometry(mm)			Average Force (kN)	FE (%)	TEA (kJ)	SEA (kJ/kg)
			Width	Length	Height				
FFTIA-L ρ -RC	1-185.22	330	249.57	62.60	63.18	8.43	17.73	2.38	3.21
	2-179.22	330	248.82	64.02	62.79	8.06	14.42	2.20	2.97
	3-191.82	330	250.39	64.35	62.83	8.22	12.66	1.97	2.62
FFTIB-L ρ -RC	1-211.00	330	249.87	62.80	66.83	8.68	17.21	2.26	2.90
	2-210.81	330	249.57	63.78	65.83	8.54	15.01	2.44	3.13
	3-251.94	330	249.19	63.00	67.70	9.34	16.71	2.49	3.00
FFTIA-M ρ -RC	1-326.14	330	251.74	65.41	62.88	10.20	15.55	2.67	2.98
	2-357.60	330	251.22	65.59	61.86	9.92	19.93	2.57	2.78
	3-338.59	330	250.76	65.61	62.36	10.33	20.67	2.95	3.26
FFTIB-M ρ -RC	1-457.99	330	249.01	66.83	66.00	12.83	32.89	2.58	2.43
	2-484.27	330	248.82	65.04	64.25	13.13	29.61	2.64	2.49
	3-418.34	330	249.62	65.99	66.59	11.32	26.29	2.76	2.62
FFTIA-H ρ -RC	1-467.87	330	250.49	65.24	65.62	11.04	27.18	2.38	2.23
	2-521.21	330	250.34	65.35	65.31	12.72	29.28	2.74	2.45
	3-514.29	330	250.58	65.06	65.48	11.92	26.70	2.76	2.48
FFTIB-H ρ -RC	1-520.47	330	250.44	63.63	62.87	14.17	36.93	2.82	2.65
	2-467.56	330	250.25	63.86	62.66	13.52	32.34	2.55	2.36

5.5 Transverse Impact of Foam Filled Tubes

Preparation of foam filled braided tube specimens required measuring 340 mm of manually compressed braided tube stock using a conventional measuring tape and cutting the braid using conventional aviation snips. The mass of braided tube utilized for each test was approximately 560 grams. Rectangular aluminum foam cores of varying density ranging from 180 kg/m³ to 520 kg/m³ were investigated within this study. Construction of the cores was completed by first cutting individual 250 mm x 65 mm x 25.4 mm and 250 mm x 65 mm x 12.7 mm sections from large foam boards using the process of water jet cutting. The water jet cutting process was selected, as it allowed for a highly precise cut of the boards with minimal risk of damage to the sensitive aluminum foam cells in

close proximity to the cutting jet. Subsequent to the water jet cutting process, the 3 individual sections were bonded together using a multipurpose adhesive with the trade name "PL Premium" by LePage. The specimens were left undisturbed for a period of at least 24 hours as indicated by the manufacturer to allow for adequate curing time of the adhesive. Any sharp edges or corners present on the core samples were rounded using a conventional belt sander to permit greater ease of insertion of the foam core into the braided tube as well as to ensure that the individual wires of the braid tows were not damaged by snagging during the process of core insertion. Prior to sanding, each rectangular foam core specimen possessed a length, width, and height of 250 mm x 65 mm x 65 mm.

Insertion of the rectangular foam cores within the stainless steel braided tubes required full manual axial compression of the tube to expand the inner diameter by increasing the tow angle. When fully compressed, tube diameter was increased to such an extent that the interior core could be inserted within the tube without distorting the alignment of the surrounding braid tows. The foam core was manually manipulated such that it was positioned in the centre of the braided tube which was subsequently released from compression. Visual inspection was completed to ensure no snags or damaged wires were present along the tube length as a result of the core insertion process. Mounting of foam filled braided tube specimens within the transverse fixtures as well as preparation of the pneumatic gun and camera were completed in a manner consistent to that previously described for empty tube specimens in Section 5.4. Prior to each impact test, distance measurements between each clamp were taken to ensure the interior foam core was not shifted during the mounting process. The assembly process of the rectangular foam filled

tube specimens is depicted graphically in Figure 12. Table 6 provides the lengths as well as the metrics computed from impact test trials on foam filled tube specimens. The specimen identification in Table 6 utilizes the convention FFTI λ - $\beta\rho$ -RC- $\#$ - α where FFTI implies (Foam Filled Transverse Impact), λ is either 'A' or 'B' implying the specimen belongs to group A or B which specifies the foam specimen was cut from the same foam board, β is either 'L','M' or 'H' implying a low medium or high foam density (ρ), 'RC' identifies the specimen as rectangular core, $\#$ indicates the respective test number of the specimen, and finally ' α ' indicates the computed density of each respective test specimen in (kg/m³).

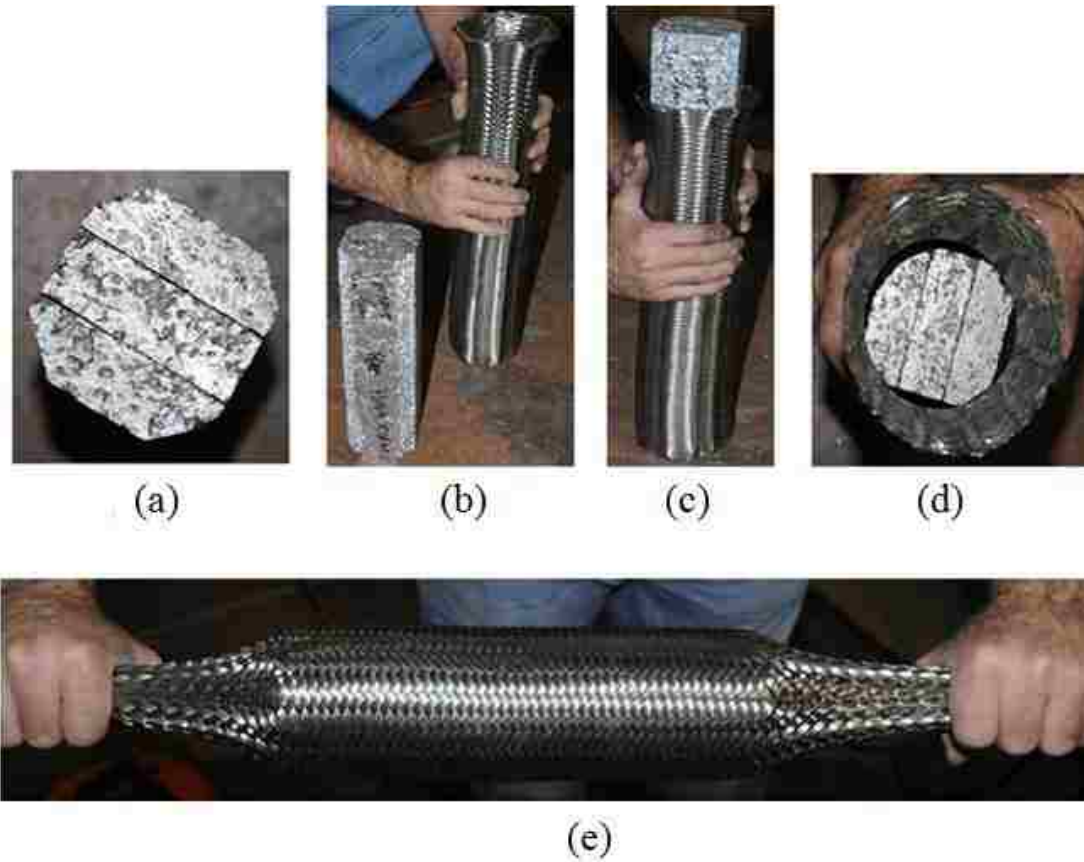


Figure 12: Assembly process of high density rectangular core foam filled braided tube.

5.6 Quasi-Static Transverse Testing of Empty and Foam Filled Tube Specimens

Quasi-static transverse tests of empty braided tube specimens were completed using a custom fabricated long stroke testing machine developed by Audysho [18-19] with a loading capacity of 300 kN and stroke length of 1.2 m. The long stroke testing machine was equipped with two identical fixture assemblies consistent to those described within Section 5.4 which were secured to the vertical columns of the machine frame and utilized to secure braided tube specimens during the transverse loading process. A secondary fixture designated as the centre fixture was secured to the translating hydraulic cylinder of the testing machine using an additional annular clamp. The centre fixture consisted of

two vertical plates and one horizontal plate. The vertical plates possess a length, width, and thickness of 260.35 mm x 101.6 mm x 25.4 mm, respectively. The horizontal plate possesses a length, width, and thickness of 250.4 mm x 101.6 mm x 38.1 mm as well as a 20.65 mm through hole which allowed for a 19.05 mm nominal diameter bolt to be fastened to the conical wedge insert incorporated within the annular clamp. Finally, a 76.2 mm solid bar was bolted between the two vertical plates such that upon vertical displacement of the hydraulic cylinder of the testing machine the bar would make contact with the braided tube specimen at the tube mid-span when fully secured within the transverse fixtures.

Preparation of empty braided tube specimens involved first cutting approximately 300 mm of manually compressed stainless steel braided tubing and cutting the tube using conventional aviation shears. The mass of the tube was approximately 500 grams. Subsequent to cutting the tube specimen, one end of the braided tube was then inserted into one of the annular clamps which were previously secured to the adapter plate of the transverse fixture assembly. The tube was then secured within the annular clamp using a taper lock conical wedge with an applied preload of roughly 10 kN. The hydraulic cylinder was lowered such that the centre axis of the tube specimen aligned with that of the centre fixture attached to the translating cylinder. After positioning the hydraulic cylinder, the remaining free end of the tube specimen was secured within the opposite side annular clamp and secured using a taper lock conical wedge with the same preload. When fully secured within the transverse fixtures an unsupported tube span of approximately 330 mm existed between the annular clamps of the transverse fixture assembly. During the transverse deformation process, displacement of the braided tube

specimen was measured using a laser displacement sensor with a functional measurement range of 1280 mm. Transverse force levels were measured using a PCB 220 kN strain gauge based load cell mounted to the translating hydraulic cylinder of the testing machine. Measurement data from both the load cell and displacement sensor were recorded using a laptop computer installed with custom programmed National Instruments LabVIEW data acquisition software. A sampling rate of 9 kHz was utilized for all experimental tests.

In addition to force and displacement measurement data, high speed visual image data was collected using a Photron SA4 high resolution camera. Time synchronization of measured and visual data sets was accomplished using custom programmed LabVIEW software and a National Instruments NI9401 transistor-transistor logic (TTL) module mounted within a NI 9274 chassis. The NI9401 module provided a high speed voltage signal to the camera to commence the collection of visual data consistent with the initiation and termination of force and displacement data collection. Time differences between force, displacement, and high speed image data sets were observed to be no greater than 1 ms over the duration of the test. All digital images were acquired using a shutter speed of 1 ms at a rate of 60 images per second and a resolution of 896 x 896 pixels². Lighting was provided by 2 ARRI 750W spot lights. Table 7 provides the specific lengths and performance metrics computed for each test. The table follows the naming convention NFFT which implies "No Foam Transverse Tensile".

Table 8: Quasi-static empty tube specimen results

Specimen ID	Test #	Tube Length (mm)	Average Force (kN)	F.E. (%)	Total Energy Absorbed (kJ)	S.E.A. (kJ/kg)
NFT	1	329	12.59	29.6	2.67	5.86
	2	329	12.24	29.9	2.37	5.21
	3	329	12.13	30.8	2.46	5.41

5.7 Quasi-Static Testing of Foam Filled Braided Tubes

Preparation of foam filled braided tube specimens involved first cutting approximately 420 mm of braided manually compressed stainless steel tubing using conventional aviation shears. The mass of tubing utilized for foam filled tests was approximately 690 grams. Preparation of rectangular foam core specimens involved first cutting 3 individual sections from aluminum foam boards using the process of water jet cutting. The 3 individual sections were bonded to one another using a multipurpose adhesive with the trade name "PL Premium" by LePage . In order to facilitate insertion of the rectangular foam core specimen within the braided tube and minimize the risk of distorting braid tow alignment, all four corners were trimmed using a conventional band saw. When fully secured within the transverse mounting fixtures of the long stroke testing machine, tube specimens were oriented perpendicular to the translating direction of the hydraulic cylinder. Tables 7 and 8 provide the dimensions as well as the performance metrics computer from quasi-static transverse test trials. Table 8 follows the naming convention FFT- $\beta\rho$ -RC where FFT implies (Foam Filled Transverse), β is either 'L' or 'H' implying a low or high foam density (ρ), 'RC' identifies the specimen as rectangular core.

Table 9: Quasi-static foam filled tube specimen results

Specimen ID	Test #	Tube Length (mm)	Core Geometry (mm)			Average Force (kN)	F.E. (%)	Total Energy Absorbed (kJ)	S.E.A. (kJ/kg)
			Width	Length	Height				
FFT-H ρ -RC	1	330	75.13	250.33	78.65	19.61	33.6	7.44	3.65
	2	330	75.47	250.04	78.97	23.11	33.3	9.13	4.32
	3	330	75.13	250.33	78.65	20.16	30.5	7.80	3.82
FFT-L ρ -RC	1	330	75.54	500.00	76.24	13.71	18.6	4.72	4.29
	2	330	75.36	500.06	76.71	11.50	16.4	4.03	3.74
	3	330	75.03	250.01	78.21	10.16	16.2	3.51	3.41

Insertion of the interior foam core within the braided tube required full manual compression of the tube to expand the diameter by enlarging the braid angle. When fully compressed, the foam core was able to be inserted within the tube without distorting or affecting the alignment of braid tows. After inserting the core the braided tube was released from compression and allowed to return to a relaxed position. Mounting of the braided tube specimen and positioning of the hydraulic ram was completed in a manner consistent to that described for empty tubes within Section 5.6.

6.0 EXPERIMENTAL OBSERVATIONS AND DISCUSSION

6.1 Experimental Observations of Aluminum Foam Core Compressive Tests

Examination of the compression test data illustrated typical elastoplastic foam compression of the cores comprised of 3 distinct regions consisting of an initial elastic region, collapse (plateau) and densification region as depicted in Appendix B. The majority of foam crushing was observed to occur between engineering strain levels of approximately 1% and 45%. Within the initial elastic region, compressive foam deformation was governed by the bending and compression of foam cell walls. The elastic region was noted to occur over strain levels ranging from approximately 0% to 2.5% for both low and high density foam specimens. The size of the plateau region was observed to be influenced by the density of foam specimens with low and high density foams exhibiting a plateau region between strain levels of roughly 3% to 40% and 2.6% to 30% respectively. Additionally, high density foam core specimens exhibited higher levels of plateau stress with plateau stress levels ranging from 3.00 MPa to 3.99 MPa for high density specimens and 0.4 MPa to 0.6 MPa for low density foam specimens. Foam deformation within the plateau region was noted to be highly localized at the cellular level resulting predominantly from buckling and brittle fracture of cell walls. These deformation mechanisms were observed to propagate throughout the specimen resulting in significant oscillations within measured stress levels. The onset of densification was reflected by a notable increase in the slope of the material stress/strain response. The estimated densification strain, elastic modulus, and plateau stress of each test specimen are listed within Tables 1 and 2 on page 31.

6.2 Experimental Results From Transverse Impact Tests

A compact disk is included with this thesis within the Appendices which includes samples of the experimental data as well as the worksheets utilized to develop the force/displacement and energy/displacement plots depicted within this chapter. Additionally, CAD prints for the projectile and input files for both FEA studies mentioned within this thesis have been included.

6.2.1 Transverse Impact Response of Empty Braided tubes

Dynamic transverse impact tests were completed on empty braided tube specimens having lengths of approximately 330 mm. The empty tube specimens examined within this study were struck at an average incident projectile velocity of 21.35 m/s with the impact event occurring over a period of roughly 10 ms. The force versus displacement and energy versus displacement responses of empty tube specimens are depicted in Figure 13. The transverse deformation process of empty tube specimen number 1 is depicted in Figure 14. Table 5 on Page 46 presents the average measured force, FE, TEA, and SEA. The captions within Figure 14 correspond with the annotations within Figure 13.

Upon impact of the projectile, empty tube specimens demonstrate a gradual linear increase in the measured force up to approximately 2 kN and an associated displacement of 40 mm. The initial linear increase in the measured response is attributed to the initial localized stacking and scissoring of the braid tows within the vicinity of the impacting cap upon development of contact between the tube and projectile as depicted in Figure 14 (a) and (b). Following the initial development of contact, the scissoring of braid tows is observed throughout the length of the empty tube specimen with braid tows located on

the contacting side of the tube (between the tube and the projectile) experiencing a greater degree of scissoring and elastic/plastic tensile deformation early in the deformation process due to the kinematic constraints imposed by the annular clamps as depicted in Figure 14 (c). Beyond displacement levels of approximately 100 mm, the force/displacement response achieved a linear profile which indicated that braid tows achieved lockup on both the contacting and non contacting surfaces of the tube resulting in elastic/plastic deformation of braid tow wires from the resulting tensile load. Subsequent to achieving tow lockup, the measured load continued to increase in a linear fashion up to approximately 41 kN and 135 mm of displacement where a momentary reduction followed by fluctuations in the measured force response were noted to develop. The fluctuations in the measured response signaled the early stages of progressive failure of the braid tow wires within the vicinity of the of the annular clamps on the contacting surface of the tube. The initiation of failure on the contacting surface of the tube was anticipated as the strands experienced a larger degree of elongation and localized bending early in the deformation process when compared to the fibres not in direct contact with the projectile.

The energy/displacement response of empty tube specimens depicted in Figure 13 possesses a similar profile to the force displacement response as it increases in a parabolic fashion throughout the displacement domain. From approximately 0 mm to 100 mm of displacement the primary mechanisms of energy absorption are a combination of (1) localized tow stacking, bending, and scissoring within the vicinity of the impacting cap and annular clamps on the contacting surface of the tube, (2) tow scissoring and locking within the straight sections of the tube, and (3) elastic/plastic tensile deformation

of braid tow wires. Displacement levels greater than 100 mm initiated a shift in energy absorption mechanisms to the plastic deformation of braid wires following tow lockup as depicted within Figure 14 (d). It should be noted that levels of absorbed energy are likely greater within the regions of the tube mid-span and annular clamps due to the presence of localized tow bending and stacking within those regions. The amount of additional energy absorbed as a result of localized stacking and bending within the impacting cap and clamp regions was not quantified within this study. The empty tube specimens examined within this study experienced the initiation of progressive failure at the contacting edge of the annular clamps at approximately 1.82 kJ of absorbed energy and a corresponding maximum displacement of approximately 150 mm.

Test trials produced repeatable results however it was noted that test number 1 experienced a transverse displacement approximately 10 mm greater than the other samples. After reviewing the visual data it was determined that the increased displacement observed in test #1 was a result of a small amount of additional slack within the tube resulting from the insertion of the conical wedges of the annular clamps. The average force, FE, and SEA were computed to be 12.20 kN, 28.23%, and 3.25 kJ/kg respectively for empty tube specimens.

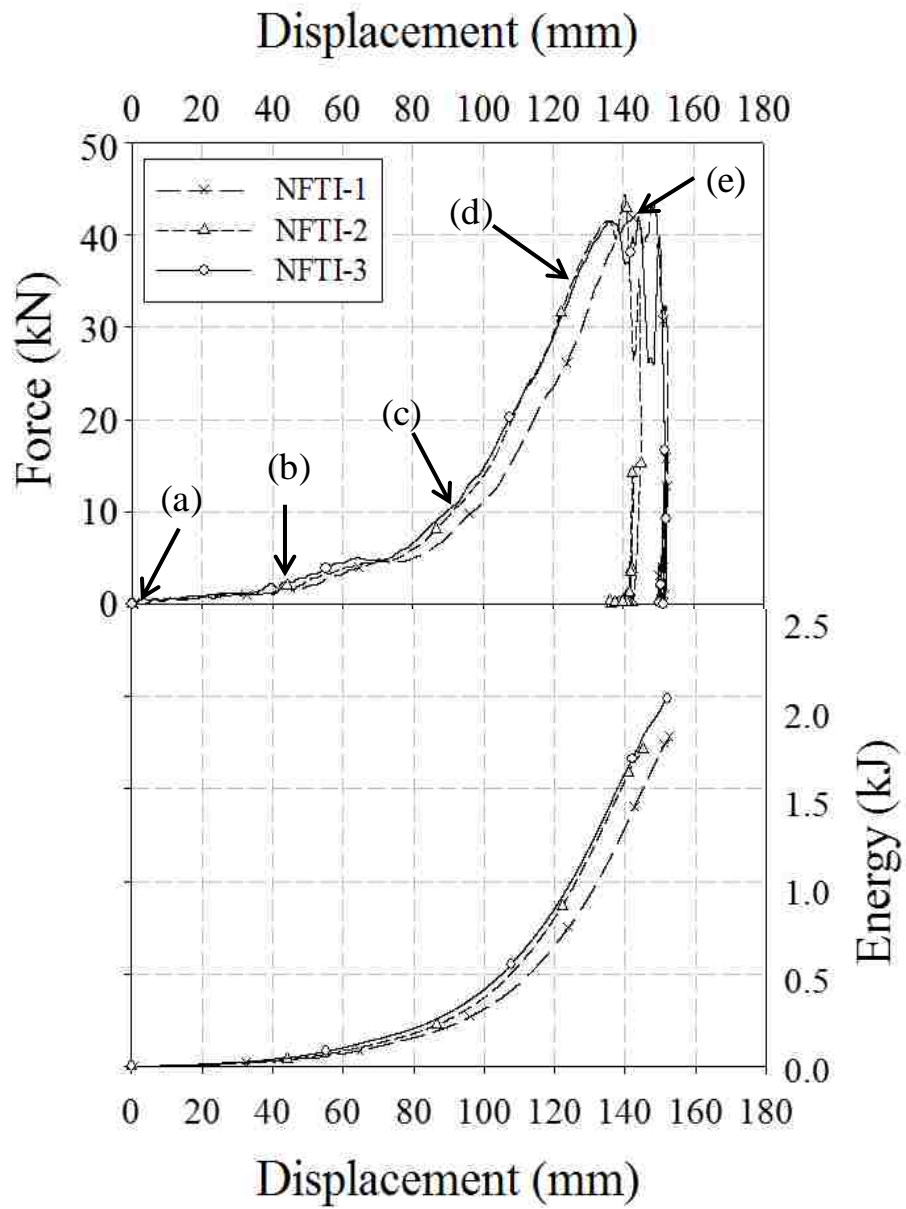


Figure 13: Force/displacement response for empty braided tube.

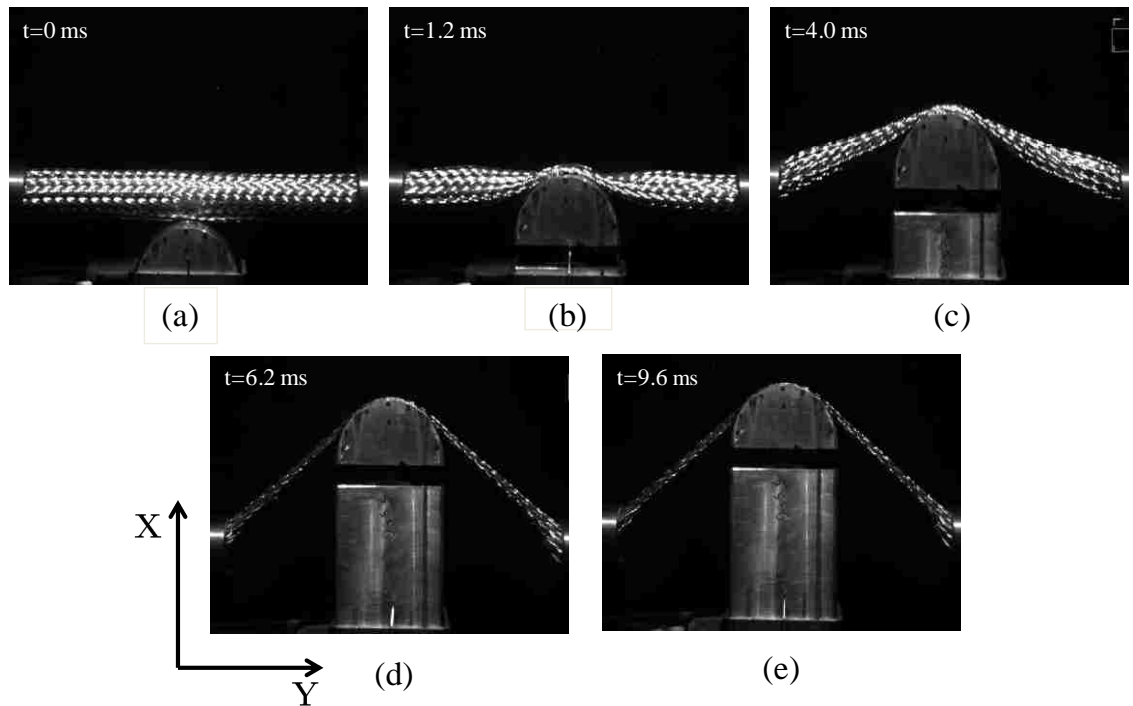


Figure 14: Photographs illustrating the transverse impact deformation process of empty stainless steel braided tube for specimen 1.

6.2.2 Transverse Impact Response of Low Density Rectangular Foam Filled Tubes

Figures 15 and 17 illustrate the transverse force versus displacement responses and energy versus displacement responses of group A and B low density rectangular core aluminum foam filled braided stainless steel tubes subjected to transverse impact. Figure 16 depicts the transverse deformation process of sample FFTIA-L ρ -RC-2-179.22, while the transverse deformation process of FFTIB-L ρ -RC-1-211.00 is illustrated in Figure 18. Annotations within Figures 15 and 17 correspond to the images within Figures 16 and 18 respectively. The average force, FE, TEA, and SEA of samples incorporating low density rectangular foam cores are presented within Table 6 on page 47.

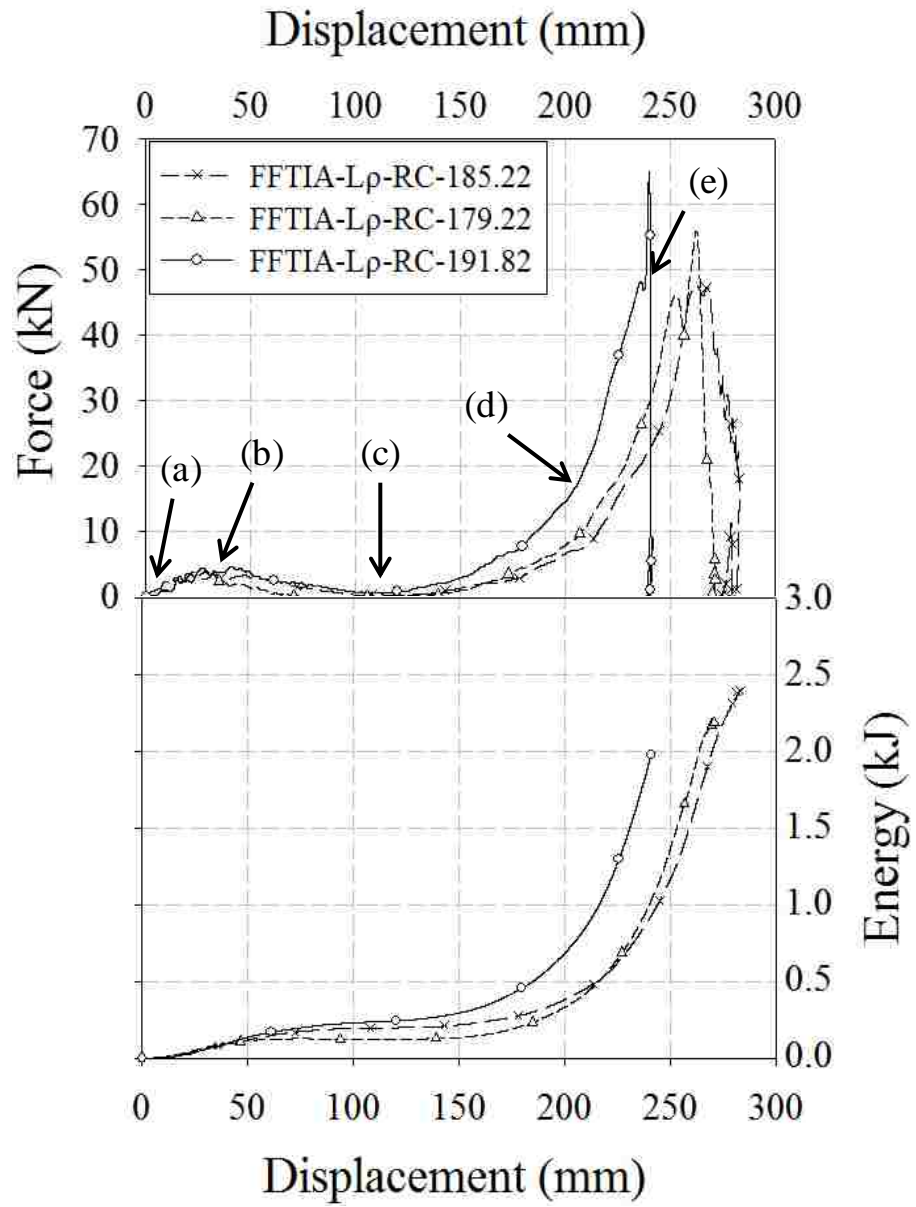


Figure 15: Force/displacement response for group A low density foam filled braided tube.

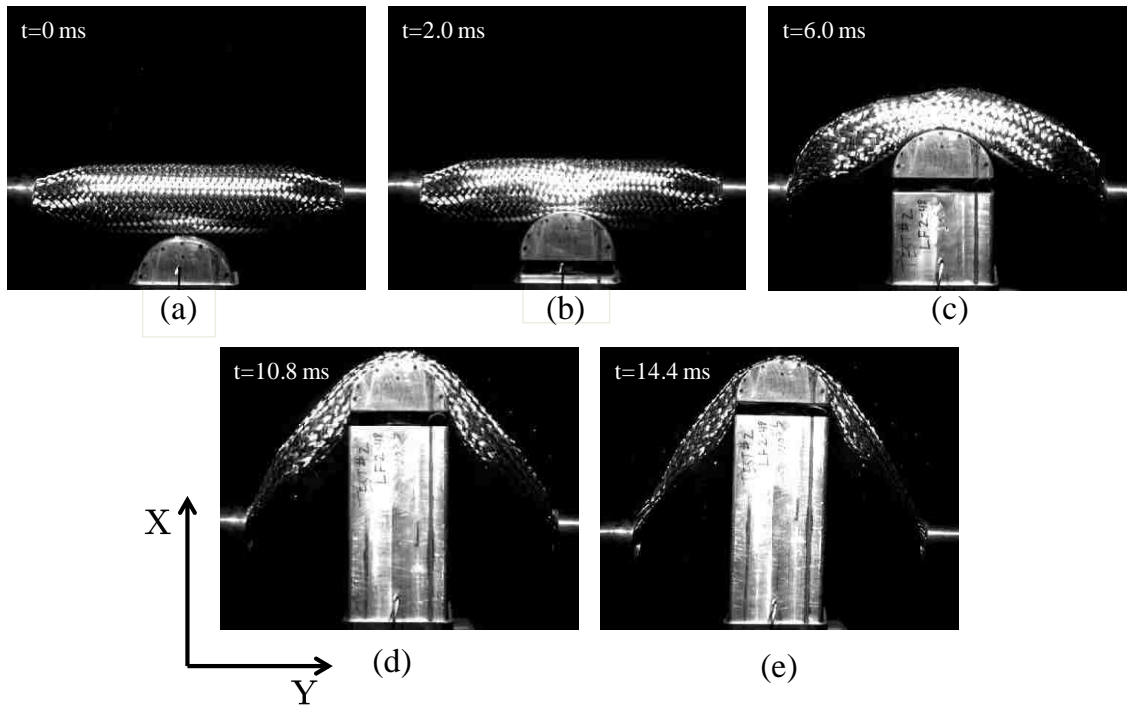


Figure 16: Photographs illustrating the transverse impact deformation process of low density group A foam filled braided tube specimen 2.

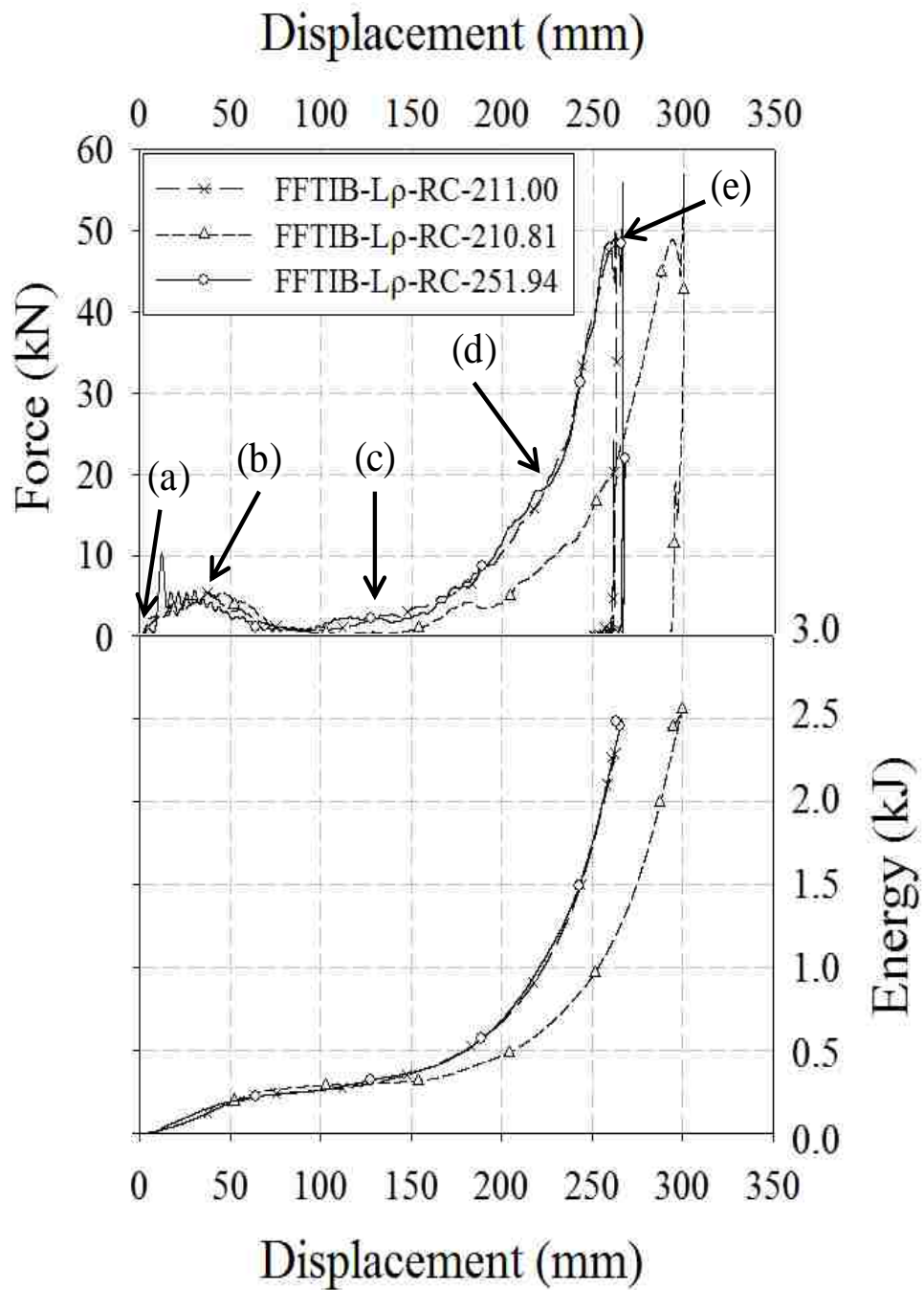


Figure 17: Force/displacement response for group B low density foam filled braided tubes

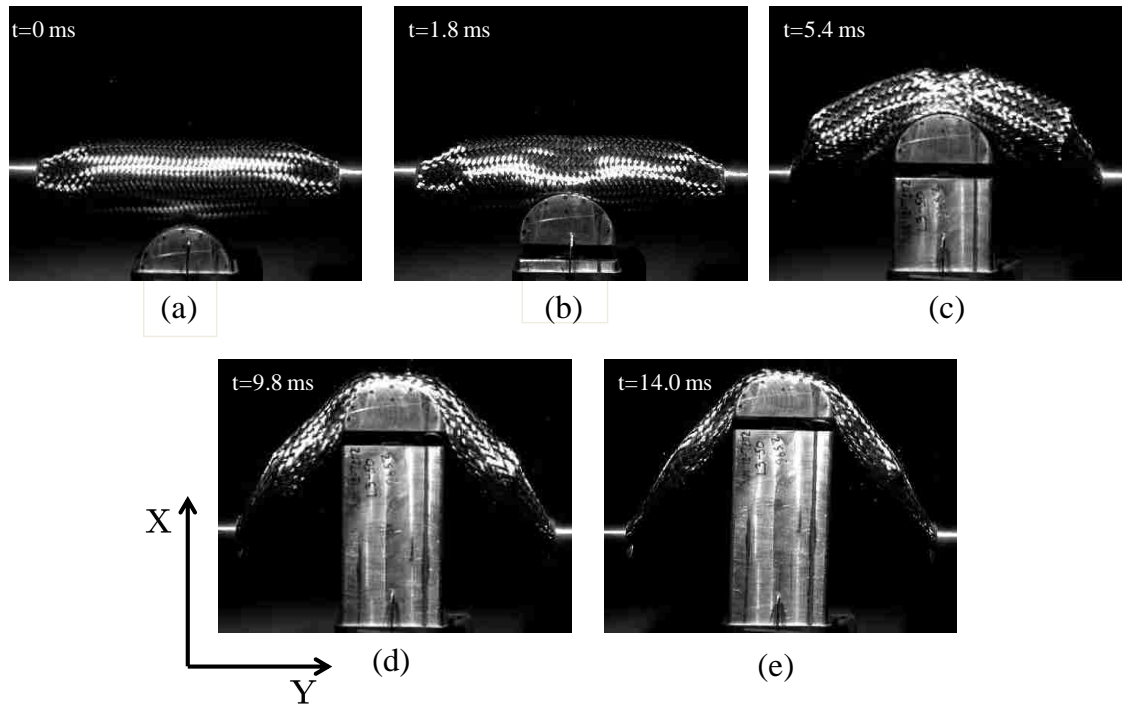


Figure 18: Photographs illustrating the transverse impact deformation process of low density group B foam filled braided tube specimen 2.

It can be observed in Figure 15 that tube specimens in group A exhibit an immediate increase in the measured force response upon impact up to a load of approximately 4kN and 35 mm of displacement. The initial increase in the measured response is attributed to the resistance of the interior foam core to penetration of the projectile upon contact as depicted within Figures 16 (a) and (b). Subsequent to the increase in measured load, a rapid drop in force is observed resulting from the fracture/splitting and localized

pulverization of the interior core by the projectile at the tube mid-span as illustrated in Figure 16 (c). The foam crushing process was noted to occur over a displacement interval of approximately 50 mm to 210 mm with the interior foam being crushed to a larger extent at the tube mid-span resulting from impact induced pulverization and within the vicinity of the annular clamps due to tight arrangement of braid tows. The foam crushing process resulted in an average reduction in tube diameter of approximately 57% within the straight sections of the braided tube. A momentary drop in the measured force succeeded by a rapid increase was noted at a displacement of approximately 250 mm and 45 kN of force. It is hypothesized that the momentary reduction in the measured force is the result of a small fraction of individual tow wires yielding on the non contacting surface of the braided tube near the annular clamp as a result of the tensile forces generated within the tube while decelerating the projectile. The kinematic constraints imposed by the presence of crushed foam within the straight sections of the braided tube as well as the highly compacted fragments present at the tube mid-span resulted in the wires on the non contacting surface of the tube being stretched to a larger extent than the wires on the contacting surface. The resulting spike in the measured force was initiated by the rapid restoration of tension within the tube subsequent to tow wire failure as the tensile load is redistributed to the intact wires on the contacting surface. Similar behavior was observed within group B low density rectangular foam filled specimens at displacement levels of approximately 260 mm and 50 kN of force.

Braided tube specimens containing low density foam cores (group B) exhibited similar behavior to group A specimens with an initial increase in the measured response followed by a load reduction beyond 5.0 kN and 40 mm of displacement. The observed load

reduction resulted from the localized splitting and pulverization of the interior foam core at the tube mid-span. Further displacement resulted in the crushing of the foam through tube diametrical reduction occurring over a displacement of approximately 60 mm to 230 mm producing an average 54.9% reduction in tube diameter. Although group B cores were constructed as one solid piece, consistent foam crushing behavior with group A specimens was observed with crushing occurring uniformly throughout the tube with a larger degree of localized crushing at the mid-span and annular clamp regions. The average crushing force for specimens in groups A and B were computed to be 4.6 kN and 5.4 kN, respectively, over the displacement ranges listed above.

FE and TEA values ranged from 12.66 to 17.73% and 1.97 kJ to 2.38 kJ for group A specimens and 15.01% to 17.21% and 2.26 kJ to 2.49 kJ for group B specimens. SEA values ranged from 2.26 kJ/kg to 3.21 kJ/kg and 2.90 kJ/kg to 3.13 kJ/kg for group A and B specimens respectively. The SEA values for group A and B low density foam filled test specimens were observed to be approximately 0.32 kJ/kg and 0.24 kJ/kg lower when compared to empty tube samples. When examining the degree of transverse elongation required to initiate failure of the tube specimens, it was noted that there were significant differences within tests FFTIA-L ρ -RC-3-191.82 of approximately 20 mm and within FFTIB-L ρ -RC-2-210.81 of approximately 40 mm when compared to other samples within their respective groups. It is hypothesized that the discrepancy observed within FFTIA-L ρ -RC-3-191.82 is simply a result of a lesser degree of slack present in the tube after mounting the tube within the transverse fixtures. The smaller degree of slack present within the tube resulted in an earlier initiation of tow scissoring and a consequently shorter period of foam crushing prior to elastic/plastic deformation of the

braided wires. Upon reviewing the visual data for test FFTIB-L ρ -RC-2-210.81 it was discovered that the increased displacement was a result of the interior foam core fracturing in a unique fashion. Rather than fracturing into two pieces of roughly equal length at the tube mid-span shortly following the initial impact of the projectile, the core utilized within test 2 fractured into 3 components. The 3 individual components were distributed such that two components of roughly equal size were present on either side of the projectile within the straight sections of the braided tube and one fragment roughly 70 mm in length remained at the mid-span. The presence of the large fragment at the tube mid-span induced a unique phenomena where isolated regions of tow scissoring were observed within the gaps between the core fragments which delayed the foam crushing process slightly. This variation in deformation does not appear to have a significant effect on the TEA, SEA, or FE metrics.

6.2.3 Transverse Impact Response of Medium Density Rectangular Foam Filled Tubes

Figures 19 and 21 depict the force versus displacement and energy versus displacement responses of group A and B medium density aluminum foam filled braided tube specimens. The transverse deformation process of specimen FFTIA-M ρ -RC-1-326.14 is depicted in Figure 20 while the deformation process of specimen FFTIB-M ρ -RC-2-418.34 is depicted within Figure 22. Consistent with Figures within Section 6.2.2, the annotations within Figures 19 and 21 correspond to the captions within Figures 20 and 22. Table 5 presents the average force, TEA, FE, and SEA values of each respective test.

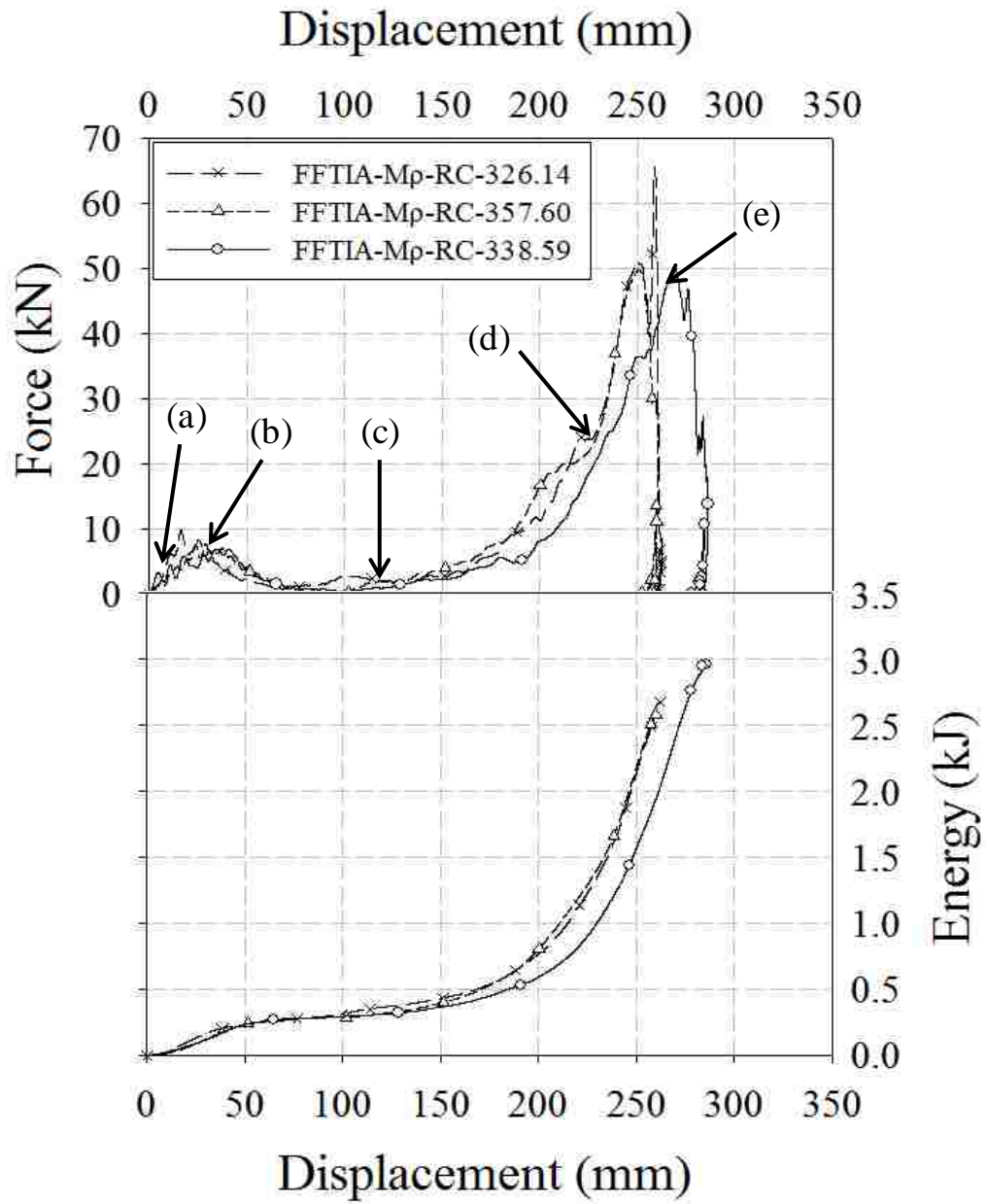


Figure 19: Force/displacement response for group A medium density foam filled

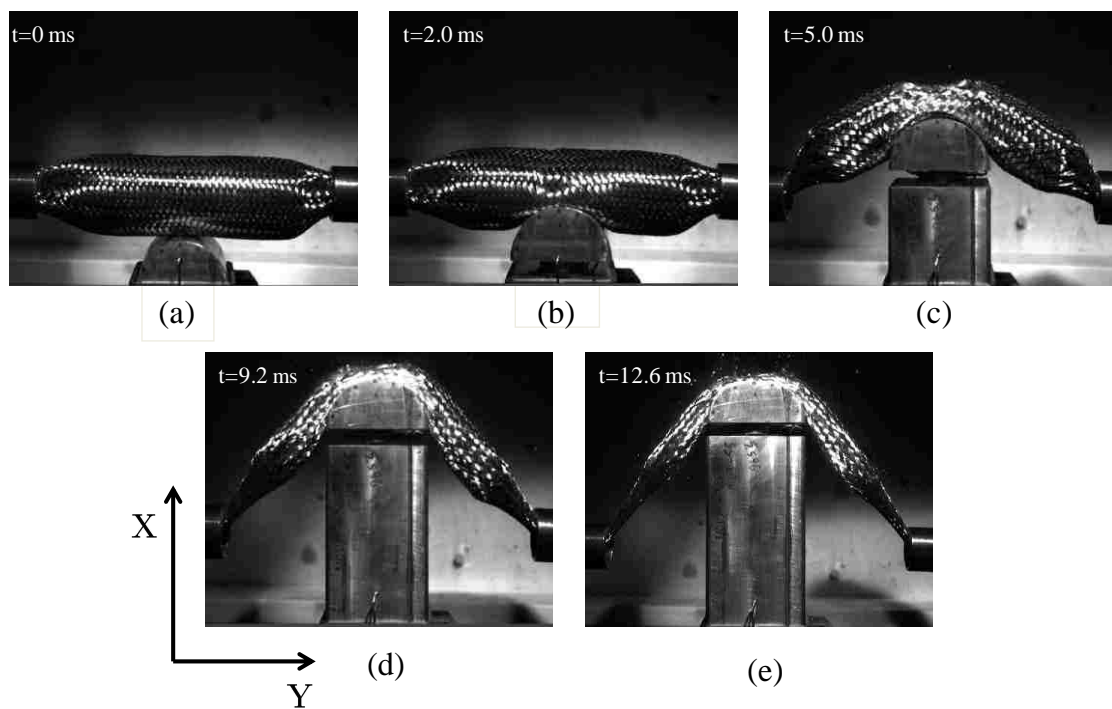


Figure 20: Photographs illustrating the transverse impact deformation process of medium density group A foam filled braided tube specimen 3.

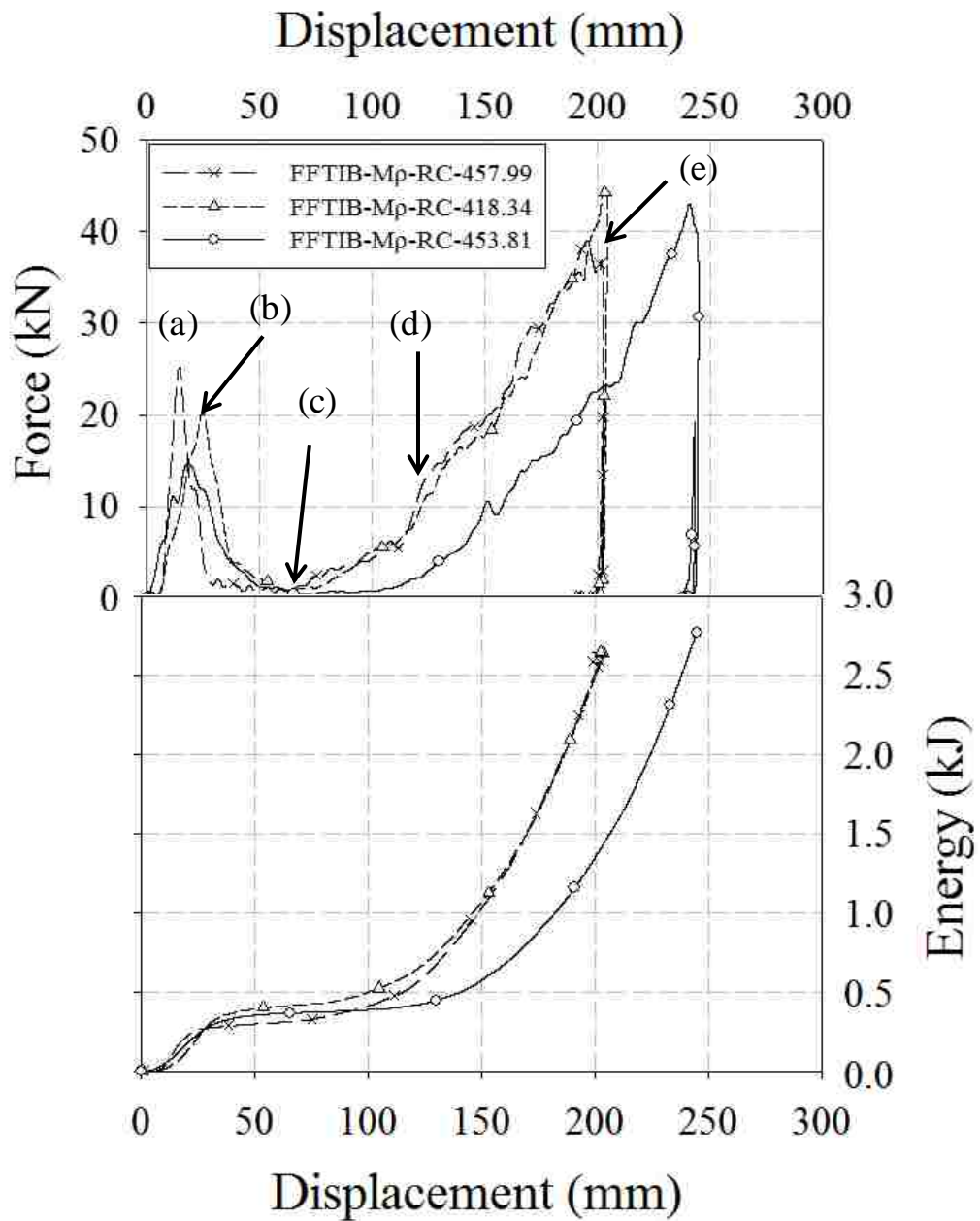


Figure 21: Force/displacement response for group B medium density foam filled braided tube

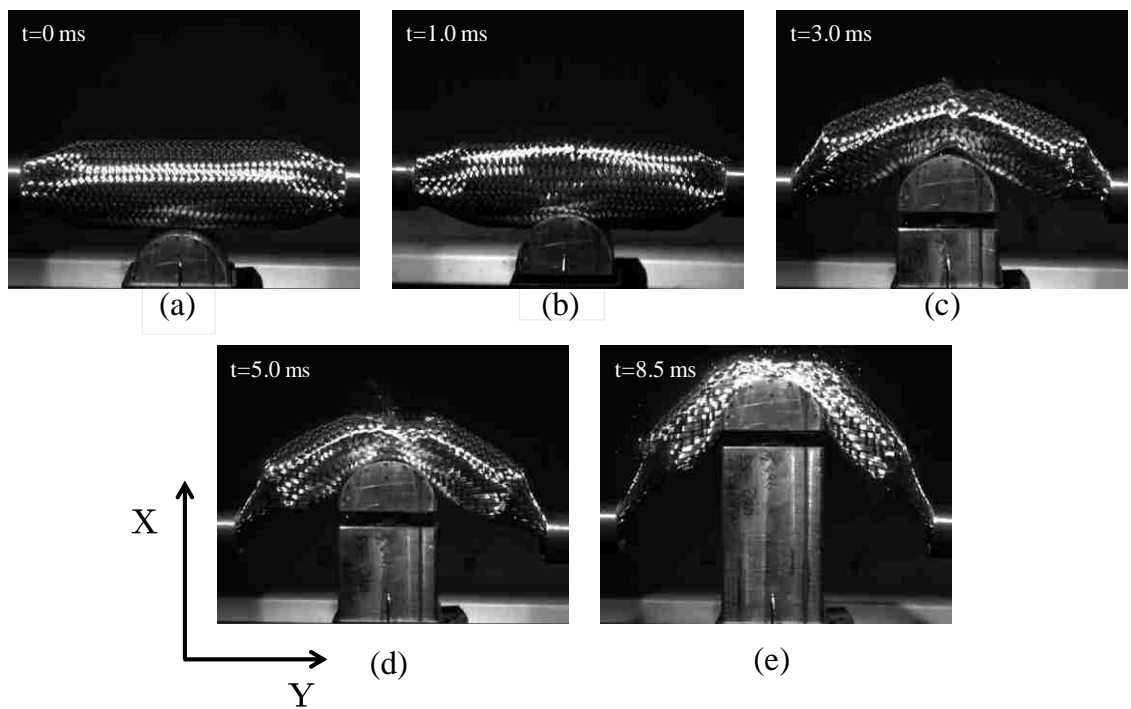


Figure 22: Photographs illustrating the transverse impact deformation process of medium density group B foam filled braided tube specimen 2

Specimens incorporating group A medium density foam cores were observed to behave in a similar fashion to braided tube specimens incorporating low density foam cores. The force/displacement profile exhibits an initial reduction beyond approximately 7 kN of force and 40 mm of transverse displacement. Fluctuations within the measured response

prior to the initial load reduction indicate that the interior foam core experiences localized pulverization and crushing at the tube mid-span as a result of penetration of the projectile prior to fracturing the core as depicted within Figure 20 (b). Group A foam specimens demonstrated consistent deformation behavior in each test with thorough foam crushing occurring over a displacement range of approximately 50 mm to 230 mm producing an average crushing force of 5.62 kN. Full tow lockup was only observed within the vicinity of the tube mid-span and annular clamps. The increased mechanical strength of the medium density group A cores did not permit braid tows to achieve full lock within the straight sections of the braided tube. A momentary load softening followed by a sharp spike in the measured response was observed during tests 1 and 3 at a force level of approximately 50 kN and corresponding displacements of 252 mm and 266 mm respectively. Observation of visual test data indicates that the momentary softening effect was a result of the same mechanism observed for low density cores where a small fraction of braid tow wires fail on the non contacting tube surface as a result of the increased elongation experienced by the fibres within the non contacting region resulting from the presence of the interior foam core.

Braided tube specimens incorporating group B medium density cores were noted to deform in a unique fashion and with a high degree of variability between tests compared to group A cores. Subsequent to contact of the projectile, the observed increase in the measured force response was noted to be significantly larger reaching levels approaching 25 kN. In addition to the increased magnitude, the profile of the force/displacement response prior to the initial fracture of the foam core at approximately 15 mm to 25 mm of displacement possessed a saw toothed shape rather than the parabolic shape observed

with group A and B low density core specimens and group A medium density specimens. The initial saw toothed shape and minimal fluctuation within force/displacement response is indicative of the limited degree of localized foam crushing at the tube mid-span from the initial penetration of the projectile as depicted within Figure 22 (b). The rapid increase in the measured force prior to the initial fracture of the interior foam is a result of the resistance of the core to bending within the braided tube prior to fracture. Subsequent to pulverization/splitting of the interior foam core, unique deformation behavior was observed within each test group B test. Within Test 1, the process of progressive foam crushing was not achieved. Braid wires in the vicinity of the tube mid-span began to fail at approximately 125 mm of transverse displacement as a result of localized plastic deformation of tow wires induced by the shifting of core fragments upon fracture. Successful foam crushing along the tube length was achieved within test 2 however the core was crushed only to a limited extent and full tow lockup was not achieved within the straight sections of the braided tube. An average crushing force of 15.2 kN was produced over a displacement of 80 mm to 205 mm with a resultant reduction in tube diameter of approximately 30%. Progressive foam crushing was achieved within test 3, however, upon fracture the two sections of the core were reoriented in such a fashion that very little foam remained within the tube mid-span. The relatively empty space created upon fracture resulted in localized scissoring of braid tows at the tube mid-span prior to initiating the crushing of the interior core within the surrounding areas. The extended tow scissoring phase was noted to occur from roughly 70 mm to 120 mm of displacement at an average force of roughly 1 kN. Foam crushing produced an average crush force of 17.8 kN computed over a displacement interval of

120 mm to 240 mm with a resultant tube diameter reduction of roughly 31%. FE and TEA values ranged from 15.55% to 20.67% and 2.57 kJ to 2.95 kJ for group A specimens and 26.29 to 32.89% and 2.58 kJ to 2.76 kJ for group B specimens. SEA values ranged from 2.78 kJ/kg to 3.26 kJ/kg and 2.43 kJ/kg to 2.62 kJ/kg for group A and B specimens respectively. Braided tube specimens incorporating group A medium density foam cores were noted to perform comparably in terms of SEA efficiency to group A and B low density specimens. However, when compared to group A and B low density cores, medium density group B specimens experienced a decrease in SEA efficiency of 14.33% and 16.61% respectively. The decreased SEA values indicate that the increased mechanical strength of the group B medium density core does not readily permit the initiation of foam crushing through braid diametrical reduction and produces an unfavorable effect most evident at the tube mid-span. The presence of this effect is reflected by the random nature of the deformation and energy absorption mechanisms observed within group B medium density core tests.

6.2.4 Transverse Impact Response of High Density Rectangular Foam Filled Tubes

This section discusses the mechanical responses of high density foam filled tube specimens subjected to transverse impact. It should be noted that although group A and B specimens are of comparable density they possess different cell sizes. Group B high density specimens possess a much smaller cell size as well as a thinner cell wall than group A specimens. Figures 23 and 25 depict the transverse force versus displacement and energy versus displacement responses of tube specimens containing group A and B cores respectively. The transverse deformation process of specimen FFTIA-H ρ -RC-3-514.29 is depicted in Figure 24 while the transverse deformation process of specimen

FFTIB-H ρ -RC-520.47 is depicted in Figure 25 with annotations in Figures 23 and 25 corresponding to those within Figures 24 and 26. The average force, FE, TEA, and SEA values of high density braided tube specimens are presented within Table 6.

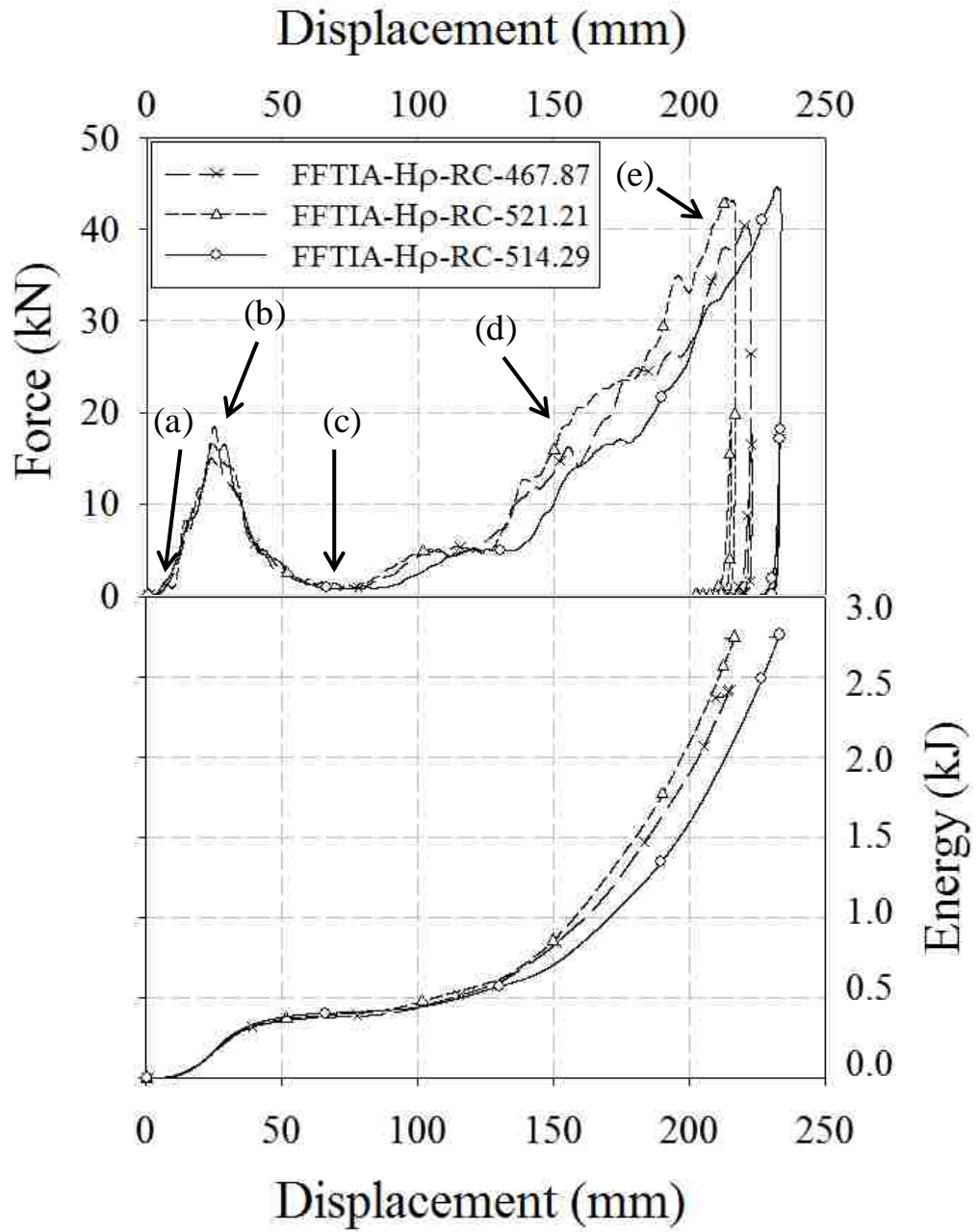


Figure 23: Force/displacement response for group A high density foam filled braided tube.

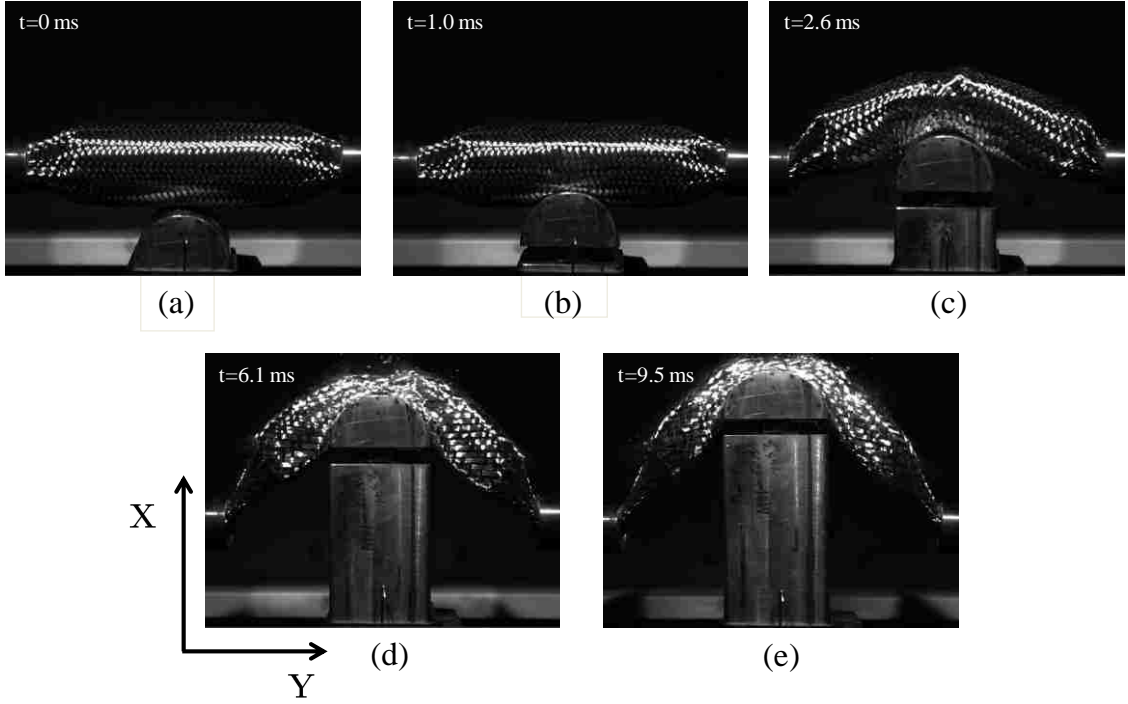


Figure 24: Photographs illustrating the transverse impact deformation process of high density group A foam filled braided tube specimen 1.

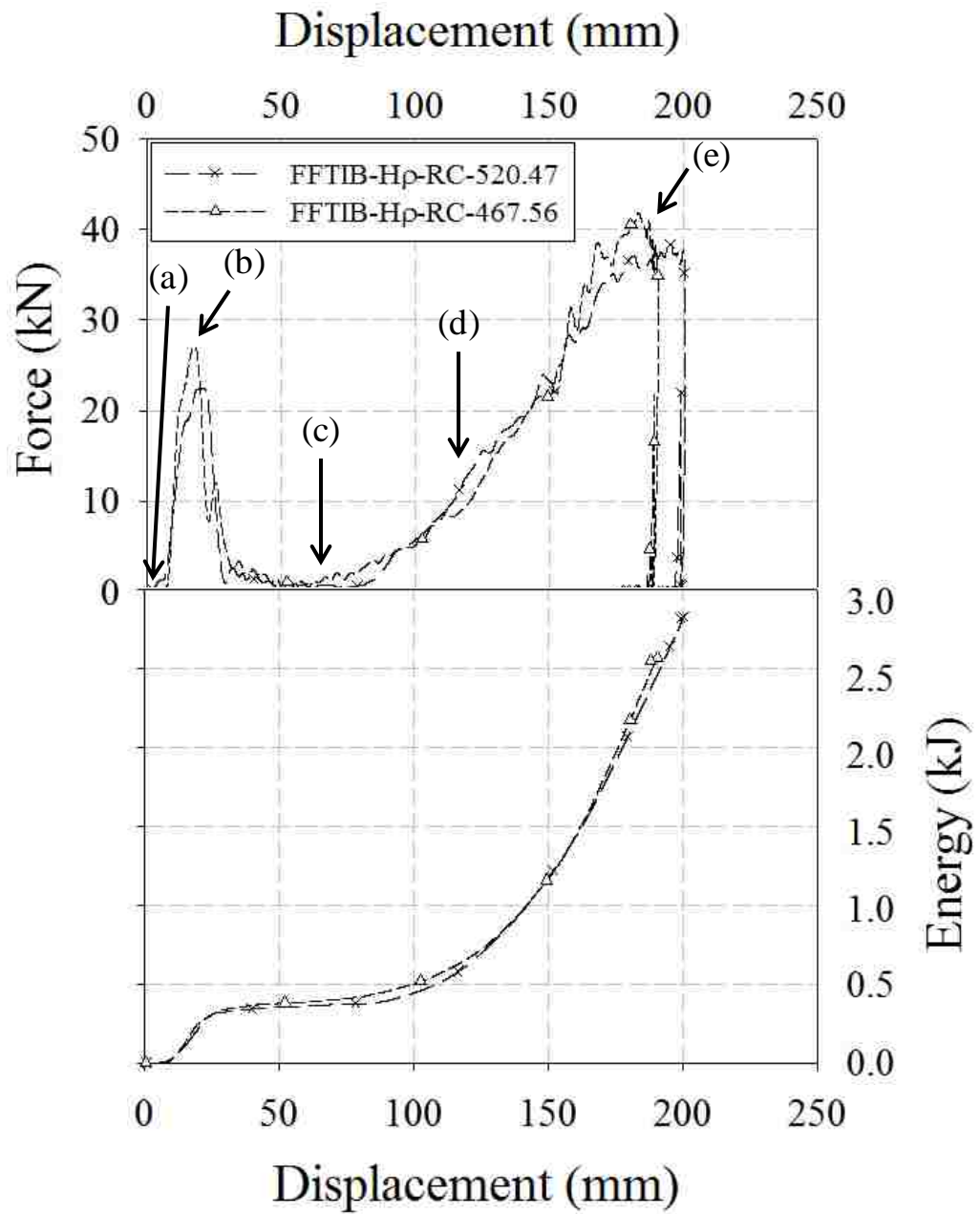


Figure 25: Force/displacement response for group B high density foam filled braided tube.

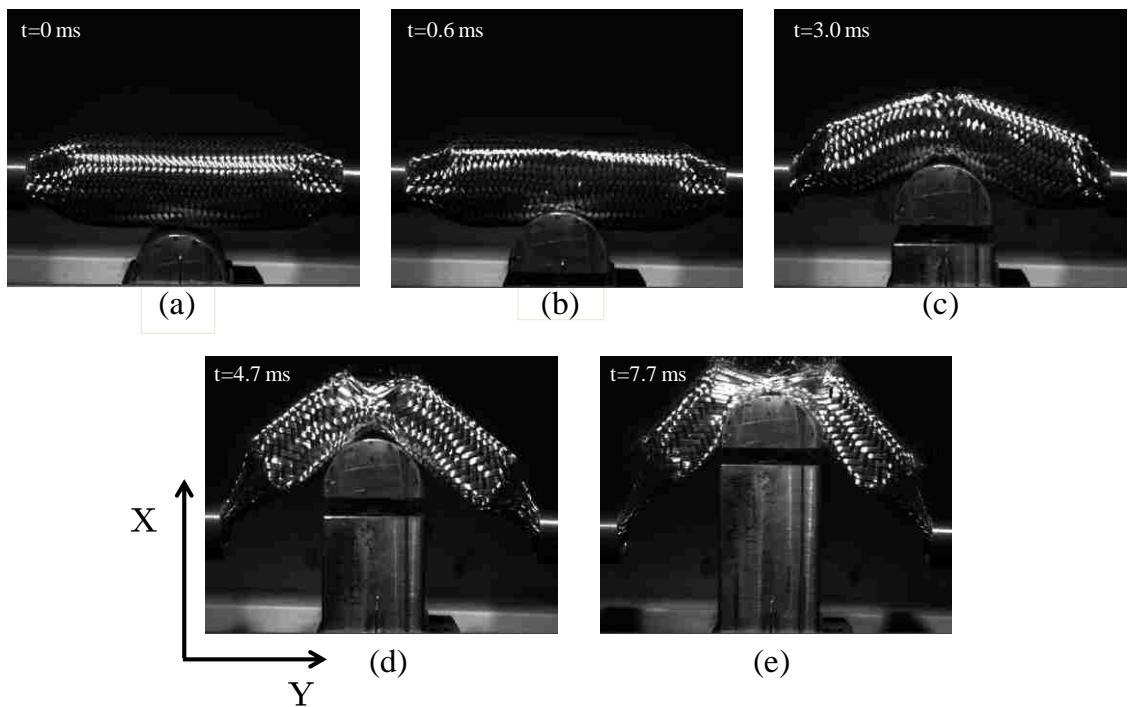


Figure 26: Photographs illustrating the transverse impact deformation process of high density group B foam filled braided tube specimen 1.

Tube specimens incorporating group A high density cores experienced a rapid load increase with very little fluctuation in the measured response early in the deformation process. The measured force was noted to increase to a peak force of approximately 17 kN at a corresponding displacement of 25 mm succeeded by a rapid load reduction following the initial fracture/splitting of the interior core at the tube mid-span. The relatively smooth profile of the force/displacement response between 0 mm and 80 mm of displacement indicates that upon impact, the projectile produces very little localized foam crushing within the immediate contact area as a result of the mechanical strength of the interior core. Significant fracturing of the core is evident without foam collapse. Subsequent to the splitting of the core, an undesirable effect was noted at the

tube mid-span. The robust mechanical strength of the core resulted in a large degree of localized elongation and shifting of braid tow wires at the tube mid-span as the two separated fragments were displaced by the impacting cap of the projectile as depicted within Figure 24 (c). Foam crushing through tube diametrical reduction was successfully achieved within all group A high density foam core tests. The process of foam crushing occurred between a displacement range of 80 mm to 225 mm producing an average crushing force of 15.87 kN. Consistent with observations from group A and B medium density cores, the mechanical strength of high density group A cores did not permit an adequate level of crushing to achieve full tow lockup. Average tube diameter reduction was noted at 27.29% within the straight sections of the braided tube after complete deceleration of the projectile.

Upon impact, tube specimens incorporating group B high density core specimens exhibited a more rapid rise within the force/displacement response than all other cores examined within this study. Prior to the initial fracture of the core at the tube mid-span, force levels were observed to rise to 27 kN at a corresponding transverse displacement of approximately 15 mm. The exceptionally steep slope observed within the early stages of the force/displacement response is attributed to the small cell size and solid construction of group B specimens which produced behavior similar to that of a brittle material under compression. Subsequent to the initial fracture of the interior core beyond 15 mm of displacement, a significant undesired interaction between the interior core and braid was observed at the tube mid-span. As the core is displaced by the forward motion of the projectile, the inability of braid tow wires on the non contacting tube surface to crush the interior core as it conformed to the impacting cap of the projectile produced a large

degree of localized tow deformation and early wire failure on the non contacting surface at the mid-span. The localized elongation and early initiation of braid tow failure are depicted within Figures 26 (c) and (d). The effect produced by the interior core resulted in a shift of energy absorption mechanisms for tube specimens incorporating group B cores. Rather than foam crushing through braid diameter reduction, the primary mechanisms of energy absorption are the initial fracture of the core followed by the progressive braid tearing at the tube mid-span beyond a transverse displacement of roughly 70 mm as depicted within Figure 26 (e).

FE and TEA values listed within Table 6 for group A specimens ranged from 26.70% to 29.28% and 2.38 kJ to 2.76 kJ while group B values ranged from 32.34% to 36.93% and 2.55 kJ to 2.82 kJ. Both group A and B high density core specimens were noted to produce FE values comparable to group B medium cores. The similarity in FE values between tube specimens incorporating high density and group B medium density cores is anticipated as the elevated mechanical strength of the cores did not permit uniform foam crushing throughout the tube length and thus produced a greater average crushing force. The additional mass added to braided tubes utilizing high density cores resulted in a reduction in SEA efficiency. SEA values for high density rectangular cores ranged from 2.23 kJ/kg to 2.48 kJ/kg for group A specimens and 2.36 kJ/kg to 2.85 kJ/kg for group B specimens. In addition to the reduction in SEA performance the presence of undesired effects arising between the interior core and braided tube suggest foam specimens of density greater than roughly 400 kg/m^3 are detrimental to the energy absorbing performance of the structure.

6.3 FEA Energy Analysis

6.3.1 Transverse Assembly F.E.A Model

When examining the TEA levels of the empty and foam filled braided tube specimens tested within this study, a discrepancy between the levels of energy absorbed by the tube and initial kinetic energy of the projectile was noted. Review of high speed image data revealed that the arms of the transverse assembly undergo a small, yet notable, degree of flexing during the impact between the braided tube specimen and projectile. It was hypothesized that the observed discrepancy in energy levels was a result of the flexing of the transverse assembly, as such, an FEA analysis of the transverse testing machine frame was conducted to ensure all energy absorbed by the braided tube sample and dissipated throughout the transverse testing machine was accounted for. Completion of the system energy balance required verifying that the sum of the respective energies absorbed by the tube specimen and long stroke testing machine frame would equate the initial kinetic energy of the projectile prior to the impact event as described in Eq. (5).

$$E_{(projectile)} = \frac{1}{2}(mv^2)_{(projectile)} = E_{(absorbed)} = TEA + E_{(elastic\ frame)} \quad (5)$$

where

$$TEA = \int F_{(measured)} dx \quad (6)$$

The amount of energy absorbed by the long stroke testing machine could not be measured directly. Therefore, a quantitative estimate of $E_{(elastic\ frame)}$ was acquired by examining the levels of absorbed energy computed by the FEA model as described in Eq. (7).

$$E_{(elastic\ frame)} = E_{(FE\ sim)} \quad (7)$$

The differences between the computed levels of energy absorbed by the long stroke machine frame and initial kinetic energy of the projectile were taken to compute TEA* as presented within Eq. (8).

$$TEA^* = \frac{1}{2}(mv^2)_{(projectile)} - E_{(FE\ sim)} \quad (8)$$

The structural model utilized within this study was an existing model previously developed by Audyscho [18-19] for simulation within LS-DYNA. Creation of the model involved using CAD modeling data generated within CATIA V5 R20 to produce IGES files to generate the geometry of the model. Discretization of the model was accomplished using Hypermesh V11 software. All structural components of the long stroke testing machine frame were represented using shell elements. The transverse assembly side plates, adapter plates, and annular clamps were represented using solid elements. The completed mesh was composed of 173260 shell elements and 52961 solid elements. All shell elements utilized within the model utilized fully integrated shell elements (ELFORM 16) and all solid elements utilized constant stress solid elements (ELFORM 1). The smallest element present within the model possessed a volume of 24.88 mm³ resulting in a minimum time step size of roughly 0.296 μ s. Bolted connections within the model were represented using constrained nodal rigid bodies (CNRB). Bolted connections between the long stroke testing machine frame and floor were represented through the implementation of boundary constraints on the nodes of the base of the machine which inhibited all translational and rotational motion. Components of the transverse testing machine frame were modeled using *MAT_ELASTIC with the

material properties of ASTM A36 steel. The properties of A36 steel used within the FE simulations are listed within Table 9.

Flexing of the transverse fixture arms was accomplished by inserting a single rigid element within the through holes of each of the annular clamps. The nodes of the rigid elements were rigidly coupled to those comprising the interior surface of the annular clamp through hole using nodal constraints. The rigid elements positioned within the annular clamps were displaced using a boundary prescribed motion. The displacement/time curve utilized to govern the motion of the arms was acquired through tracking the flexing motion of the transverse assembly in visual test trial data within the plane of impact using ProAnalyst [32] motion analysis software. Due to the relatively simple nature of the simulation, the complete geometric model was utilized. Although the impact event occurred over a period of roughly 10 ms, a termination time of 40 ms was utilized to ensure the arms were permitted to return to a low energy state prior to completing the simulation. The FEA simulation was noted to complete within a clock time of roughly 3 hours and 20 minutes and no mass or time scaling techniques were implemented in the numerical modeling process.

Table 10: Mechanical properties for ASTM A36 steel

Material	Density (kg/m³)	Young's Modulus (GPa)	Poisson's Ratio	Yield Stress (MPa)	Ultimate Stress (MPa)	Elongation (%)
A36	7830	210	0.28	248	441	21

6.3.2 Simulation Results

Examination of the internal energy levels produced from the bending of the transverse fixtures confirmed that a significant quantity of energy was being dissipated as a result of flexing of the transverse mounting arms. Rather than completing an individual simulation for each respective test, the test in which the transverse fixture assembly flexed to the greatest extent was simulated using the FEA model. The resulting internal energy of the testing machine was plotted against the displacement of the transverse fixtures within Mathcad engineering software [36]. A 7th order polynomial regression curve fit was implemented on the energy/displacement data. The resulting fitting curve possessed a Pearson's correlation coefficient approaching unity indicating a strong fit between the data sets. The resulting fitting function was then utilized to predict the levels of energy absorbed by the transverse fixture assembly during each respective test. The results of the system energy balance are presented within Table 10. Examination of the energy balance of the system revealed a strong degree of correlation between TEA and TEA* values with a maximum difference of approximately 3.5%.

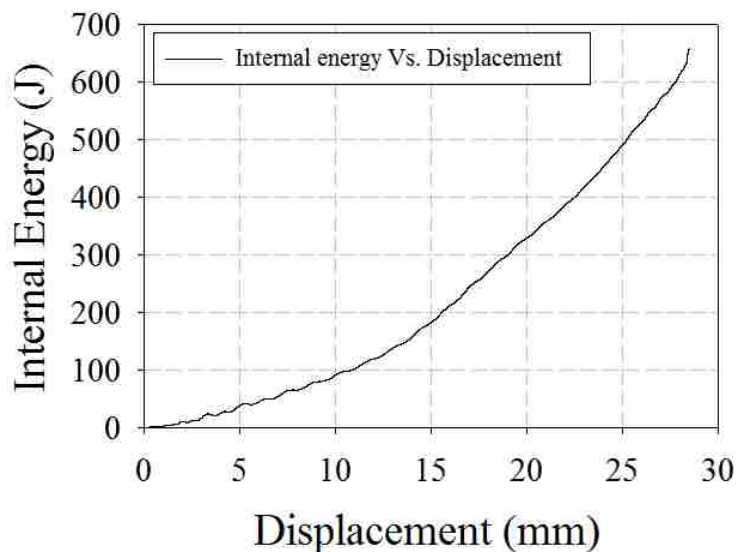


Figure 27: Fixture Internal Energy versus Transverse Displacement

Table 11: FEA energy balance results

Specimen ID	Test #	Incident Velocity (m/s)	Arm Displacement (mm)	$E_{(FE\ sim)}$ (kJ)	$E_{(projectile)}$ (kJ)	TEA (kJ)	TEA* (kJ)
NFTI	1	21.10	20.89	0.406	2.17	1.78	1.76
	2	21.02	22.77	0.464	2.15	1.70	1.69
	3	21.92	20.99	0.416	2.34	1.99	1.92
FFTIA-L ρ -RC	1-185.22	23.83	23.80	0.474	2.76	2.38	2.29
	2-179.22	23.12	19.50	0.363	2.60	2.20	2.24
	3-191.82	22.95	23.91	0.500	2.56	1.97	2.06
FFTIB-L ρ -RC	1-211.00	24.41	24.94	0.536	2.89	2.26	2.35
	2-210.81	25.15	24.42	0.547	3.08	2.44	2.53
	3-251.94	25.27	24.91	0.535	3.11	2.49	2.58
FFTIA-M ρ -RC	1-326.14	26.05	25.13	0.543	3.30	2.67	2.76
	2-357.60	25.63	25.84	0.570	3.20	2.57	2.63
	3-338.59	26.64	25.56	0.559	3.45	2.95	2.89
FFTIB-M ρ -RC	1-457.99	26.03	26.96	0.617	3.30	2.58	2.68
	2-484.27	26.51	28.28	0.685	3.42	2.64	2.74
	3-418.34	26.93	28.36	0.690	3.53	2.76	2.84
FFTIA-H ρ -RC	1-467.87	25.40	28.35	0.689	3.14	2.38	2.45
	2-521.21	26.05	27.53	0.644	3.30	2.74	2.66
	3-514.29	26.76	28.36	0.700	3.48	2.76	2.78
FFTIB-H ρ -RC	1-520.47	26.96	27.57	0.645	3.54	2.82	2.90
	2-467.56	25.80	26.47	0.596	3.24	2.55	2.64

7.0 QUASI-STATIC VERSUS DYNAMIC TEST RESULT COMPARISON

This chapter provides a comparison between the experimental findings collected from dynamic impact test trials on empty and aluminum foam filled braided tube specimens and the quasi-static test results collected within [18]. Although the density levels of the aluminum foam cores investigated within each respective study are not identical, the comparison provides some important insight towards the influence of loading rate on the energy absorbing performance of the composite structure under the transverse loading condition.

7.1 Quasi-Static versus Dynamic Transverse Tensile Response of Empty Braided Tubes

During the quasi-static transverse loading process, tube specimens were loaded at a constant rate of 18.8 mm/s until the braided tube experienced complete mechanical failure. Dynamic test trials involved striking the tube specimen at an incident projectile velocity of 21.10 m/s to 21.92 m/s with the impact event occurring over a time period of roughly 10 ms. The force versus displacement and energy versus displacement responses of empty braided tube specimens subjected to both quasi-static and dynamically applied transverse tensile loads are shown within Figures A1 and A2. The transverse deformation process of quasi-static test NFFT-1 is depicted within Figure 28 and the transverse deformation process of dynamic impact test NFTI-1 is depicted within Figure 14 on page 60. Tables 5 and 7 on pages 46 and 53 present the average force, TEA, FE, and SEA values for dynamic and quasi-static tests, respectively.

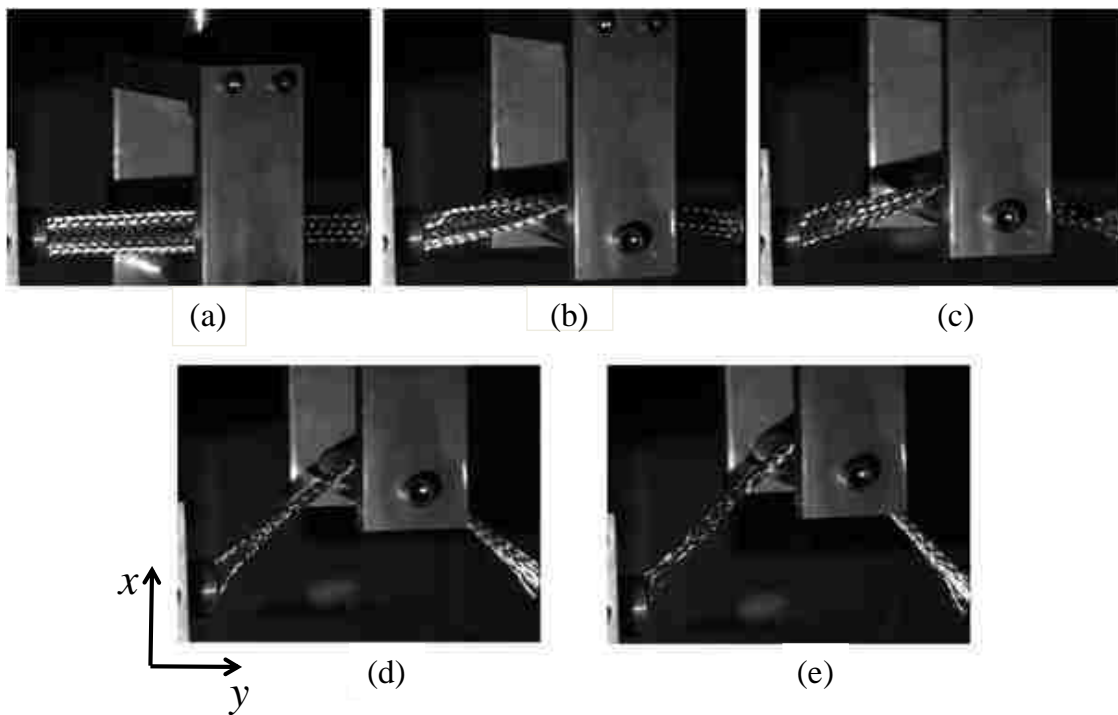


Figure 28: Quasi-static deformation process of empty braided tube

Within quasi-static test trials, the force/displacement response was observed to increase gradually up to approximately 1.5 kN of force and an associated displacement of approximately 55 mm. This initial response was noted to be a result of the development of contact between the centre loading bar and contact surface of the braided tube specimen which resulted in the localized stacking and scissoring of braid tows at the tube

mid-span. Transverse displacement levels beyond 55 mm induced a steep linear increase in the measured force response as a result of tow scissoring occurring throughout the tube length followed by the elastic/plastic deformation of braid tow wires as tensile forces developed throughout the braided tube as depicted within Figure 28(b) and (c). Continued loading of the braided tube resulted in material failure of braid tow wires which was noted to develop in a progressive manner within the vicinity of the annular clamps on the contacting surface of the braided tube as a result of the tensile forces and highly localized bending present within the clamp regions as depicted within Figure 28(d) and (e). The initiation of progressive braid failure was reflected as a load softening within the measured response which continued until the tube specimen experienced complete material failure. Peak load values reached roughly 40 kN at a corresponding crosshead displacement of approximately 150 mm for quasi-static tests. The increased loading rate within dynamic test trials was observed to produce a significant effect on the force/displacement response of empty braided tube specimens when compared to quasi-static test trials. From approximately 0 mm to 40 mm of transverse displacement, the measured response increased in a linear fashion up to a force of approximately 1.25 kN as a result of the initial development of contact between the impacting cap of the projectile and contacting tube surface. At approximately 45 mm of transverse displacement, a momentary spike within the measured response of roughly 1 kN in magnitude was observed as a result of the contacting surface of the braided tube colliding with the non contacting surface due to the penetration of the projectile as depicted within Figure 14 (b). Transverse displacement levels beyond 45 mm induced a steep linear increase within the measured response resulting from the scissoring of braid

tows followed by the elastic/plastic deformation of individual braid wires consistent with behavior observed within quasi-static tests. A momentary reduction within the measured force followed by a sharp linear increase was noted at roughly 70 mm of displacement within impact test trials. Analysis of visual test data revealed that the momentary reduction in force was a result of a brief reduction of contact between the impacting cap of the projectile and contacting surface of the braided tube prior to achieving full tow lockup. The initiation of progressive tube failure occurred at approximately 135 mm of transverse displacement and a peak force value of 41 kN within dynamic test trials. Consistent behavior was observed between quasi-static and dynamic test trials with braid failure initiating on the contacting surface of the tube specimen within the vicinity of the annular clamps.

Examination of the performance metrics listed within Tables 5 and 7 revealed that empty braided tube specimens produced consistent results with average force and average FE values of 12.32 kN and 30.1% for quasi static test trials and 12.21 kN and 28.23% for dynamic test trials. Average TEA and SEA values were 2.5 kJ and 5.49 kJ/kg for quasi-static test trials and 1.82 kJ and 3.25 kJ/kg for dynamic test trials. The larger TEA and SEA values observed within quasi-static tests are due to the approximately 15 mm of additional transverse displacement required to initiate braid failure when compared to dynamic tests. It is hypothesized that within dynamic test trials tube specimens began to fail at a smaller degree of transverse displacement due to the increased loading rate combined with the highly localized tensile stresses and bending present within the clamp regions. Although strain rates along the tube length were not quantified within this study, the failure behavior observed within dynamic test trails exhibited similar trends to those

identified within the work of [38] where it was noted that the failure strain of 304 stainless steel specimens subjected to axial tensile loads decreased with increasing strain rate. Additionally, the early failure behavior observed within dynamic test trials exhibits similarities to the findings of Menkes and Opat [39] examining the effects of increasing impulse velocity when striking fully clamped 6061-T6 beams at the mid-span. The findings from the study indicated a transition in deformation mechanisms with increasing impulse velocity from large inelastic deformation of the entire beam proceeded by a shift to tensile tearing at the beam supports and finally transverse shear failure at the beam supports beyond a critical velocity value.

7.2 Quasi-static versus Dynamic Transverse Tensile Response of Low Density Foam Filled Tubes

Quasi-static transverse tests on foam filled specimens were completed at a crosshead speed of 18.8 mm/s until the tube experienced complete failure consistent with the methodology utilized for empty braided tube specimens. Within dynamic test trials, tube specimens incorporating group A and group B low density foam cores were impacted at incident velocities of 22.95 m/s to 23.12 m/s and 24.41 m/s to 25.27 m/s, respectively. The force versus displacement responses of group A and B low density rectangular core foam filled tube specimens as well as the findings collected from low density quasi-static tests are depicted within Figures A3 and A4 respectively. The energy displacement responses of group A and B specimens are depicted within Figures A5 and A6. The transverse deformation process of quasi-static test TFFT- $L\rho$ -RC-1 is depicted within Figure 29. The deformation processes of dynamic test FFTIA- $L\rho$ -RC-2-185.22 is depicted within Figure 16 and the deformation process of test FFTIB- $L\rho$ -RC-2-210.81 is

depicted within Figure 18. Tables 6 and 8 on pages 47 and 54 present the average force, FE, TEA, and SEA values for quasi-static and dynamic foam filled test trials respectively.

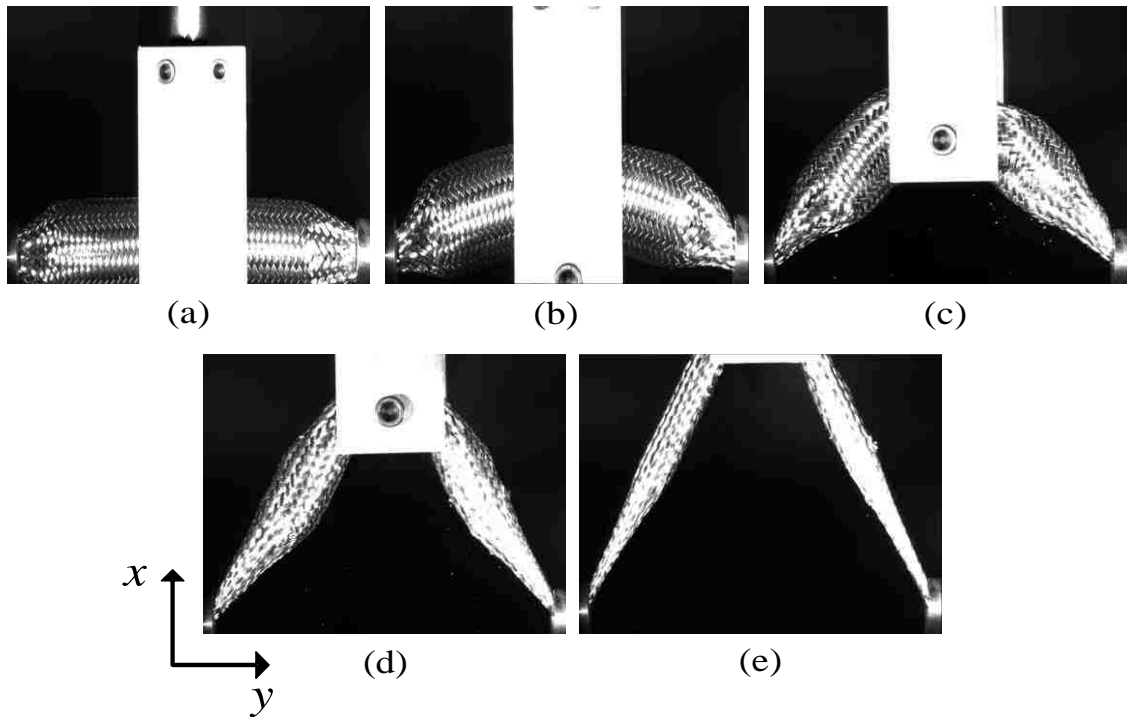


Figure 29: Quasi-static deformation process of low density foam filled braided tubes

It can be observed within Figures 16 and 18 that the dynamic loading process had a significant effect on the mechanical response of braided tubes incorporating both group A and B low density rectangular core specimens when compared to quasi-static low density rectangular foam tests. During quasi-static test trials, the measured response was

observed to increase in a relatively linear fashion up to roughly 1.5 kN of force and a corresponding transverse displacement of roughly 30 mm. Transverse displacement levels greater than roughly 35 mm resulted in the fracture of the interior foam core which was reflected as a very rapid drop within the measured response followed by a slow linear increase as the process of foam crushing through braid diametrical reduction was initiated as depicted within Figure 29 (b) and (c). The process of foam crushing was noted to occur over a displacement range of approximately 50 mm to 250 mm producing an average crushing force of 2.14 kN. Within dynamic impact test trials, immediately following the initial impact of the projectile, the measured response of low density foam filled tube specimens was observed to rapidly increase up to peak loads of roughly 4.5 kN and 5.5 kN for group A and B specimens, respectively, at an associated displacement level of approximately 40 mm. In addition to the more rapidly rising force levels observed within dynamic tests, significant fluctuations within the measured response were noted immediately upon impact as a result of localized pulverization of the interior core from penetration of the projectile as depicted within Figures 16 (b) and 18 (b). Displacement levels greater than roughly 40 mm resulted in the fracture of group A and B foam cores at the tube mid-span with continued foam collapse in the vicinity of the tube mid-span subsequent to fracture. The localized foam crushing at the tube mid-span induced by the impulse of the projectile was noted to produce elevated levels of absorbed energy early in the deformation process when compared to quasi-static test trials as depicted within Figures A5 and A6. For group A specimens the foam crushing process occurred over a displacement range of roughly 50 mm to 210 mm producing an average crushing force of 4.6 kN. The foam crushing process occurred over a displacement range

of approximately 60 mm to 230 mm for group B cores producing an average crushing force of 5.4 kN. Continued transverse loading beyond the foam crushing phase resulted in the measured response regaining a linear profile with minimal fluctuations within quasi-static and dynamic test trials as tow lockup was achieved throughout the tube length and braid tow wires experienced elastic/plastic deformation. A smaller degree of transverse elongation was required to initiate tube failure within dynamic test trials consistent with the observations noted for empty tube specimens. It is hypothesized that the observed reduction in displacement is a result of the same mechanisms noted for empty tube specimens. Tube failure was noted to initiate on the contacting surface of the braided tube specimen within the vicinity of the annular clamp for both quasi-static and dynamic test trials.

Examination of the metrics listed within Tables 6 and 8 for dynamic and quasi-static test trials revealed that the increased loading rate within dynamic test trials influenced the energy absorbing performance of the structure. Quasi-static test trials produced average force and average FE values of 11.8 kN and 17% respectively. Dynamically impacted low density foam filled tube specimens produced average force and average FE values of 8.24 kN and 14.94% for group A specimens and 8.85 kN and 16.31% for group B specimens. A roughly 47% and 41% reduction in TEA performance was noted for group A and B low density foam specimens respectively when compared to low density quasi-static transverse tests.

7.3 Quasi-static versus Dynamic Transverse Tensile Response of Medium Density Foam Filled Tubes

Dynamic transverse impact test trials on medium density foam filled braided tube specimens were completed at incident projectile velocities ranging from 25.63 m/s to 26.64 m/s and 26.03 m/s to 26.93 m/s for group A and B specimens respectively. The dynamic force versus displacement response of group A medium density cores is plotted alongside the force versus displacement response of quasi-statically tested low density foam cores within Figure A7. The dynamic force versus displacement response of group B medium density foam cores is plotted alongside the force versus displacement response of quasi-statically tested high density foam core specimens within Figure A8. The energy displacement responses of group A and B medium density cores are shown within Figures A9 and A10 respectively. The transverse deformation process of quasi-static test FFT-H ρ -RC-1 is depicted within Figure 29.

Upon impact, the force displacement response of dynamically loaded braided tube specimens incorporating medium density group A cores increased in a relatively linear fashion up to a peak load of approximately 8 kN and a corresponding transverse displacement of roughly 30 mm. A significant degree of fluctuation within the measured response was noted as a result of the localized pulverization of the interior foam core at the tube mid-span initiated by the penetration of the projectile as depicted within Figure 20 (b). Transverse displacement levels beyond 30 mm resulted in fracture of the interior core at the tube mid-span with continued localized foam crushing present at the mid-span subsequent to core fracture. The rapidly rising force levels coupled with the localized foam crushing at the tube mid-span resulted in braided tube specimens incorporating

medium density group A cores absorbing energy at faster rate than low density foam filled braided tube specimens tested quasi-statically in the early stages of deformation as depicted within Figure A9. The foam crushing process of medium density group A cores was noted to occur over a displacement interval of roughly 50 mm to 230 mm producing an average crushing force of 5.62 kN. Braided tube specimens incorporating medium density group A cores exhibited a similar measured response to quasi-statically tested low density foam filled tube specimens subsequent to core fracture. However, failure of group A specimens was noted to initiate at displacement levels approximately 100 mm less than those observed during low density foam quasi-static tests. Consistent failure behavior was observed within low density quasi-static tests and medium density group A tests with braid failure initiating on the non contacting surface of the tube in the vicinity of the annular clamp. Dynamically impacted braided tube specimens incorporating group B medium density cores experienced a rapid increase within the measured force response upon impact with force levels reaching up to 25 kN at a corresponding displacement of roughly 20 mm prior to core fracture. In addition to the rapid rise in force, medium density group B cores exhibited very little fluctuation within the measured response prior to and following fracture of the interior core due to a minimal amount of localized foam collapse present at the tube mid-span resulting from the increased mechanical strength of the core. The measured response of quasi-statically tested high density aluminum foam filled braided tube specimens was observed to increase in a linear, more gradual fashion than group B cores up to a peak load of roughly 8 kN at a corresponding transverse displacement of roughly 45 mm. Minimal fluctuations within the measured response were noted prior to and immediately following the fracture of the interior core consistent

with the behavior observed within group B medium density impact tests. The foam crushing process occurred over a displacement interval of roughly 50 mm to 200 mm and 80 mm to 200 mm within high density quasi-static foam filled tests and group B medium density impact tests producing respective average crushing forces of 10.5 kN and 15.2 kN. Braid failure was noted to initiate at transverse displacement levels approximately 150 mm less than those observed within quasi-static high density foam core test trials.

Quasi-statically tested low density foam filled braided tube specimens performed comparably in terms of FE performance to dynamically impacted medium density group A specimens producing average FE values of 17.1% and 18.72% for quasi-static and dynamic tests respectively. The 100 mm reduction in transverse displacement required to initiate braid failure observed within group A impact tests was noted to produce an average reduction in TEA and SEA performance of roughly 1.36 kJ and 0.47 kJ/kg respectively when compared to low density quasi-static tests. The 150 mm reduction in transverse displacement required to initiated braid failure within dynamically loaded medium density group B specimens resulted in a significant reduction in average TEA and SEA performance of 5.45 kJ and 1.42 kJ/kg compared to high density quasi-statically tested specimens.

7.4 Quasi-static versus Dynamic Transverse Tensile Response of High Density Foam Filled Tubes

Dynamic impact test trials on high density foam filled braided tube specimens were completed at incident projectile velocities ranging from 27.52 m/s to 28.37 m/s and 25.8 m/s to 26.96 m/s for group A and B specimens respectively. The force versus

displacement responses of group A and B high density rectangular core foam filled tube specimens as well as the findings collected from low high quasi-static tests are depicted within Figures A11 and A12 respectively.

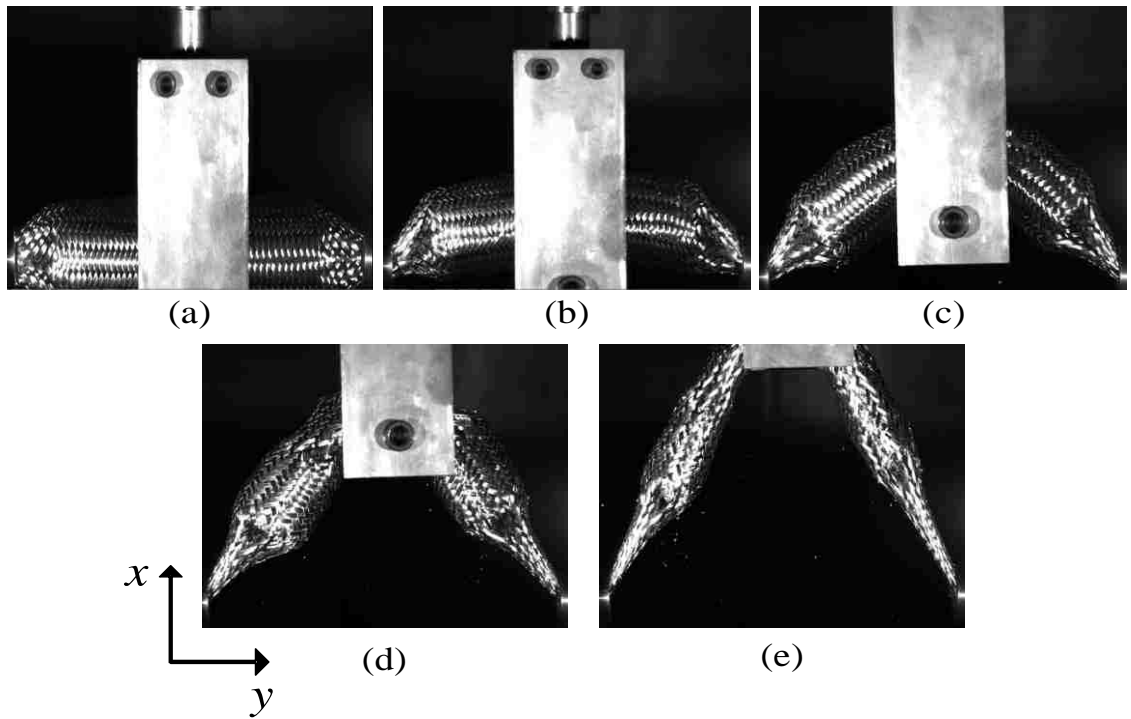


Figure 30: Quasi-static deformation process of high density foam filled braided tubes

The measured responses of dynamically impacted braided tube specimens incorporating group A and B high density foam cores were noted to exhibit similar behavior to that observed within quasi-static test trials completed on high density foam filled specimens. Minimal localized foam collapse at the tube mid-span within the immediate contact area was noted in both quasi-static as well and dynamic impact test trials. The absence of foam collapse resulted in the measured force response possessing a relatively smooth profile prior to the initiation of foam crushing through braid diametrical reduction. Force levels increased much more rapidly within dynamic impact test trials prior to the initial fracture of the interior foam core at the tube mid-span. Force levels were noted to reach 17 kN at a displacement of 25 mm and 27 kN at a displacement of 15 mm for group A and B specimens respectively. Subsequent to the fracture of the foam core, dynamically and quasi-statically tested high density foam filled tube specimens responded in a similar fashion with a rapid drop within the measured response. The increased loading rate utilized within dynamic impact test trials was noted to produce a negative effect on the foam crushing process compared to that observed for quasi-statically tested braided tube specimens. Braided tube specimens incorporating group A cores experienced foam crushing over a displacement interval or roughly 80 mm to 225 mm producing an average crushing force of 15.87 kN however, the core was crushed to a lesser extent than that observed within quasi-static test trials. Braided tube specimens incorporating group B cores experienced only minimal foam crushing as a result of the robust mechanical strength of the core mitigating the desired tow scissoring effect. Transverse displacement levels beyond roughly 70 mm resulted in tensile tearing of the braid at the tube mid-span as depicted within Figure 26 (e). In addition to the reduction in foam crushing

performance, early initiation of braid failure was noted for tube specimens incorporating group A and B high density foam cores when compared to quasi-static transverse tensile tests. Braid failure was noted to initiate at transverse displacement levels roughly 130 mm and 150 mm less than those observed within quasi-static test trials for group A and B specimens respectively.

The reduction in foam crushing experienced within dynamic impact test trials resulted in a significant reduction in TEA and SEA performance compared to quasi-statically tested tube specimens. Tube specimens incorporating group A high density foam cores experienced an average reduction in TEA and SEA performance of 5.49 kJ and 1.54 kJ/kg compared to quasi-statically tested high density cores while group B specimens exhibited a reduction in TEA and SEA values of 5.45 kJ and 1.42 kJ/kg.

8.0 VARIABILITY ANALYSIS OF DYNAMIC IMPACT TEST RESULTS

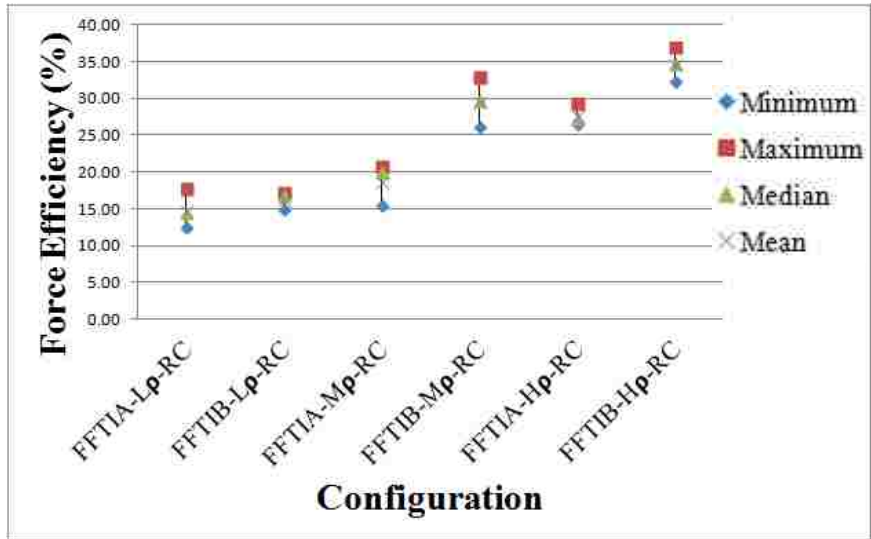
A brief variability analysis of the transverse dynamic impact results on foam filled braided tube specimens listed within Table 6 is completed within this chapter. The plots presented within this section list the FE, TEA, and SEA values for a given foam core density. The plots presented within Figure 31 list the maximum, minimum, median, mean, as well as range bars which indicated the difference between the maximum and minimum values for each given testing configuration.

8.1 Transverse Impact Tests of Rectangular Foam Filled Tube Specimens

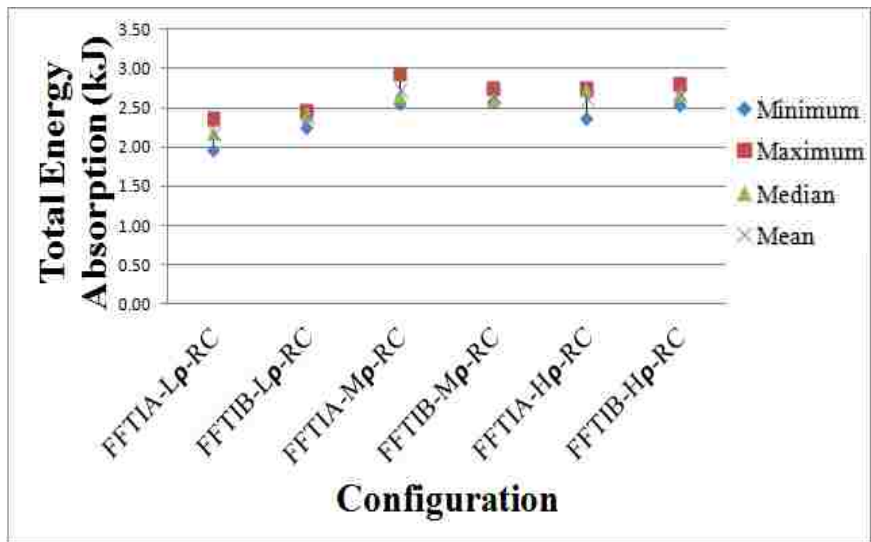
From Figure 31(a) it can be observed that both low density group A and B foam cores as well as medium density group A cores exhibited a lower mean FE value than medium density group B and high density foam core specimens. This trend is anticipated as braided tube specimens incorporating foam specimens of density levels ranging from approximately 179.22 kg/m^3 to 357.60 kg/m^3 were observed to experience more thorough foam crushing compared to high density cores resulting in a reduced average force as a result of sustained foam collapse through a larger portion of the displacement domain. The degree of variation within TFE values for all foam filled dynamic impact tests was relatively small regardless of the interior core density. Braided tube specimens incorporating low density group B cores exhibited the smallest degree of variation within the collected test data with TFE values ranging from 15.01% to 17.21 % and a mean TFE value of 16.31%. Medium density group B cores exhibited the highest degree of variation within TFE results with values ranging from 26.29% to 32.89% and a mean value of 29.60%.

Figure 31(b) presents the total energy absorbed (TEA) values for each testing configuration. It can be observed within Figure 31(b) that all test specimens tested under transverse impact produced very repeatable TEA results. The largest degree of variation with TEA results was observed within results from medium density and high density group A cores. It is hypothesized that the larger degree of variation observed within TEA values collected from medium and high density group A cores is associated with the process of foam crushing. Although foam crushing through the action of braid diametrical reduction was successfully achieved within each of the aforementioned groups, the core was not completely pulverized throughout the entire tube length during the impact event. As such, the amount of energy absorbed within each respective test will be dependent on factors governing the extent of foam crushing such as irregularities within the cellular structure of the interior foam core.

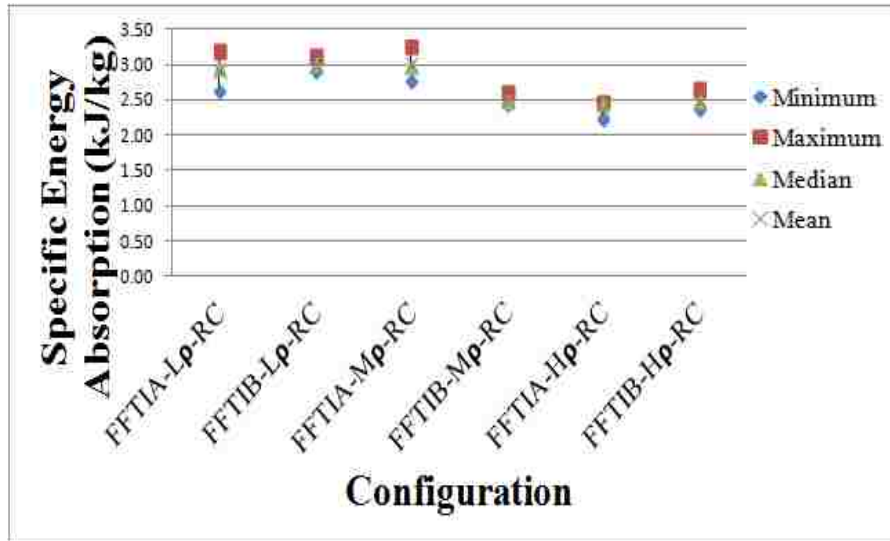
The specific energy absorption (SEA) values for each testing configuration are presented within Figure 31(c). SEA values were noted to be fairly consistent for all foam densities tested. Foam specimens incorporating medium density group B cores as well as both group A and B high density cores were noted to experience an approximate 0.5 kJ/kg decrease in mean SEA values compared to group A and B low density as well as group A medium density cores.



(a)



(b)



(c)

Figure 31: Minimum, maximum, mean, and median values of metrics computed from foam filled impact test trials (a) FE, (b) TEA, and (c) SEA

9.0 Potential Applications of Aluminum Foam Filled Braided Stainless Steel Tubes

The aluminum foam filled braided stainless steel tubes examined within this study have a wide range of potential applications. Within personal safety equipment, these tubes have the potential to be integrated into devices such as fall arrest systems to assist in decelerating personal safely after a fall. Additionally, due to their ability to provide the benefits of energy absorption under both an axial and transverse mode of deformation as well as the ability to scale the structure for a required application, foam filled braided tubes would be well suited for integration within road barriers as well as containment vessels such as those surrounding a turbine. Finally, if the braided stainless steel and aluminum foam combination was not well suited for a particular application the structure can be further modified through the implementation of a difference interior foam or exterior braid material.

10.0 CONCLUSIONS

10.1 Conclusions for Transverse Dynamic Impact Test Trials

The 5 research objectives outlined within Section 3.0 have been successfully completed within this research study. The mechanical response of empty and aluminum foam filled braided stainless steel tube specimens subjected to transverse impact loads were examined within this study through the collection of both measured and visual test data (objectives 1 and 2). Integration of a high speed DAQ system within the projectile permitted collection of force data within a previously unexplored loading condition. Digital image data was utilized to examine the tow kinematics as well as the deformation and failure mechanisms associated with the transverse impact deformation process (objectives 3 and 4). The primary findings from dynamic impact test trials are as follows:

1. Empty braided tube specimens were observed to fail within the vicinity of the annular clamps on the non-contacting surface of the braided tube. Failure of empty tube specimens was noted to initiate within the vicinity of the clamps as a result of the larger degree of tow scissoring and localized bending present within the clamp region. Failure was noted to initiate at either the left or right clamp with no observed pattern.
2. Foam filled braided tube specimens incorporating group A and B low density rectangular foam cores failed in a similar fashion with an observed load softening effect followed by a rapid increase in the measured load upon initiation of tube failure. Thorough foam crushing was observed within both group A and B low foam tests with foam crushing occurring to a greater

extent within the mid-span and annular clamp regions as a result of the localized bending and stacking of braid tows observed within those regions. The presence of crushed foam within the tube resulted in tube failure initiating on the non-contacting surface of the braided tube within the annular clamp region.

3. The average TEA for specimens containing low density group A and B cores was determined to be 2.18 kJ and 2.40 kJ respectively.
4. The average FE and SEA values for group A low density core specimens were determined to be 14.94% and 2.93 kJ/kg while the average FE and SEA values were determined to be 16.31% and 3.01 kJ/kg for group B specimens.
5. Braided tube specimens incorporating medium density group A cores exhibited consistent foam crushing behavior within each test as well as a load softening effect upon the onset of tube failure similar to that observed within low density foam tests. Medium density group B specimens exhibited a higher degree of variability in foam crushing behavior between tests resulting from the presence of an interaction effect between the braid and interior foam core.
6. The average TEA for specimens containing medium density group A and B cores was determined to be 2.18 kJ and 2.40 kJ respectively
7. The average FE and SEA values for group A medium density core specimens were determined to be 18.72% and 3.00 kJ/kg while the average FE and SEA values were determined to be 29.60% and 2.51 kJ/kg for group B specimens.

8. Group A high density foam filled braided tube specimens successfully achieved foam crushing though braid diametrical reduction despite the presence of a minor undesired effect at the tube mid-span. The solid construction and small cell size of group B cores resulted in tearing of the braided tube early in the deformation process at the tube mid-span. The tearing of the braid initiated by the shifting of the core fragments upon fracture was observed to be the primary mechanism of energy absorption for group B high density cores.
9. The average TEA for specimens containing high density group A and B cores was determined to be 2.63 kJ and 2.69 kJ respectively. Average FE and SEA values for group B high density core specimens were determined to be 27.72% and 2.39 kJ/kg while average FE and SEA values for group B high density core specimens were determined to be 34.64% and 2.51 kJ/kg.
10. Experimental observations suggest that use of aluminum foam core specimens above density levels of roughly 450 kg/m³ generate an undesired effect upon fracture of the core, which is detrimental to tube performance.

Finally, research objective 5 was completed through the completion of a preliminary comparison of the data collected within dynamic impact test trials and the transverse test data collected within the quasi-static transverse tests completed within [18]. The primary findings from the comparison are as follows:

11. Empty braided tube specimens demonstrated fairly consistent behavior within both quasi-static and dynamic test trials with peak force levels reaching

roughly 40 kN. Braid failure was initiated on the non contacting surface of the tube within the vicinity of the annular clamps within both quasi-static and dynamic impact tests. The increased loading rate within dynamic test trials produced a 15 mm reduction in transverse displacement required to initiate tube failure. The reduction in transverse elongation resulted in an average reduction in TEA performance of 0.68 kJ for dynamically impacted empty tubes.

12. Low density foam filled braided tube specimens displayed similar behavior within quasi-static and dynamic impact test trials. Dynamically impacted low density tube specimens exhibited greater levels of absorbed energy prior to fracture of the interior core due to the presence of localized foam collapse within the vicinity of impact. An approximate 1.91 kJ and 1.69 kJ reduction in TEA performance of 1.91 kJ and 1.69 kJ was noted for tube specimens from group A and B low density cores when compared to quasi-static tests.

13. Dynamically impacted braided tube specimens incorporating medium density group A and B cores experienced a respective 100 mm and 150 mm reduction in transverse displacement required to initiate failure when compared to quasi-static transverse tests. The reduction in transverse displacement observed within dynamic test trials produced a reduction in TEA and SEA performance of 1.36 kJ and 0.47 kJ/kg, and 5.46 kJ and 1.42 kJ/kg for group A and B cores respectively.

14. A significant reduction in foam crushing was noted within dynamic impact test trials on tubes incorporation both group A and B high density foam cores when compared to high density quasi-static tests. The robust mechanical strength of group B cores mitigated the desired tow scissoring effect resulting in braid tearing at the tube mid-span. The lesser degree of foam crushing combined with the early initiation of braid failure resulted in a reduction in TEA and SEA performance of 5.49 kJ and 1.54 kJ/kg for group A core and 5.45 kJ and 1.42 kJ/kg for group B cores compared to high density quasi-static transverse tests.

RECOMMENDATIONS FOR FUTURE WORK

Based on the findings collected from this research study the following recommendations are presented to further understand the potential of aluminum foam filled braided stainless steel tubes.

1. Investigate a wider variety of interior foam core geometrical configurations such as sectioned cores. Investigating alternatives such as a sectioned core offers the potential to further tailor the mechanical response of the structure by minimizing the bending stiffness of the structure immediately upon impact.
2. Perform an optimization study to determine the optimum density and geometry of interior aluminum foam to maximize the amount of energy absorbed through the action of foam crushing. A study of this nature would be very beneficial as it could significantly improve the performance of the structure under both quasi-static and dynamic loading conditions.
3. Investigate the implementation of alternative braid and foam combinations. The use braid materials woven from alternative metallic alloys should be investigated in an attempt to minimize the loading rate sensitivity of the structure. Additionally, more extensive material testing could be completed on the existing structure could be completed to quantify the effects of the increased loading rate experienced during dynamic test trials such as the confirmation of the formation of martensite within failed braid tow wires.

ACKNOWLEDGEMENTS

The financial support of the Natural Science and Engineering Research Council of Canada (NSERC) as well as the Ontario Graduate Scholarship (OGS) program is gratefully acknowledged.

REFERENCES

- [1]. SMARTRISK. (2009). The Economic Burden of Injury in Canada. SMARTRISK: Toronto, Ontario.
- [2]. (2015, March 25). Quick facts and statistics. Retrieved from <http://www.parachutecanada.org>
- [3]. (2015, March 25). Young Worker Focus Report. Retrieved from http://www.worksafebc.com/publications/reports/focus_reports/
- [4]. IHSA. (2013). IHSA Member Injury Performance for 2013. IHSA.ca
- [5]. Wilkins. K and Mackenzie. S G, (2015, March 25). "Work Injuries". Retrieved from <http://www.statcan.gc.ca>
- [6]. iCasualties.org. IED Fatalities, 2009.
- [7]. Ramasamy A, Hill AM, Masouros S, Gibb I, Phillip R, Bull AM, et al. "Outcomes of IED foot and angle blast injuries". *J Bone Joint Surg Am* 2013;95:1–7
- [8]. World Health Organization (WHO), Global Status Report on Road Safety 2013, Retrieved from <http://who.int>
- [9]. "Magnesium Vision 2020: A North American Automotive Strategic Vision for Magnesium" Automotive Metals Division, United State Automotive Materials Partnership (USAMP) (December 2004).

- [10]. Mutua J. M., Kihiu J.M., Rading G.O., "Use of magnesium alloys in optimizing the weight of automobile: Current trends and opportunities", Sustainable research and innovation, vol. 2, p. 2, 2010.
- [11]. Wagner. D.A., Logan. S.D., Wang. K, Skszek. T, Salisbury. C.P., "Test results and FEA predictions From Magnesium AM30 Extruded Beams in Bending and Axial Compression", TMS The Minerals, Metals and Materials Society (2009)
- [12]. Majumder. A, Altenhof. W, Vijayan. V and Jin. S.Y., "Quasi-static axial cutting of AA6061 T4 and T6 round extrusions", Journal of Materials Design and Applications, 222 (2008), 183-195.
- [13]. Jin. S.Y., Altenhof. W, Li. Z, " A parametric study on extrusion geometry and blade quantity during axial cutting deformation of circular AA6061-T6 extrusions under impact and quasi-static loading", International Journal of Impact Engineering, 49 (2012), 165-178.
- [14]. Hall. I.W., Guden. M, Claar, T.D., "Transverse and longitudinal crushing of aluminum - foam filled tubes", Scripta Materialia, Volume 46, Number 7, 11 April 2002, pp. 513-518(6)
- [15]. A&P Technology Inc. Frequently asked questions. Available from: (<http://www.braider.com>) [accessed in March 2015].
- [16]. Altenhof. W, Powell. C, Harte. A.M., Gaspar. R, "An experimental investigation into the energy absorption and force/displacement characteristics of aluminum foam filled braided stainless steel tubes under quasi-static tensile loading conditions", Int J Crashworthiness 2005;10(1):21–31.

- [17]. Cheng. Q, Altenhof. W, Jin. S.Y., Powell. C, Harte. A.M., "Energy absorption of aluminum foam filled braided stainless steel tubes under quasi-static tensile loading conditions", *Int J Mech Sci* 2006;48:1223–33.
- [18]. Audysho. R, Smith. R, Altenhof. W, Patel. K, "Aluminum foam core density and geometry influences on the deformation mechanisms of foam filled braided tubular structures in tension", *Materials & Design*, Vol. 54 (2014), pp. 394–413.
- [19]. Audysho. R, Smith. R, Altenhof. W, "Mechanical assessment and deformation mechanisms of aluminum foam filled stainless steel braided tubes subjected to transverse loading, *Thin-Walled Structures*", Vol. 79 (2014), pp. 95–107.
- [20]. Jenq. S.T. and Mo. J, "Ballistic impact response for two-step braided three-dimensional textile composites", *AIAA Journal*, Vol. 34, No. 2 (1996), pp. 375-384.
- [21]. Gong. J.C. and Sankar. B.V., "Impact Properties of Three-Dimensional Braided Graphite/Epoxy Composites", *Journal of Composite Materials*, Vol. 25, No. 2 (1991), pp. 15-731.
- [22]. Gning. P.B, Tarfaoui. M, Collombet. F, Riou. L, Davies. P, "Damage development in thick composite tubes under impact loading and influence on implosion pressure: experimental observations", *Composites: Part B*, Vol. 36, No. 4 (2005), pp. 306–318.
- [23]. Karbhari. V.M., Haller. J.E., Falzon. P.K., Herszberg. I, "Post-impact crush of hybrid braided composite tubes", *International Journal of Impact Engineering*, Vol. 22, No. 4 (1999), pp. 419-433.

- [24]. Zhang. Y, Jiang. L, Sun. B, Gu. B, "Transverse impact behaviors of four-step 3-D rectangular braided composites from unit-cell approach", *Journal of Reinforced Plastics and Composites*, v 31, n 4 (2012), p 233-46.
- [25]. Borvik T, Hopperstad O S, Reyes A, Langseth M, Solomos G, and Dyngeland T., "Empty and foam filled circular aluminum tubes subjected to axial and oblique quasi static loading". *International Journal of Crashworthiness*, 2003; 8:5:481-494.
- [26]. Bambach. M.R., Jama. H, Zhao. X.L., Grzebieta. R.H., "Hollow and concrete filled steel hollow sections under transverse impact loads", *Engineering Structures*, Vol. 30, No. 10 (2008), pp. 2859–2870.
- [27]. Kavi. H, Toksoy. A, Guden. M, "Predicting energy absorption in a foam-filled thin-walled aluminum tube based on experimentally determined strengthening coefficient", *Materials and Design*, v 27, n 4 (2006), p 263-269.
- [28]. Zarei. H, Kroger. M, "Crashworthiness Investigation and Optimization of Empty and Foam Filled Composite Crash Box", *Woven Fabric Engineering*, p 343-62, 2010
- [29]. Gu B, Li Y. "Ballistic Perforation of Conically Cylindrical Steel Projectile into Three-Dimensional Braided Composites", *AIAA Journal*, 2005;43
- [30]. Lipa. S and Kotelko. M, "Lateral Impact of Tubular Structure – Theoretical and Experimental Analysis. Part 1 – Investigation of Single Tube", *Journal of Theoretical and Applied Mechanics*, Vol. 51, No. 4 (Warsaw 2013), pp. 873-882.
- [31]. Zeng. T, Fang. D, Lu. T, "Dynamic crashing and impact energy absorption of 3D braided composite tubes". *Materials Letters* 59 (2005) 1491–1496

- [32]. Xcitex Inc., ProAnalyst User's Manual, Cambridge, MA, USA, 2004.
- [33]. Cymat Technologies Ltd., Aluminum Foam Technology Applied to Automotive Design, Mississauga, Ontario, Canada, 2002.
- [34]. Ashby. M, Evans. A, Fleck. N, Gibson. L, Hutchinson. J.W, Wadley. H.N.G, "Metal foams – a design guide", Burlington, MA: Butterworth-Heinemann (2000), pp. 8–9.
- [35]. Harte. A.M, and Altenhof. W, "Uses for stabilized aluminum foam in crashworthiness and strengthening applications", SAE paper no. 2003-01-1295. Society of Automotive Engineers, (2003).
- [36]. PTC Inc., Mathcad User's Manual, Needham, MA, USA, 1985.
- [37]. PCB Piezotronics, Inc., Model 203B ICP® quartz force ring, 20k lb comp., 0.25 mV/lb Installation and Operating Manual, 2014.
- [38]. Lino. Y, Svejcar. J, Dlouhy. L, Forejt. M, "Effects of Strain Rate 10^{-4} to 10^3 on Room Temperature Tensile Properties and Notched Plastic Zone of Type 304 Stainless Steel", Paper presented at 17th European Conference on Fracture, 2-5 September, 2008, Brno, Czech Republic.
- [39]. Menkes, S.B and Opat, H. J., "Broken beams", Experimental Mechanics, 13 (1973), pp. 480-486.

APPENDIX A: QUASI-STATIC AND DYNAMIC TRANSVERSE TEST DATA

COMPARISON

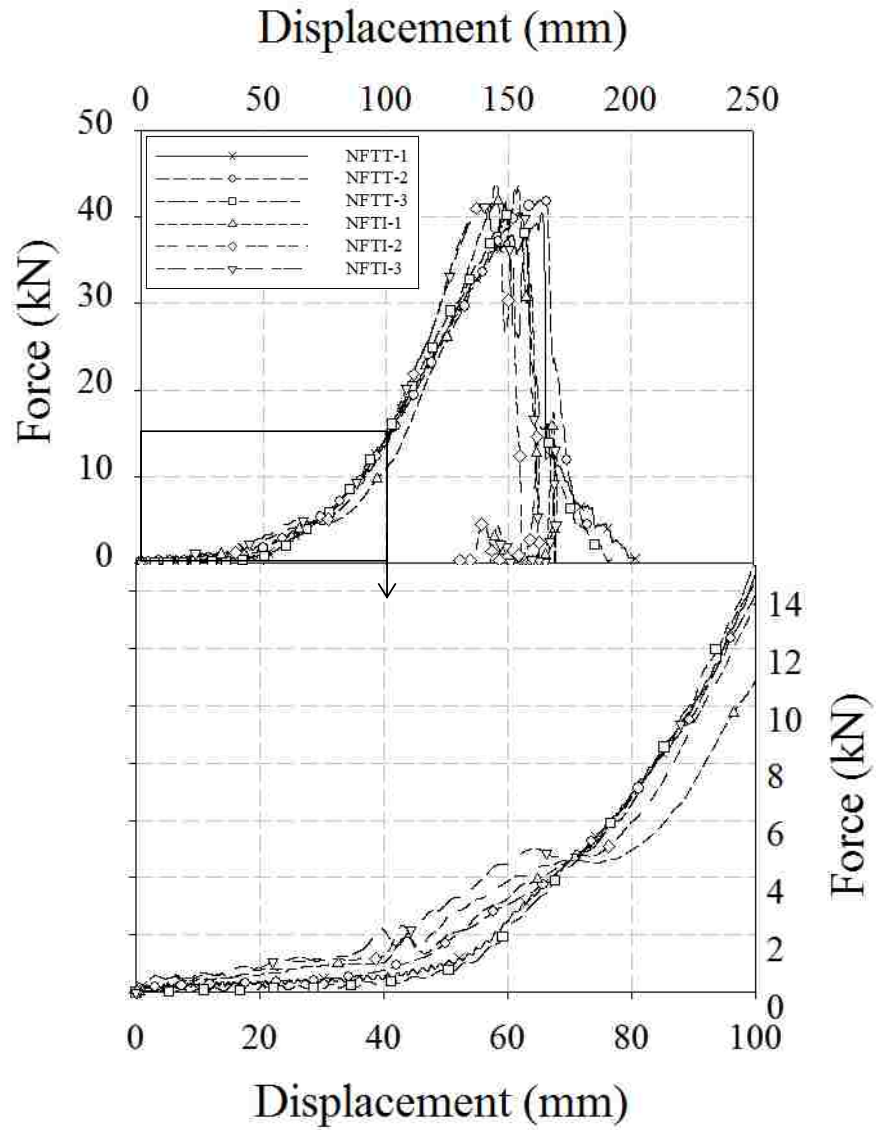


Figure A1: Force/displacement response of empty braided tubes

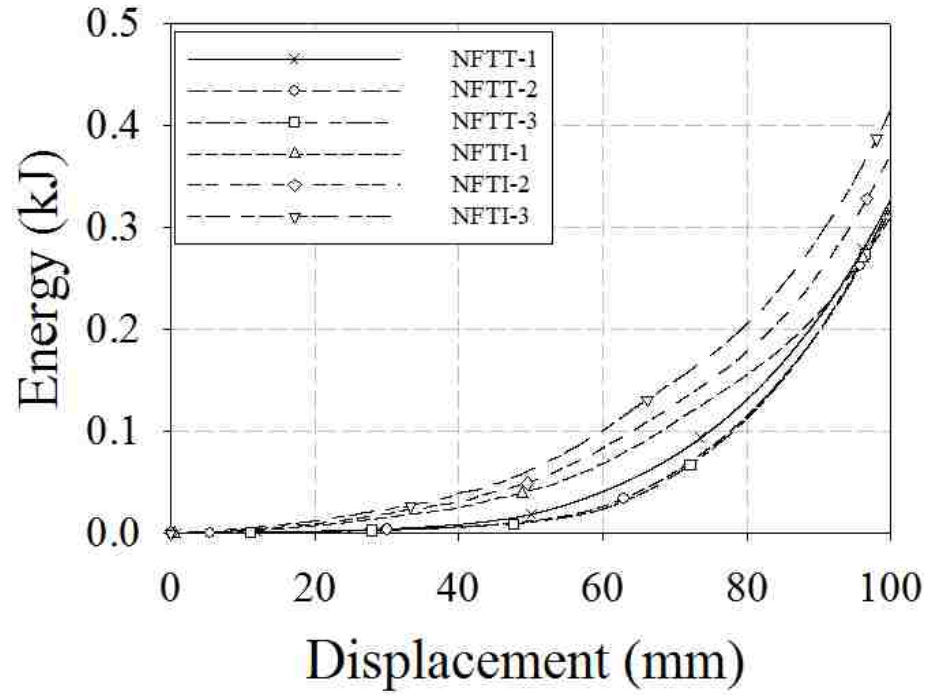


Figure A2: Energy/displacement response of empty braided tubes

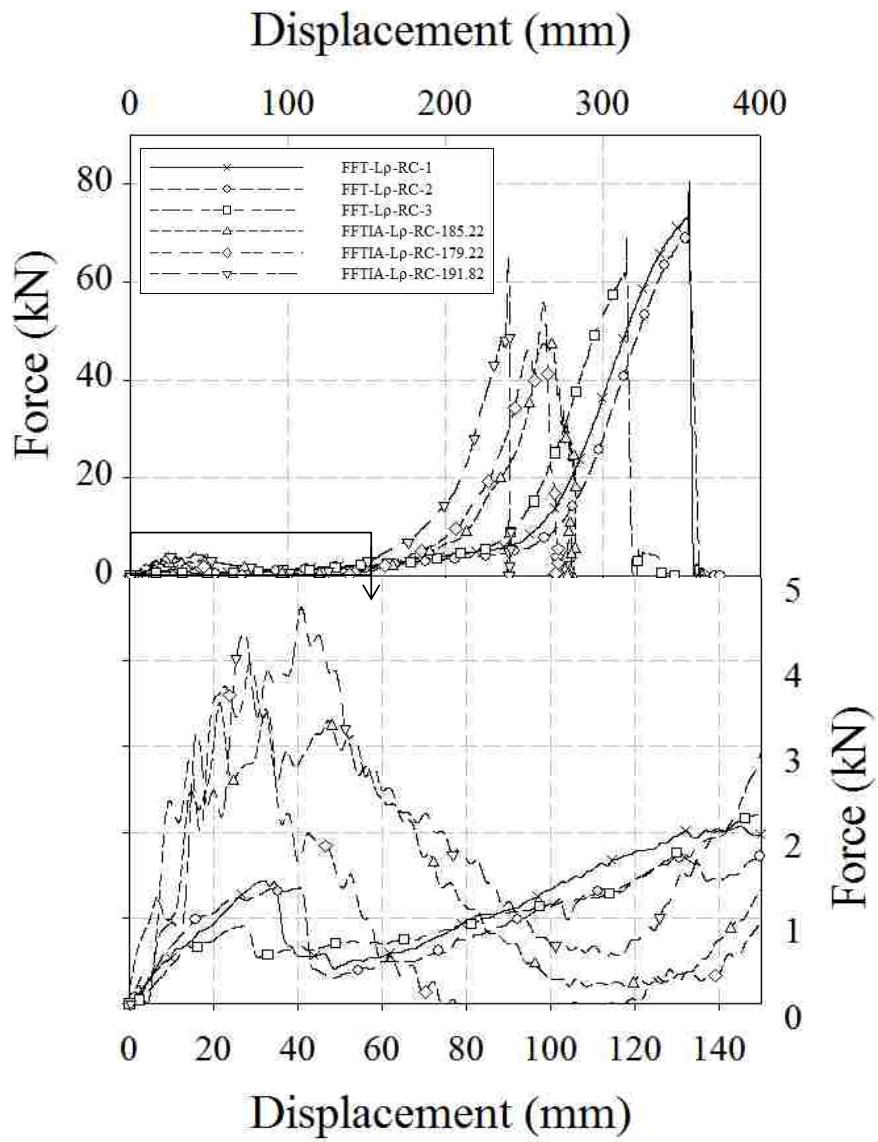


Figure A3: Force/displacement response of low density group A cores

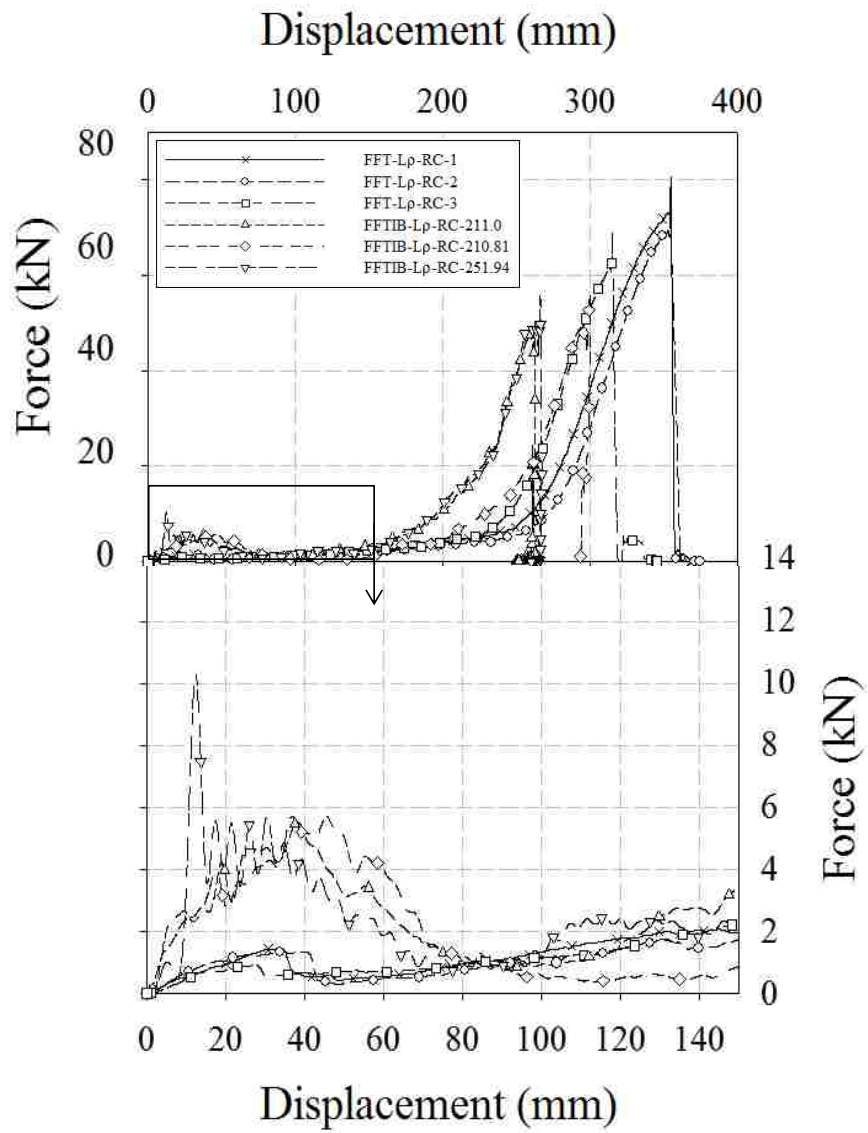


Figure A4: Force/displacement response of low density group B cores

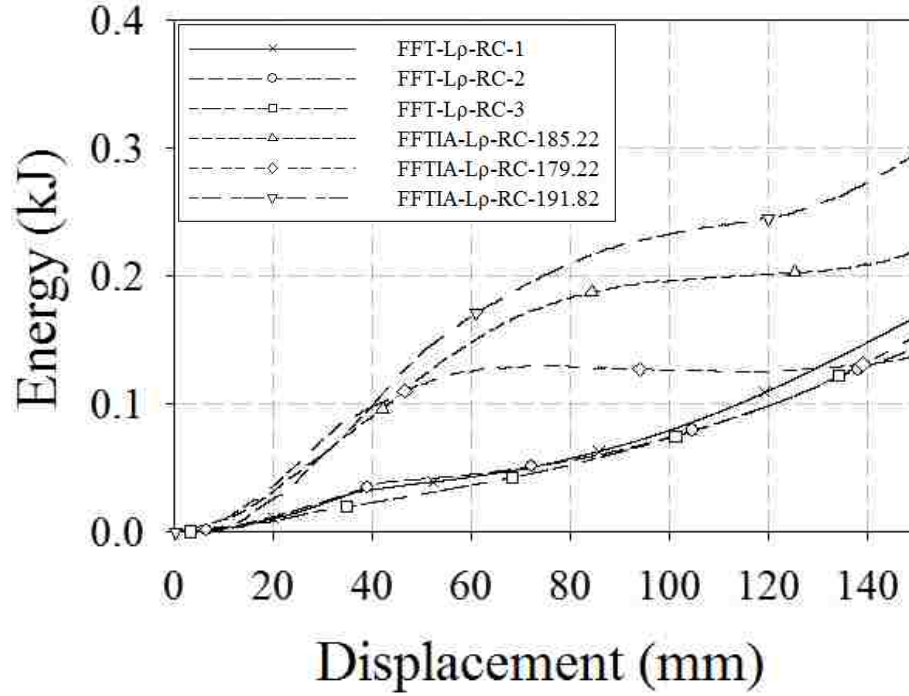


Figure A5: Energy/displacement response of low density group A cores

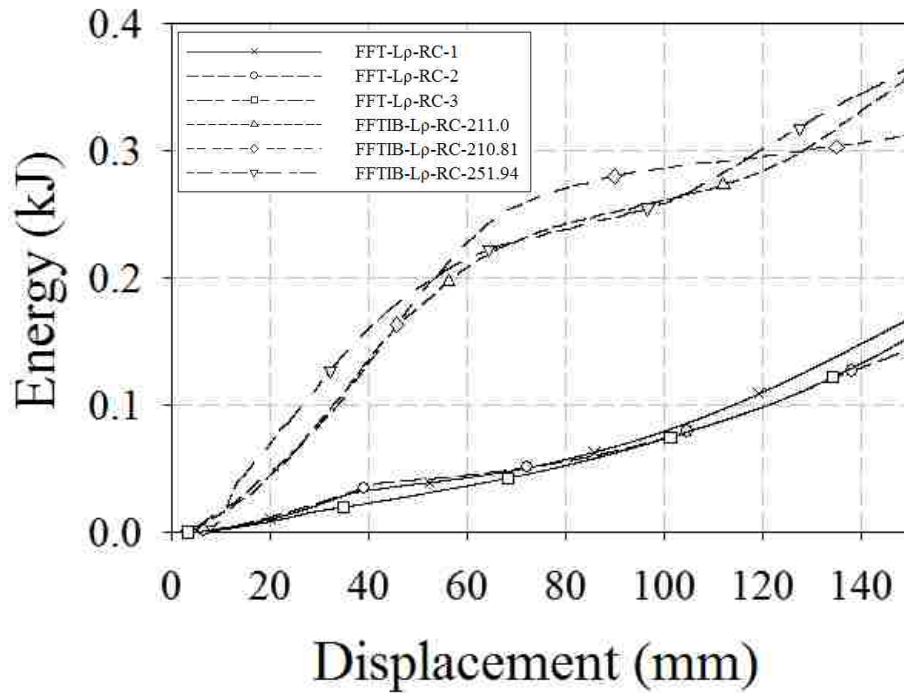


Figure A6: Energy/displacement response of low density group B

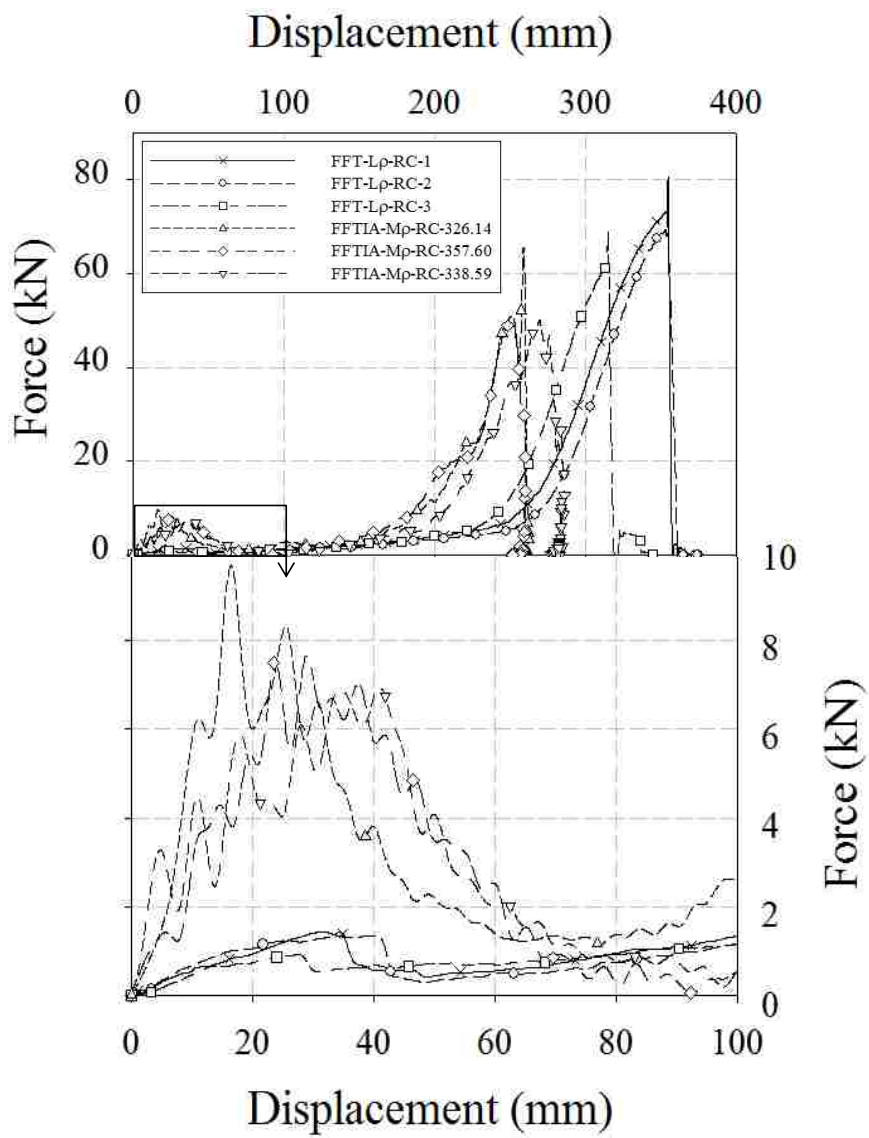


Figure A7: Force/displacement response of medium density group A cores

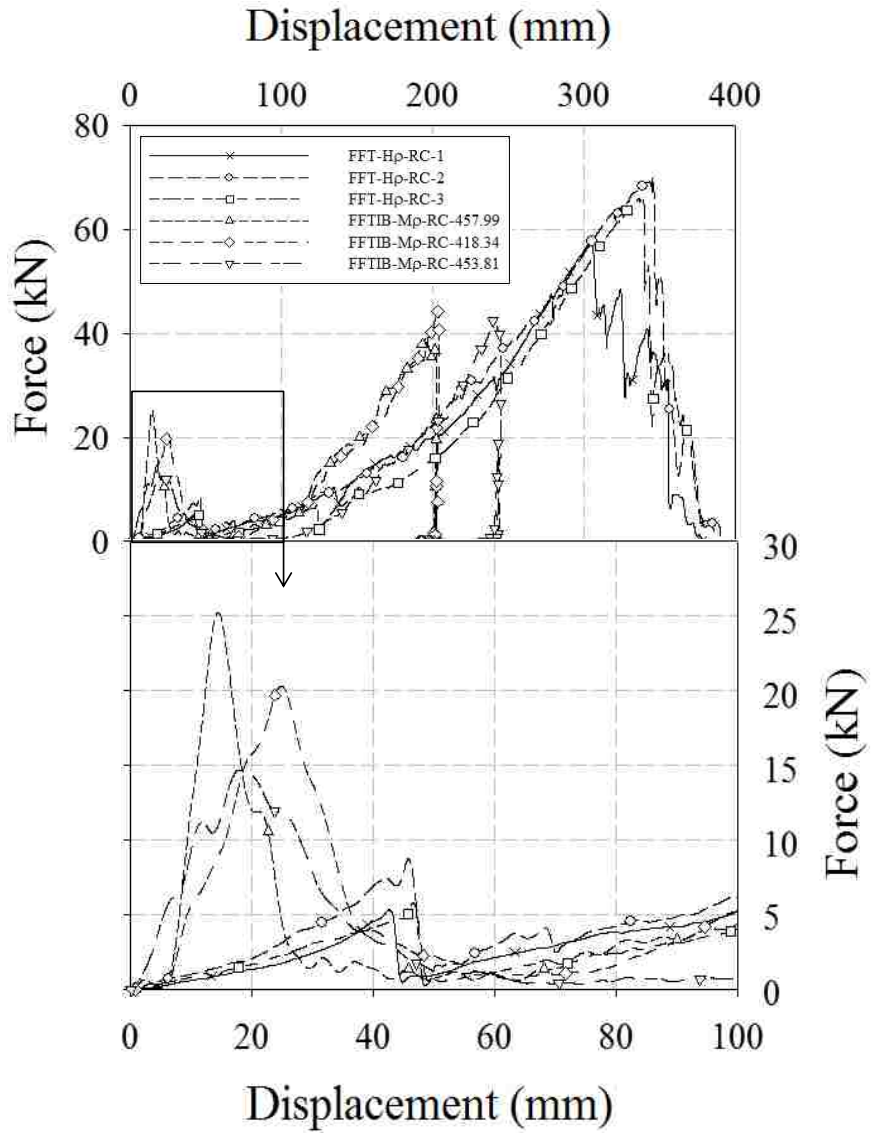


Figure A8: Force/displacement response of medium density group B cores

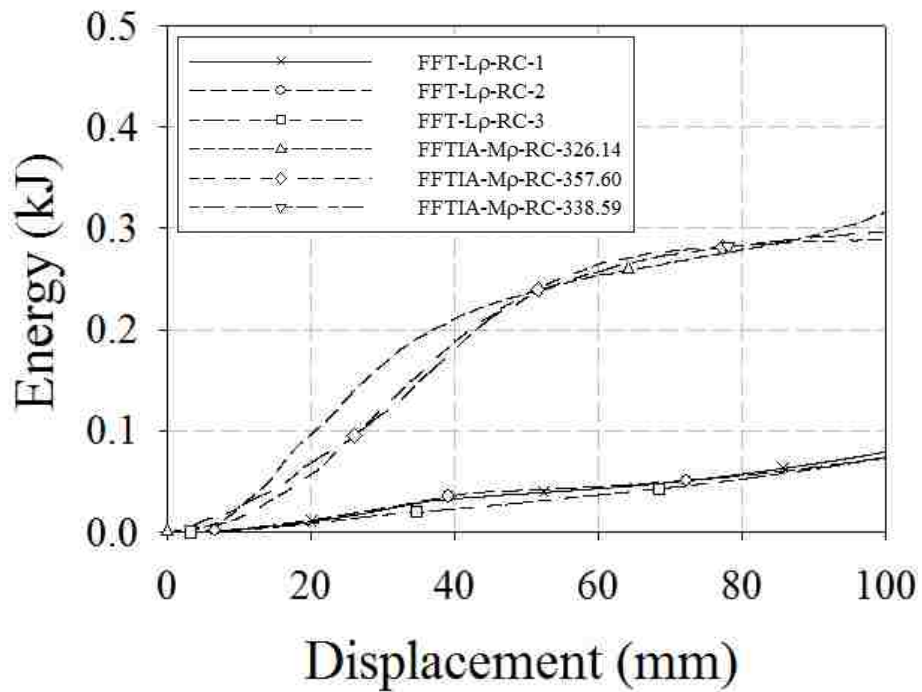


Figure A9: Energy/displacement response of medium density group A cores

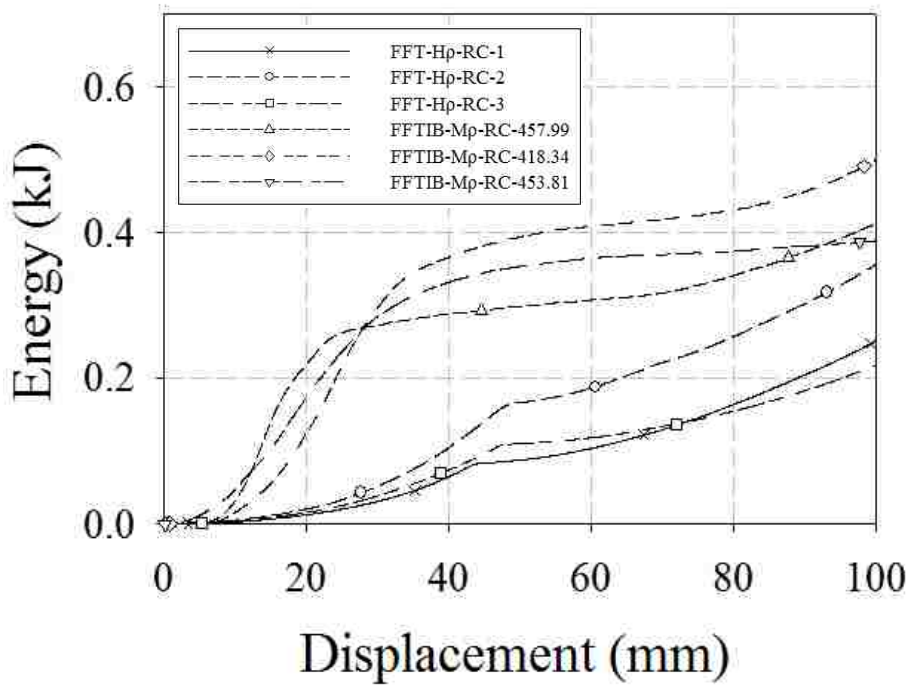


Figure A10: Energy/displacement response of medium density group B

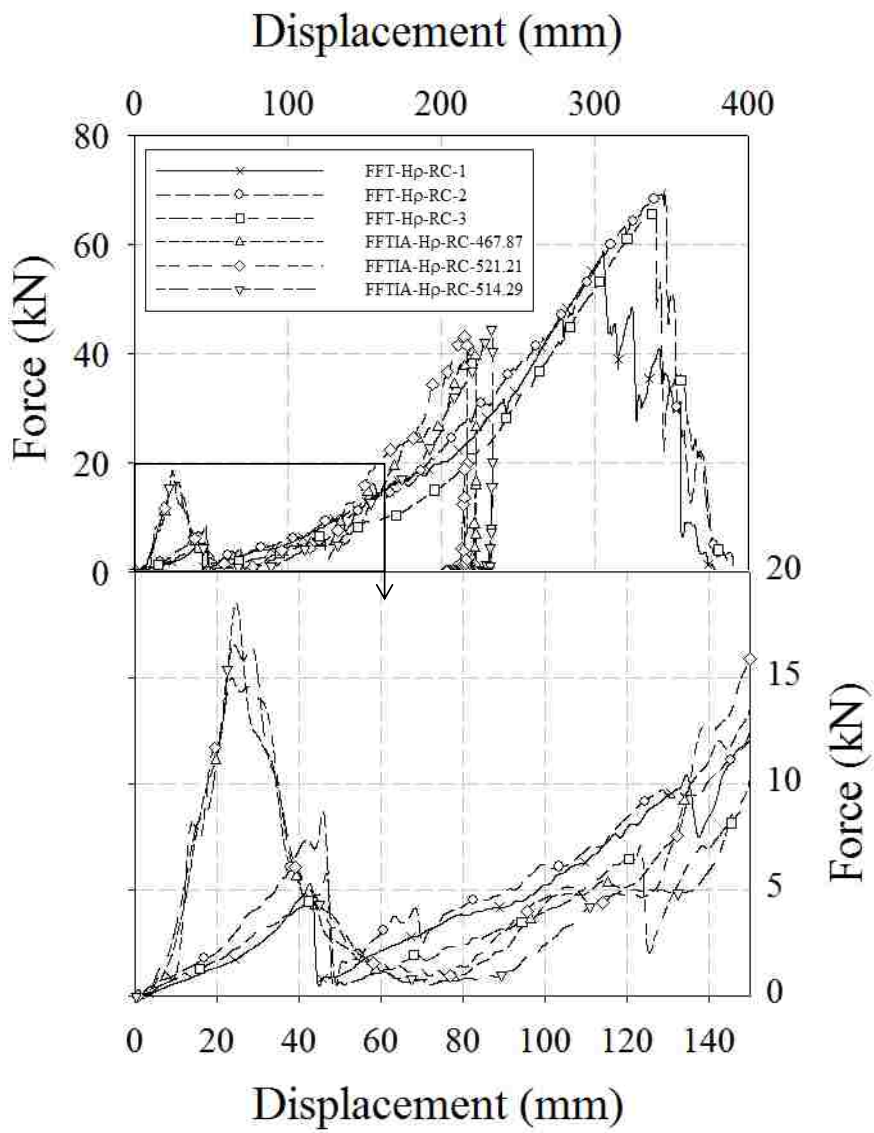


Figure A11: Force/displacement response of high density group A cores

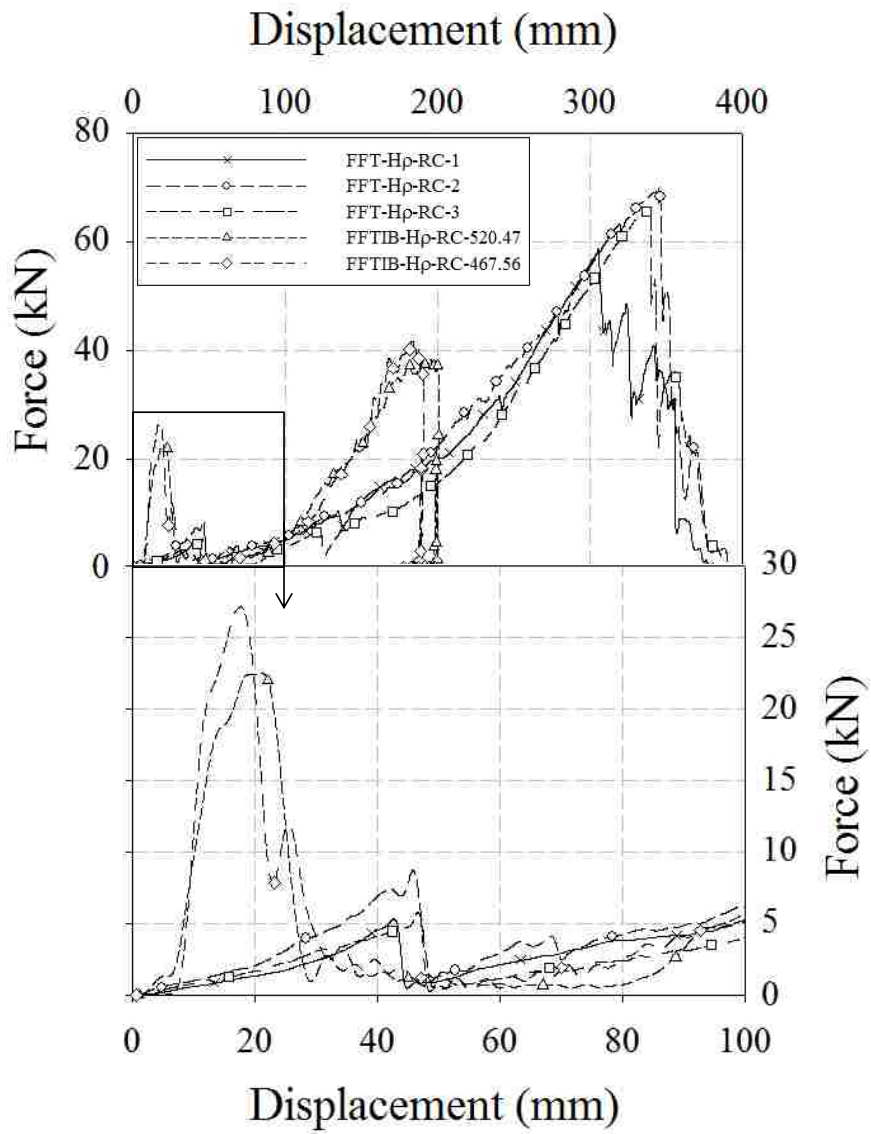


Figure A12: Force/displacement response of high density group B cores

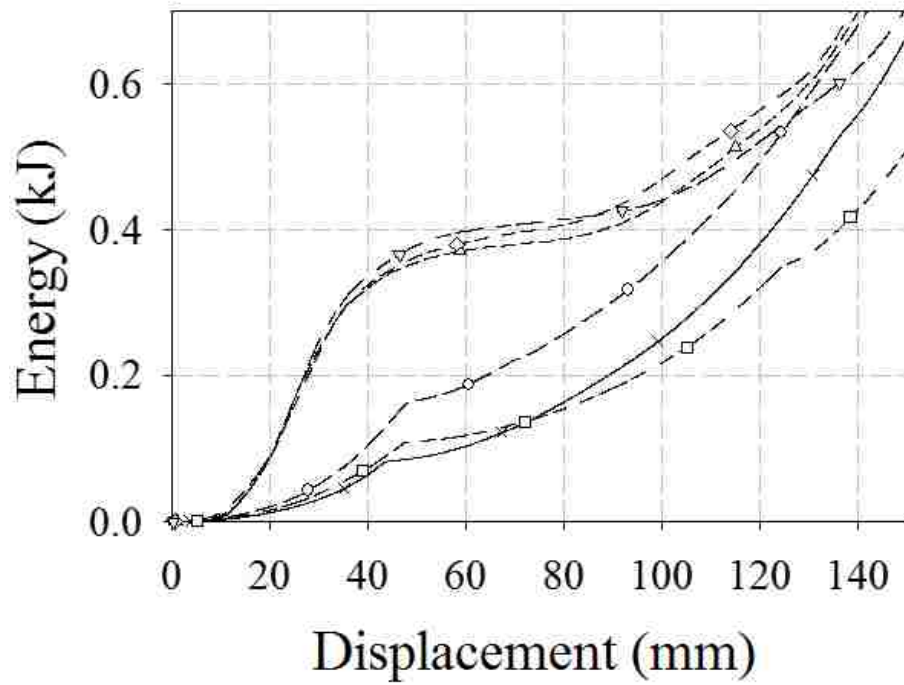


Figure A13: Energy/displacement response of high density group A cores

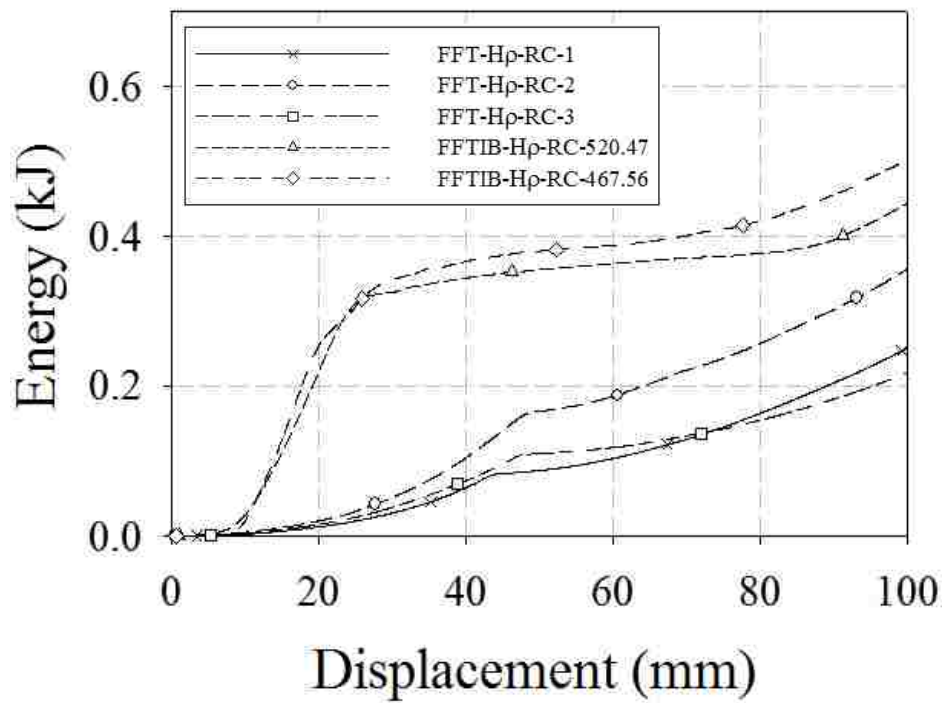


Figure A14: Energy/displacement response of high density group B

**APPENDIX B: ENGINEERING STRESS/STRAIN RESPONSES OF ALUMINUM
FOAM CORE SAMPLES**

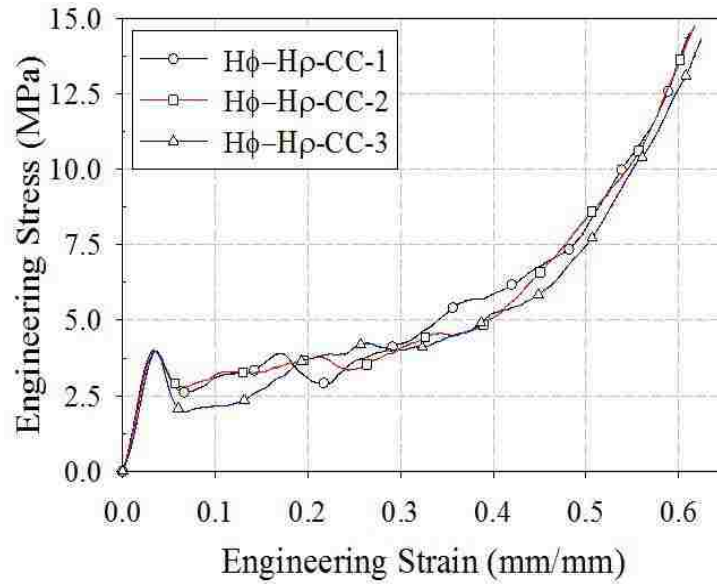


Figure B1: Stress/strain response of high diameter high density circular cores.

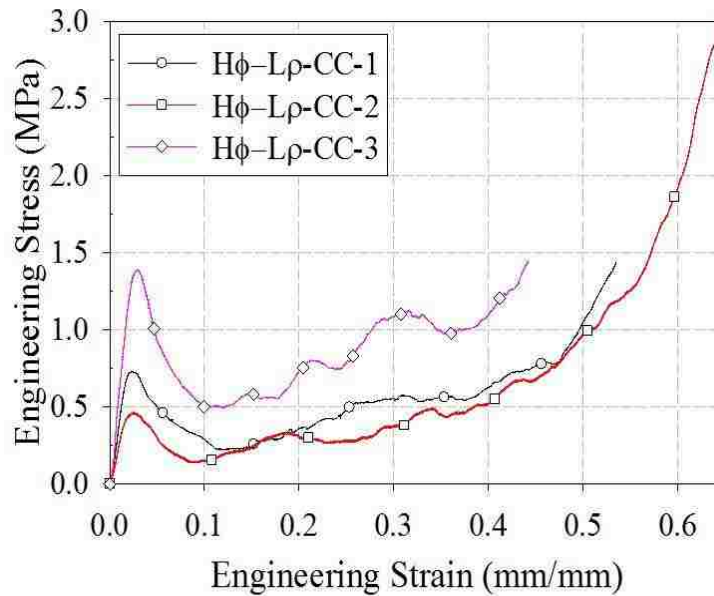


Figure B2: Stress/strain response of high diameter low density circular cores.

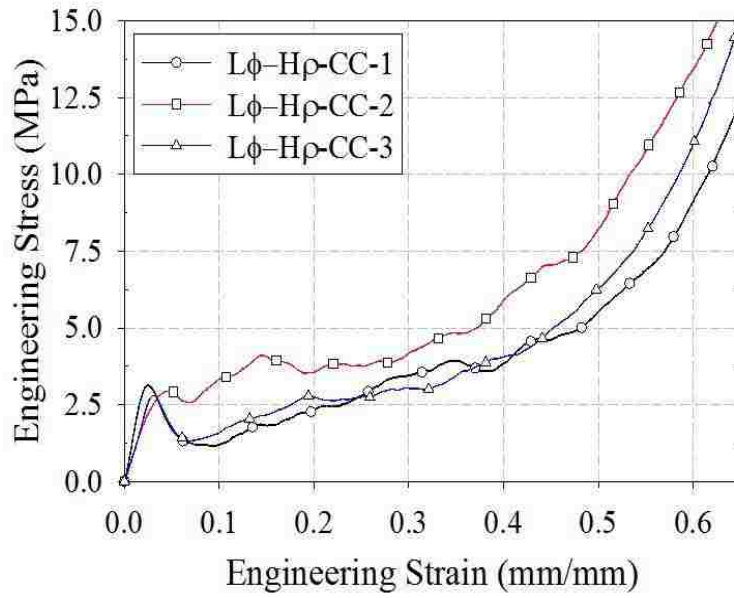


Figure B3: Stress/strain response of low diameter high density circular cores.

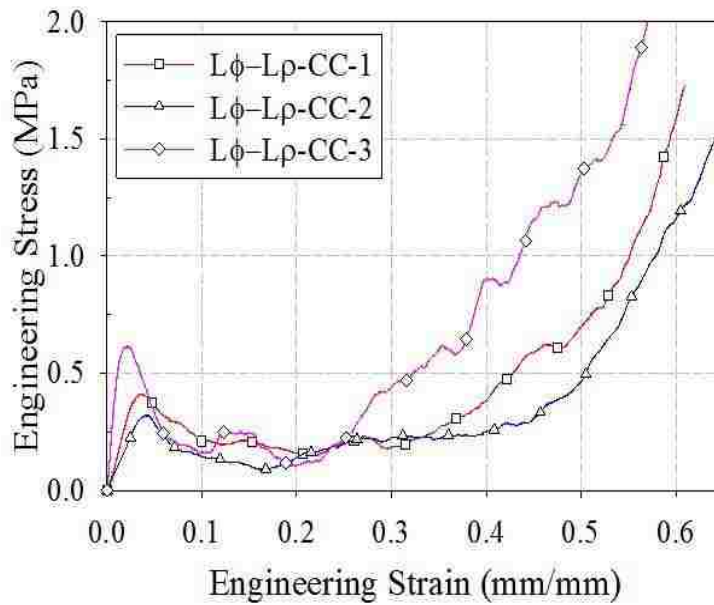


Figure B4: Stress/strain response of low diameter low density circular cores.

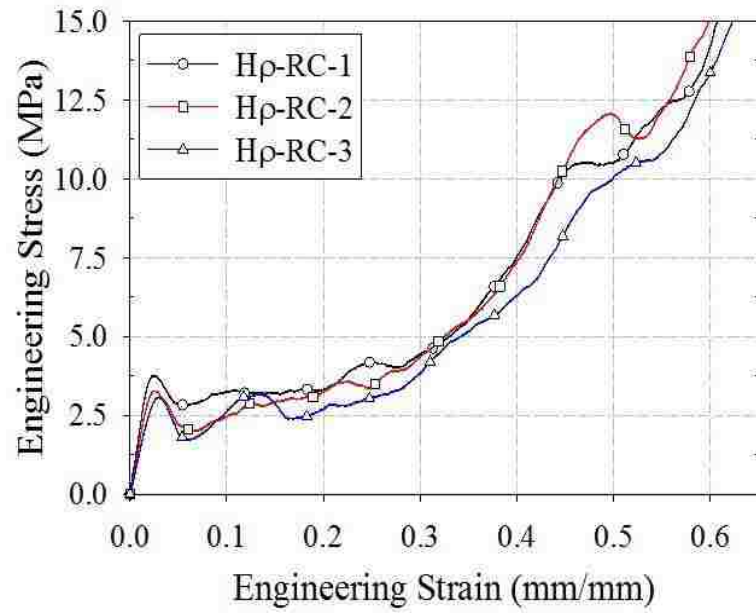


Figure B5: Stress/strain response of high density rectangular cores.

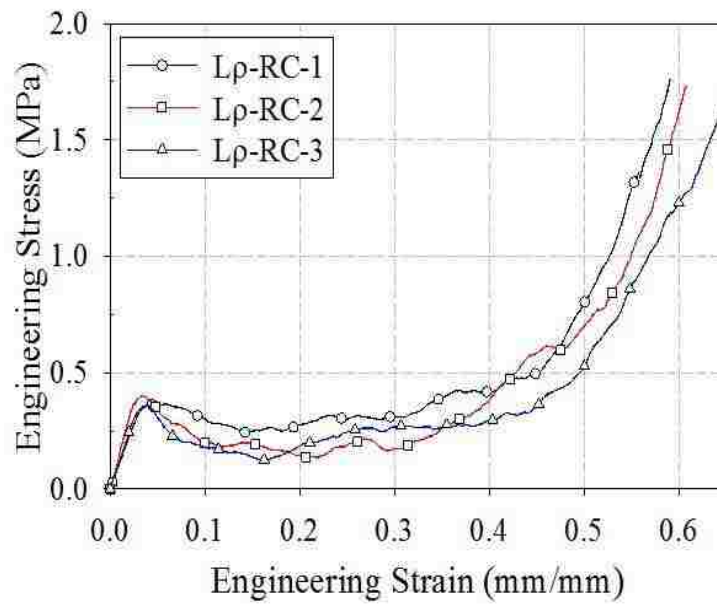


Figure B6: Stress/strain response of low density rectangular cores.

APPENDIX C: ENGINEERING PRINTS FOR PROJECTILE AND IMPACTING
CAP

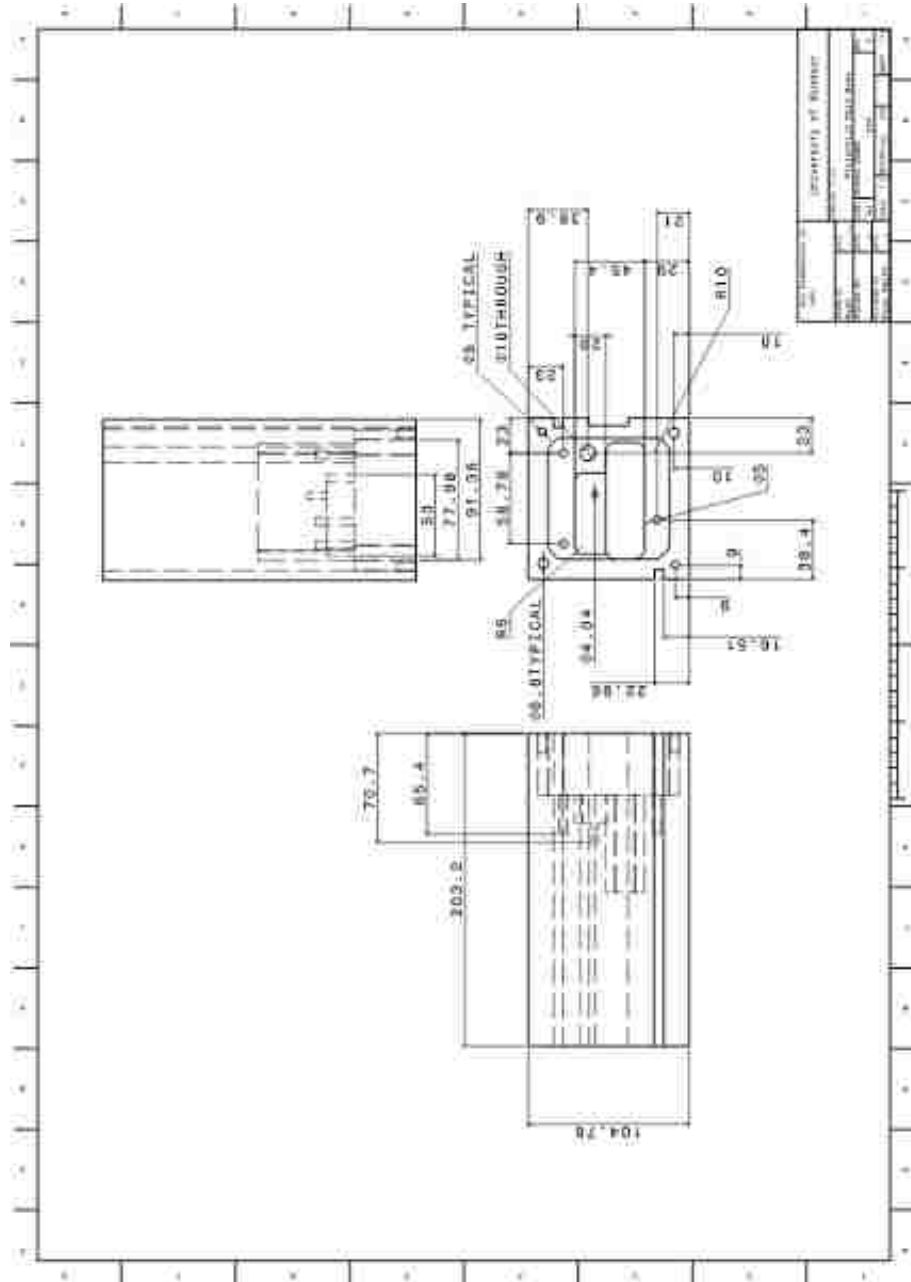


Figure C1: Projectile Main Body

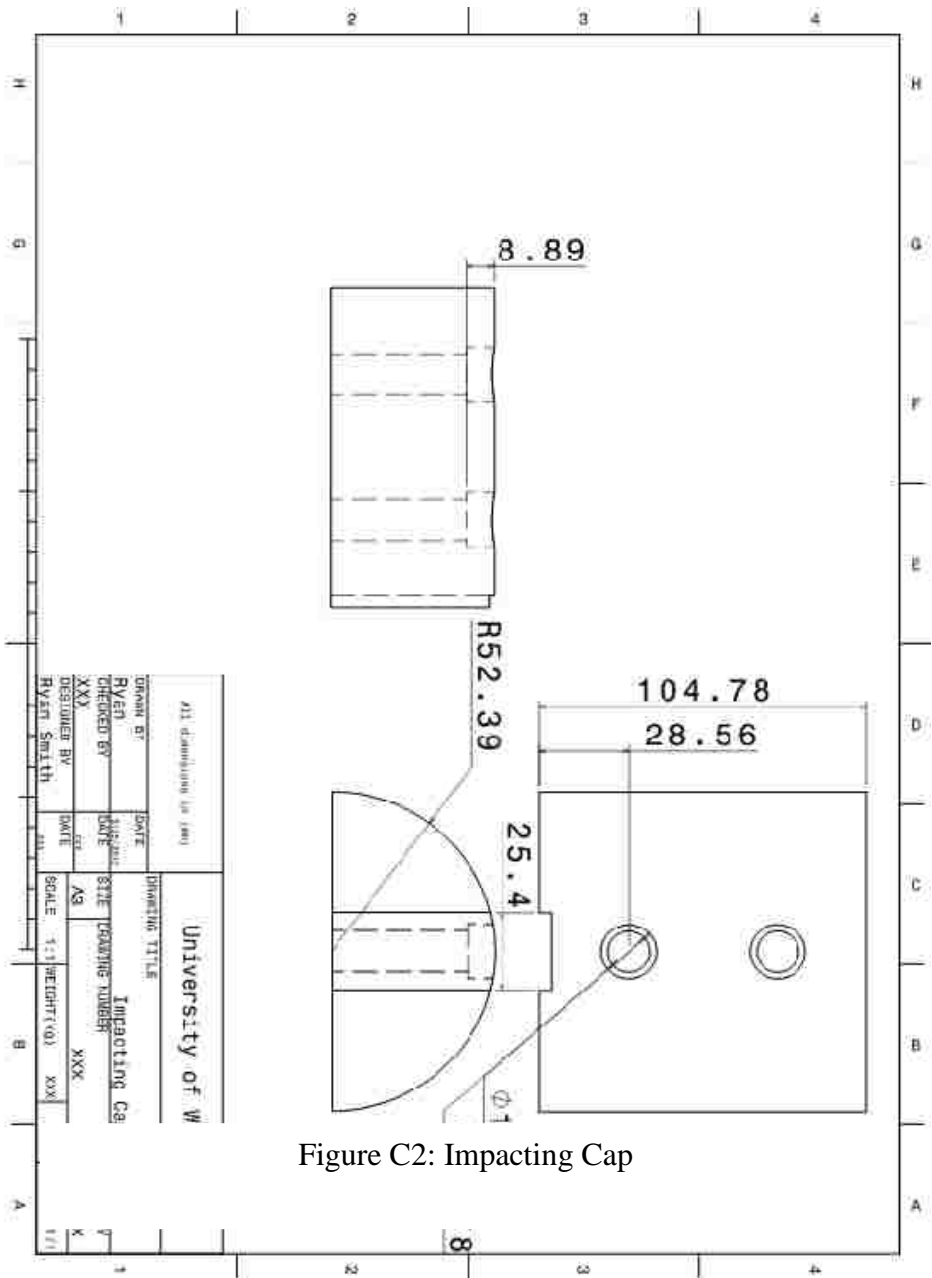


Figure C2: Impacting Cap

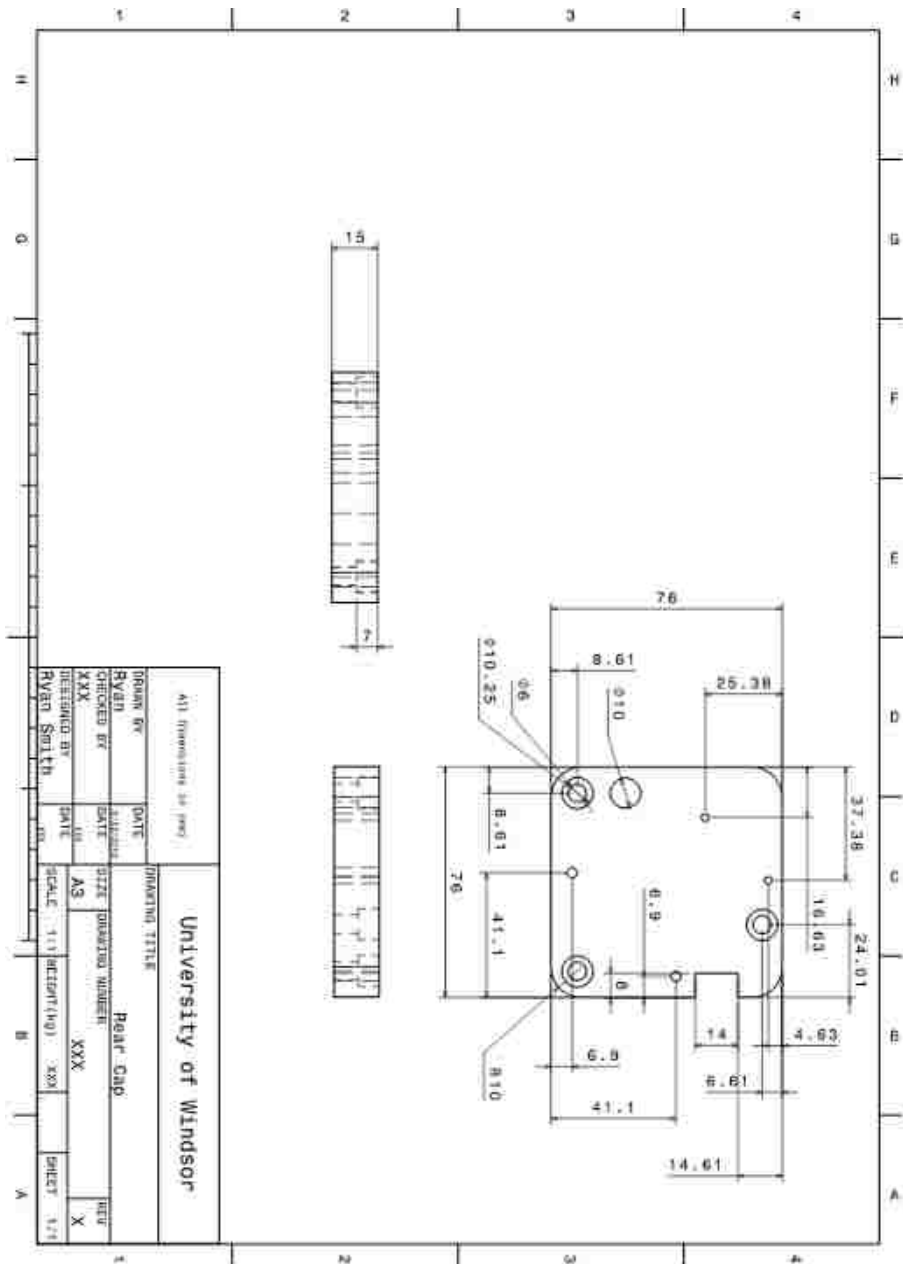


Figure C3: Rear Cap

VITA AUCTORIS

NAME: Ryan Smith

PLACE OF BIRTH: Windsor, ON

YEAR OF BIRTH: 1988

EDUCATION: General Amherst High School, Amherstburg, ON,
2007

University of Windsor, B.A.Sc., Windsor, ON, 2011

CANDIDATE: University of Windsor, M.A.Sc., Windsor, ON, 2015